University of Alberta

DEVELOPMENT AND APPLICATION OF LABRADOR SEA CLIMATOLOGIES

by

Nilgün Çetin

A thesis submitted to the Faculty of Graduate Studies and Research in partial fulfillment of the requirements for the degree of **Doctor of Philosophy**.

Department of Earth and Atmospheric Sciences

Edmonton, Alberta
Fall 2007

Canada

Abstract

Two yearly climatologies of the Labrador Sea are developed. One is based on the traditional geopotential coordinates, and the other employs isopycnal coordinates in the vertical. The analysis of the results show that the isopycnal climatology has more skill at describing the mean state of the Labrador Sea, without smoothing out important flow features such as strong boundary currents and fronts.

Seasonal climatologies based on the isopycnal coordinates in the vertical are also developed to study seasonal variability of the Labrador Sea hydrography and freshwater and heat fluxes. The greatest seasonal variability is observed in winter, the season in which deep convective overturning takes place.

By using the objective analysis technique which successfully represented the dynamics of the Labrador Sea, a pseudo time-series of water properties is developed to study their inter-annual variability.

The contribution of the West Greenland Current to the interior Labrador Sea freshwater budget is found to be greater than that of the Labrador Current, even though the Labrador Current has a larger freshwater content. Diagnostic calculations

show that the Labrador Current flows southward mostly parallel to the isobaths without much of its fresher waters ever crossing into the interior Labrador Sea.

To the memory of my father, Yılmaz Baybağ (1937-1980)

Acknowledgements

There have been many people who have contributed to the successful completion of this work, both on a scientific and personal level. It is my great pleasure to have the opportunity now to acknowledge their much appreciated efforts.

First and foremost, I want to express my gratitude to Dr. Paul Myers for supervising my research with continuous encouragement and support. I am indebted to him for the time he has so generously invested in me by not only providing scholarly advise, but also allowing me to learn from my mistakes. Thank you for never loosing your cheerful enthusiasm about the project since the day I started working on it and for making me always feel that you trusted in me to complete it, even at times when I doubted myself.

I would like to thank my supervisory committee members, Dr. Edward Lozowski and Dr. Andy Bush for accepting the responsibility of carefully watching the progress of my research since the time I transferred to the University of Alberta. Also, I would like to acknowledge Dr. Gordon Swaters, Gerhard Reuter, and Dr. Brad de Young for their suggestions, which improved the presentation of this work.

This journey which led to a Ph.D. degree in Physical Oceanography has been a very long one, which could not have been completed without the help of many friends along the way. It started on the Island of Newfoundland in the Department of Physics and Physical Oceanography at the Memorial University of Newfoundland. I would like to thank some of the faculty members from whom I took various courses in oceanography: Dr. Brad de Young, Dr. Len Zedel, Dr. Paul Myers and Dr. Serpil Kocabıyık. A special thank-you to Cristina S. Tollefsen for warming up cold and drizzly Newfoundland winters with her friendship.

Then the journey took me far from the ocean, to Edmonton, where I became a graduate student in the Department of Earth and Atmospheric Sciences. I would like to thank everyone in the department for making this transition as smooth as possible. During this time our research group grew and I had the pleasure of working with graduate students from a diverse background. They are -in the order they joined our group- Daniel Deacu, Mark Cheeseman, Duo Yang, Michelle Li, Jennifer Jackson, Yan Tsehtik, and Sanjay Rattan.

Then I found myself in the West Coast of Canada before the dissertation was completed. This work would have stayed incomplete if it was not for the support I received from Germaine Gatien and Howard Freeland. They generously opened their home to me and helped me stand on my own feet again. I am grateful to you both for making me feel like I have a family to whom I can turn to at troubled times. Germaine's editorial help improved the readability of the manuscript very much. Thank you Germaine for tirelessly reading the chapters over and over again.

The Department of Earth and Ocean Sciences at the University of British Columbia and the Institute of Ocean Sciences have been my workplaces since I moved to the West Coast. I would like to express my deepest gratitude to Dr. Susan Allen of the EOS-UBC for becoming a mentor more than a boss and for encouraging me to complete my thesis. I have received a very warm welcome from everyone at IOS and enjoyed working alongside many of you. There are too many names to mention here. I would like to give special thanks to Dr. Howard Freeland for being my mentor and host, and to Dr. Robin Brown for letting me have a workplace at IOS and reminding me that I must finish writing the thesis whenever I was unmotivated.

During the course of my PhD studies, I came to realize how strongly we rely on our friends and how lucky I must be for having so many wonderful friends. The fact that this dissertation is ever completed is the proof of this belief. When I was going through a very difficult time and thought nothing could ever be normal again, I found the best friend I have ever had, Tsuyoshi Wakamatsu. Thank you Tsuyoshi for sharing the good and the bad times with me. Without your never-failing optimism and strength I could have never reached the end.

Contents

List of Figures

List of Tables

Chapter 1

Introduction

The atmospheric and oceanic circulation on Earth results from the meridional variation in solar radiation. To balance the discrepancy in heat distribution, the atmosphere and ocean move in such a way as to carry heat from the tropics, where there is an excess of it, to the polar regions where there is a deficit. The Ocean's role in this system is to transport heat from the equatorial regions to high latitudes in relatively fast and narrow currents concentrated on the western boundary of ocean basins, such as the Gulf Stream.

When warm waters reach higher latitudes, they loose their heat to the atmosphere by convection; as a result, the atmosphere is warmed and the surface waters are cooled. The density of seawater is a function of temperature, salinity, and pressure. Lowering the temperature causes an increase in density. When denser water is

formed near the sea surface by convective cooling, the water column becomes unstable and the denser water sinks until it reaches its neutral density surface in the water column. This process is called convective overturning (e.g. Marshall and Schott, 1999). Newly formed deep waters then flow back to equatorial regions as deep currents. The circulation cell set up by changes in heat and/or salt content of the water mass is known as the Thermohaline Circulation (THC).

Deep waters of the world oceans are formed at a few sites, where local atmospheric and oceanic circulation and their interaction favour convective overturning; one of these sites is the Labrador Sea. Surface waters of the Labrador Sea loose buoyancy when subjected to strong atmospheric forcing in winter; as a result, they sink to intermediate depths forming a new water mass known as the Labrador Sea Water (LSW). Even though the LSW is not the deepest convective product to be formed at high latitudes, it is closely linked to the global thermohaline circulation, and the associated poleward heat transport by the North Atlantic ocean (e.g. Weaver and Sarachik, 1991; Marsh et al., 2005). The North Atlantic Ocean has a deep, pronounced thermohaline circulation due to deep water formation (e.g. Lazier and Wright, 1993); therefore, the zonally- and vertically-integrated time-averaged northward heat transport by the North Atlantic is greater than that of the North Pacific Ocean (e.g. Talley, 2003). Effectively, most of the oceanic heat transport in the Northern hemisphere occurs in the North Atlantic, although the North Pacific has a larger volume.

Also, the poleward heat transport associated with the thermohaline circulation in the North Atlantic contributes substantially to the Earth's energy balance (Trenberth and Caron, 2001). The North Atlantic's greater role in the global heat balance makes this basin, especially the deep water formation sites, a key component of the climate system. Moreover, the LSW's low salinity balances the high salinity intermediate waters of the Atlantic Ocean once it is advected out of the Labrador Sea (e.g. Talley and McCartney, 1982).

In recent years, various climate change scenarios have been debated in the light of a long-term warming of the atmosphere since the beginning of industrialization. A similar warming of the world oceans is also reported (Levitus et al., 2000). A large number of observational and numerical studies have been undertaken to determine whether or not a climate shift is already occurring, and how to detect and predict it (see IPCC (1996) report for an extensive list of references). The oceans with their high heat capacity, deep water formation sites, and through their interaction with other elements of the climate system, regulate climate over a wide range of temporal and spatial scales.

The focus of this study is one of the prominent deep water formation sites in the North Atlantic Ocean, the Labrador Sea. In the following sections, various aspects of the Labrador Sea, such as its circulation, deep water formation, and the atmosphere-ocean interactions are summarized from the literature. The Labrador Sea, owing

to the reasons stated above, is one of the most extensively studied regions of the world's oceans. The rationale of choosing the Labrador Sea for this research project, the objectives, and the structure of the dissertation are provided in the last section, where a summary of the major outcomes of this study is also included.

1.1 An introduction to the Labrador Sea and its water masses

The Labrador Sea (Figure 1.1) is located at the northern extremity of the Atlantic Ocean, roughly between Labrador and Newfoundland on the west and Greenland on the east. It is connected to the Arctic Ocean through Baffin Bay on the north and open to the Atlantic Ocean on the south. The proximity of the Labrador Basin to continental northern Canada and the Arctic makes it not only susceptible to changes in the local climate, such as the intensification of the hydrological cycle in the Northern Hemisphere (e.g. Frich et al., 2002), but also a profound contributor to the regional and possibly to the global climate (e.g. Dickson et al., 1996; Curry et al., 1998).

The basin-scale circulation pattern in the Labrador Sea is cyclonic, as it is part of the cyclonic subpolar gyre. At the surface, cold and fresh boundary currents flow as narrow jets concentrated over the steepest topography, with relatively large current
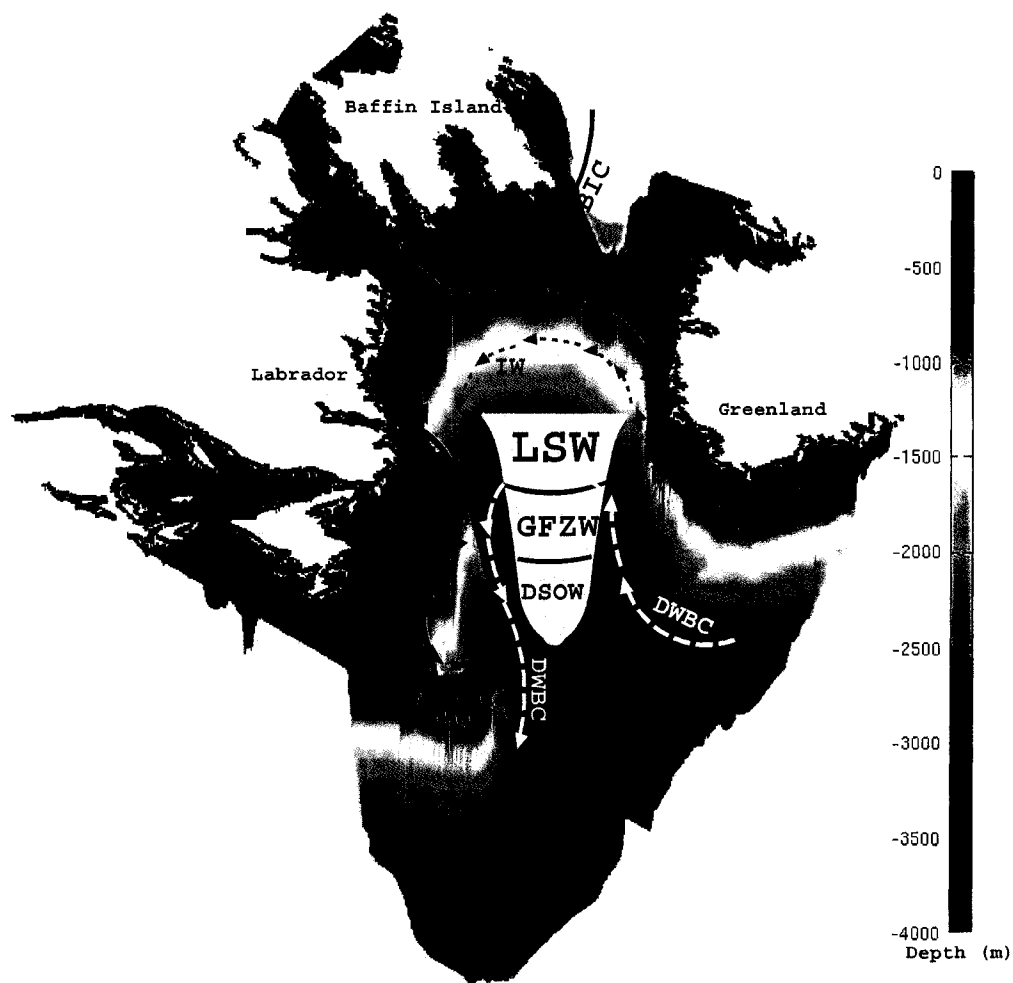
Figure 1.1: A cartoon of the Labrador Sea showing the bathymetry (color coded, in metres), and surface (black), near surface (gray) and deep (white) currents and the water masses found in the interior Labrador Sea (gray shading). Abbreviations are as follows. Surface Currents: East Greenland Current (EGC), Baffin Island Current (BIC), Hudson Bay Water (HBW). Near surface currents: Irminger Water (IW). Interior water masses: Labrador Sea Water (LSW), Gibbs Fracture Zone Water (GFZW), Denmark Strait Overflow Water (DSOW), Deep Western Boundary Current (DWBC).

velocities (approximately 30 cm/s, Flatau et al., 2003).

On the Greenland side, a northwestward-flowing boundary current known as the West Greenland Current (WGC) brings low salinity (S < 34.5[1]), near-freezing (T $\approx$ -1.8 °C) waters of Arctic origin as it enters the Labrador Sea around the tip of Cape Farewell (Clarke, 1984). Over the wider continental shelf and shelf break off Labrador, there lies the southeastward-flowing Labrador Current (LC). The LC is composed of three fresh and cold water masses: Baffin Island Current (BIC), which carries Arctic water to the south through the Canadian archipelago (T $\approx$ -1.5 °C and S $\leq$ 34, Lazier and Wright, 1993), a branch of the WGC, and Hudson Bay Water (HBW). The resultant LC has a salinity of < 34 over the shelf, $\approx$ 34 at the shelf break, and $\geq$ 34 over the continental slope (Lazier and Wright, 1993). Moreover, Lazier and Wright (1993) reported a second branch of the LC, concentrated over the $2500m$ isobath, offshore of the "classical" LC, and named it the "deep" LC, accordingly. The classical LC is primarily baroclinic, and the deep LC has a strong barotropic component. More than 90% of the total volume is carried in the barotropic branch with mean surface velocities reaching 50 cm/s (Lazier and Wright, 1993), while the baroclinic branch is much weaker with mean surface velocities of about 20 cm/s (Petrie and Andersen, 1983). The deep LC is considered to be part of the large-scale subpolar gyre circulation (Thompson et al., 1986), which is stronger in winter and

---

[1]Salinity is measured as a conductivity ratio, therefore, does not have physical units

weaker in summer (Greatbatch and Goulding, 1989) with a mean barotropic velocity of $4 - 5cm/s$.

At depth, the Labrador Sea circulation is still cyclonic and it acts as a pathway for the various components of the Deep Western Boundary Current (DWBC). The deepest part of the central Labrador Sea is filled with the convective product of Nordic Seas, known as the Denmark Strait Overflow Water (DSOW), because it enters the Labrador basin after spilling over the sill in Denmark Strait, between Greenland and Iceland. The DSOW is occasionally called North Atlantic Bottom Water (NABW), as it lies within a few hundred meters of the bottom (e.g. Clarke, 1984); a slightly modified version of this water mass is also called lower North Atlantic Deep Water (lNADW, Fischer et al., 2004). DSOW is slightly fresher than the overlying water mass, but its low temperature (T $\approx$ 0.8 to 1.5 °C, S $\approx$ 34.9, $\sigma_\theta{}^2$ > 28.88) makes it the densest of all North Atlantic water masses.

Above the DSOW, there lies the Northeast Atlantic Deep Water (NEADW), whose origin is the Iceland-Scotland ridge Overflow Water (ISOW), and it fills the northeastern Atlantic basin after spilling over the ridge (T $\approx$ 3 °C, S $\approx$ 34.95, 28.80 > σ_θ> 28.88). In recent literature, this water mass is referred to as the Charlie Gibbs Fracture Zone Water (GFZW) (e.g. Smethie and Swift, 1989) since it enters the western basin through the Charlie Gibbs Fracture Zone. The GFZW is also called

---

[2] $\sigma_\theta = \sigma(S, \theta, 0)$ is the density of a parcel of water would have if it raised adiabatically and without salinity exchange to the surface.

middle North Atlantic Deep Water (mNADW) in older literature. For the sake of consistency, the bottommost component is called DSOW, and the overlying water mass is called GFZW, throughout the rest of this dissertation. Both the DSOW and GFZW move cyclonically around the Labrador Sea and leave the basin east of Flemish Cap (Fischer et al., 2004). The GFZW is older and saltier than the DSOW as it has mixed with higher salinity Mediterranean water while it was in the eastern basin (Fischer et al., 2004).

The LSW lies above the two deep components of the DWBC, the GFZW and DSOW, and below the warmer, saltier Irminger Sea Water (ISW or IW) (Fischer et al., 2004). Fischer et al. (2004) defines the LSW as the water mass whose potential density is in the range of $\sigma_\theta= 28.74 - 28.80$. The same density definition is adopted in this study as well. Even though the T and S values of the LSW are known to exhibit inter-annual and inter-decadal variability (e.g. Dickson et al., 1996), the density of the LSW is almost invariable over time. This is because the temperature and salinity changes are compensating in density (e.g. colder/fresher or warmer/saltier LSW products are similar in density) (Clarke and Gascard, 1983; Talley and McCartney, 1982), except during the intense convection events of the early 1990s, when the LSW penetrated into the salty NEADW underneath and became denser. Even so, the density fluctuations of the LSW would be very subtle according to Talley and McCartney (1982).

The interior waters of the Labrador Sea are warmer and saltier than the bound-

ary currents. Lateral fluxes of heat and salt from the northwest corner of the North Atlantic Current (NAC; T $\approx$ 9.5°C and S $\approx$ 35.35, Clarke, 1984), and from the IW (T $\approx$ 4.5°C and S $\approx$ 34.95, Cuny et al., 2002), keep the Labrador Sea interior ice free (Lilly et al., 1999; Lazier, 1973). Thus intensified air-sea heat fluxes in winter can cause enough buoyancy loss to produce the LSW, a mid-depth water mass which fills the basin roughly between 500 and 1500m, via convective overturning. This newly-formed water mass lies roughly between 500 and 1500 metres of the water column. However, it should be noted that the maximum depth the convective overturning reaches in a particular year is found to be significantly variable (e.g. Lazier, 1980; Pickart et al., 2002). The process of LSW formation and its variability is further discussed in the following section.

1.2 Convective overturning in the Labrador Sea

The Labrador Sea is one of the few oceanic sites where surface waters are converted into mid-depth waters via open-ocean deep convection (Marshall and Schott, 1999), providing a link between the atmosphere and the mid-depth ocean (Curry et al., 1998). Clarke and Gascard (1983) and Gascard and Clarke (1983) discussed the physical processes that govern deep convection on three spatial scales as listed below.

[i] The largest-scale constraints on the deep convection are a basin-scale cyclonic circulation, a low stratification in the underlying water column, and a strong buoyancy forcing, which is supplied by the cold dry winds in the proximity of continental Canada.

[ii] The second set of constraints involves mesoscale structures, such as a localized cyclonic current on the scale of the Rossby deformation radius, which is about 10 km in the Labrador Sea, that brings dense water to the surface by the doming of isopycnals and lets it be subjected to further cooling by the atmosphere (Gascard and Clarke, 1983). Based on Lagrangian float data, Lavender et al. (2000) showed that the interior circulation is dominated by $O(10\text{km})$ cyclonic recirculation cells around the periphery of the Labrador Sea, approximately enclosed by the $\sim$ 3000m isobath, and an anticyclonic counter-current to the north of Flemish Cap. One of the cyclonic recirculation cells is adjacent to a well-known convection site (see Figure 13 in Lavender et al., 2005 for an improved representation) at around 53°W and 57°N where deep water convection was observed by Clarke and Gascard (1983) in the winter of 1976. Therefore, the second set of constraints is also satisfied in the Labrador Sea.

[iii] The smallest-scale constraint is related to mixing mechanisms within a mesoscale cyclone, which is rather challenging to observe in the field or simulate numer-

ically, as it involves eddy fields. However, literature available on this topic is increasing owing to innovative observational methods from the use of satellite altimetry (e.g. Lilly et al., 2003; Brandt et al., 2004) to surface drifters, Lagrangian float deployments (e.g. Fratantoni, 2001; Cuny et al., 2002) and high-resolution models (e.g. Eden and Böning, 2002; Spall, 2004). These tools, which became available only in recent years, provide insight into the small-scale ocean processes and their role in maintaining the deep convection in the Labrador Sea. A major outcome of these studies is the importance of Greenland eddies both in the re-stratification of the water column after the deep convection by removing the buoyancy and in balancing heat and salt budgets through lateral fluxes (e.g. Katsman et al., 2004).

Information about where the convective overturning occurs is as valuable as understanding how the process works. For example, there have been reports of newly-ventilated LSW reaching subtropical regions in a very short time (e.g. Molinari et al. (1998) reported a LSW transit time of about 10 years from the Labrador Sea to the Bahamas, at 26°30'), thus, rapidly transporting the high-latitude climate signal to the deeper parts of the equatorial ocean. Motivated by the rapid spreading rates and sparseness of direct observations of the Labrador Sea convection (the same conditions that make deep water formation possible, cold winds and harsh winters, also make *in situ* observations very difficult) an active convection experiment was set up during

the winter of 1997 (Lab. Sea Group, 1998). During this experiment, in addition to the "classical" deep convection site offshore of the 3000m isobath in the central Labrador Sea, another deep convection site within the boundary current (< 3000m), at the edge of the ice margin is observed (Pickart et al., 2002). The convective product of the "boundary" is found to be lighter than the "classical" LSW (often called LSW and sometimes referred as cLSW) with slightly warmer temperatures ($T_{boundary} \approx 3.1°C$ as compared to $T_{classical} \approx 2.8°C$). This lighter "boundary" product is named upper LSW (uLSW) by Pickart et al. (1997); they explained the rapid spreading of the LSW by the advection of the uLSW within the fast flowing boundary currents. Furthermore, another site for the LSW formation, outside the Labrador Sea basin, is suggested by Pickart et al. (2003). A cold atmospheric jet formed by the orography near the southern tip of Greenland can cause buoyancy loss great enough to convectively overturn the surface waters southeast of Greenland up to 2000m (Pickart et al., 2003). They calculated the volume of newly formed LSW in the Irminger Sea to be comparable to that of LSW formed in the Labrador Sea for the winter of 1996-1997.

1.3 Sources of variability in the LSW production

There are a number of factors, such as the magnitude of the heat exchange between the atmosphere and the Labrador Sea, freshwater input from the Arctic regions and physical properties of previously formed LSW, that can alter the rate of

LSW production. While the regional circulation patterns (e.g. cyclonic gyre circulation, persistent northwesterly winds) and intense atmosphere-ocean interactions favour deep convection, surface freshwater flux and stratification work against it. There have been a limited number of direct observations of the deep convection in the Labrador Sea; however, available data show that the depth of convection can reach up to $2300m$ (Lazier et al., 2002). On the other hand, there have been winters without any deep water formation (Lazier, 1980). Although it varies greatly with location and time, on average the depth of the deep convection can be considered to be 1750 meters (Lilly et al., 1999).

Atmosphere-ocean coupling is pronounced over winter due to the wind-induced vertical mixing processes and air-sea heat fluxes. Deser and Blackmon (1993) studied 90 years of winter observations by using an objective analysis method (Empirical Orthogonal Function – EOF) on four components of the climate system: Sea Surface Temperature (SST), air temperature, wind, and Sea Level Pressure (SLP) in order to find a dominant frequency of the surface climate variability in the North Atlantic. As a result of the statistical analysis, it is found that all of the four climate variables represent fluctuations around quasi-decadal time scales with two different decadal spectral peaks, one at 9 years and the other at 12 years, indicating that decadal oscillations are not regular. There is a strong correlation between the thickness of LSW, which is related to the strength of the winter convection, and the North Atlantic

Oscillation (NAO) index. The NAO index is defined as the difference between the sea level pressure of the low pressure cell over Greenland and the high pressure centre over the Azores (Hurrell, 1995). Curry et al. (1998) report that LSW layer thickness increases with increasing westerly winds (i.e. high NAO index). However, the correlation between the wind strength and LSW is not always strong; for example, during some special events called the Great Salinity Anomalies (GSA) when there is a large freshwater influx (See *Section* 1.4 for a review of past GSAs).

Besides being an important component of the northern limb of the global Meridional Overturning Circulation (MOC), the LSW is one of the major sources of low-salinity mid-depth waters in the North Atlantic ocean. Its contribution to the global thermohaline circulation is two-fold, through entrainment into more saline Nordic overflows (e.g. McCartney, 1992), and through direct advection. The advection pathways of LSW are described as towards the south and then out of the basin from the eastern edge of the Flemish Cap as part of the DWBC, directly towards the northeast into the Irminger Basin and finally to the southeast across the North Atlantic underneath the NAC (e.g. Talley and McCartney, 1982; Rhein et al., 2002).

1.4 Great Salinity Anomaly (GSA)

An episode of anomalously fresh surface waters in the North Atlantic is called a Great Salinity Anomaly (GSA). GSAs propagate cyclonically around the subpolar

gyre and enter the Labrador Sea, causing a collapse or severe reduction in the deep water formation. To date, two GSAs have been reported, while the most recent episode in the 1990s is currently being investigated (e.g. Häkkinen, 2002). The first anomaly to be reported occurred in the early 1970s (Dickson et al., 1988) and the second in the 1980s (Belkin et al., 1998). GSA events are also associated with low temperatures and extended ice coverage in the Labrador Sea. The formation and advection of GSAs are very important processes since they have pronounced effects on the regional and global climate systems.

Belkin et al. (1998) proposed that the two GSAs were caused by different mechanisms. The GSA of the 1970s was caused by the high freshwater/sea ice input from the Arctic into the Greenland Sea and Iceland Sea, which was then advected to the Labrador Sea. On the other hand, the GSA of the 1980s was created locally in the Labrador Sea by harsh winters in the early 1980s, with a possible contribution of fresh water inflow from the Canadian Archipelago. The large positive sea-ice anomaly observed during the GSA of the 1980s, around the Labrador Sea, without a counterpart in the Greenland Sea, stresses the importance of local climate effects and conditions. The analysis of salinity and sea-ice anomalies indicates that in coastal regions a number of different processes (e.g. winds, ice advection, and local freshwater influx) play a role in determining the distribution of salinity and sea-ice (Mysak et al., 1990).

1.5 A review of previous climatologies

LSW formation and spreading rates, and physical properties of the LSW and other water masses of the Labrador Sea are known to vary on a number of time scales from seasonal to decadal (e.g. Dickson et al., 2002). Therefore, the descriptions of temperature, salinity and flow field derived from individual surveys (e.g. Lazier, 1973; Clarke and Gascard, 1983; Lazier and Wright, 1993; Pickart et al., 2002), which are irregularly distributed over time and space, cannot represent the mean state of the Labrador Sea.

To know the mean state of the Labrador Sea, a climatology needs to be compiled. An ocean climatology is assembled by taking an average of water properties observed over a number of years. During the averaging process, transient features are filtered out and replaced by persistent features. In a region where the variability is high, such as the Labrador Sea, one can ask whether a climatology can ever represent the actual hydrography of the region. However, to understand the variability in a region, one must first know the mean state around which the system is changing. Therefore, a climatology of the Labrador Sea is required to get a clear picture of its mean state, and then to be used as a benchmark for interpreting observations, model results, and its variability. Additionally, gridded mean property fields produced from the climatology are of use for the initialization and validation of numerical models.

In this study, two new climatologies of the Labrador Sea are compiled. The

methods, interpretations and various applications of these climatologies are discussed in the chapters to follow. Compiling two climatologies by using the same data but different methods allows us to examine the strengths and weaknesses of these methods. The new climatologies are also compared to climatologies produced from other studies. The next paragraph gives an overview of some of the well-known climatologies involving our study area.

Examples of climatologies that include the Labrador Sea are:

- Climatological Atlas of the World Ocean (Levitus, 1982), and it updates in 1994 (Levitus, 1994), 1998, 2001 (Stephens et al., 2002; Boyer et al., 2002 (hereinafter WOA-82, WOA-94, WOA-98, and WOA-01 respectively).

- Reynaud (1994) climatology of the north Atlantic.

- deYoung et al. (1994) climatology of the northwest Atlantic.

- Lozier et al. (1995) climatology of the north Atlantic.

- Grey and Haines (1999) climatology of the north Atlantic based on Lozier et al. (1995) climatology.

- Yashayaev and Zveryaev (2001) seasonal climatology of the north Pacific and north Atlantic.

Some of these have been used in diagnostic and modelling studies (e.g. Reynaud

et al., 1995; Cooper and Gordon, 2002; Myers et al., 2005). Some of the climatologies were produced for the global ocean while others focused on a particular basin. Climatologies built for the world ocean (e.g. WOA-82 and WOA-94) require a coarse resolution ($1° \times 1°$) to account for the large, data-sparse regions in the Southern Ocean. Although the Lozier et al. (1995) climatology for the North Atlantic utilized the same horizontal resolution as the global climatologies, the smoothing scale was smaller due to increased data volume, and thus overall resolution was increased. In our study, even greater data volumes reached during the 1990s enabled us to avoid additional smoothing between the iterations. deYoung et al. (1994) used a very fine resolution ($1/12° \times 1/12°$). However using such a high resolution causes unfilled grid points in the northern latitudes where the data coverage is limited, especially in winter. We thus choose to use a resolution of 1/3 degree, as did Reynaud (1994) whose climatology might be the closest work to ours with respect to the choice of domain, resolution and objective analysis scheme. A significant difference between the geopotential climatology produced as the first part of this study and the work of Reynaud et al. (1995) is the large amount of additional data that has become available over the last decade, permitting the use of smaller search radii and a tighter depth dependence. The inclusion of the large number of recent measurements as a result of regional and global programs, such as the Labrador Sea Experiment and World Ocean Circulation Experiment, in the hydrographic database has provided a supplementary motive to

carry out this study. The details of the data coverage and quality control procedures can be found in the next chapter.

Spatial smoothing is introduced when unevenly-distributed real observations are mapped onto regular grid points in the horizontal and vertical, a process known as objective analysis. However the degree of smoothing can be kept to a minimum by applying an appropriate objective analysis technique. Traditionally, the data are first binned in the vertical, according to either their depth (geopotential coordinates) or potential density (isopycnal coordinates) range. Isopycnal coordinates provide a more natural system since water tends to flow along isopycnals rather than along isobaths. The advantages of using isopycnal coordinates over geopotential coordinates are discussed in detail in Lozier et al. (1995); they have been widely used in climatological studies of the World Oceans (Grey and Haines, 1999; Lozier et al., 1995; MacDonald et al., 2001). One of the advantages is to eliminate the effects of over-smoothing by averaging properties on an isopycnal surface. Unrealistic mixing of water properties is avoided by binning data over isopycnal surfaces. Furthermore, isopycnal-averaging preserves baroclinicity of the flow field, which will be highlighted in our results, especially with respect to the Deep Western Boundary Currents (DWBC).

1.6 Objectives and the structure of the thesis

As mentioned above, the Labrador Sea experiences variability on a number of time scales imposed by the other components of the climate system, with which it interacts closely. However, it should be stressed that the Labrador Sea is not a simple conduit passing the climate signal from higher latitudes to lower latitudes; it leaves its signature by modifying and buffering these signals. To know the current state of the Labrador Sea in relation to its long-term averaged mean state is important to assess and track these changes up and downstream. A snapshot of the current conditions can be obtained through *in situ* observations, but to know the mean state, a climatology is necessary.

One of the reasons for choosing the Labrador Sea for a climatological study is that it is one of the best-sampled oceanographic regions for an open ocean system even though winter data volumes are limited. The number of available observations determines the grid resolution and the smoothing scales. Working with large volumes of data improves results by reducing the amount of smoothing needed. Also, the increased resolution allows smaller-scale prominent features to be preserved in the climatological fields. Provided that an appropriate method of objective analysis is chosen, a climatology can even capture some of the finer details of the circulation, as evidenced by the results of the current study. The results are discussed along vertical cross-sections and in terms of their relation to the key regions. Figure 1.2 shows the

location of these sections and regions.

The data included in this study and the methods used to analyze it are detailed in *Chapter* 2. The objective analysis scheme chosen for the analysis is one that takes into account the close relationship between the bathymetry and circulation pattern. The velocity fields and transport rates for various water masses are calculated by a diagnostic model, which is also explained in *Chapter* 2.

The effects of vertical coordinates are investigated by binning the same data on two different vertical coordinates, geopotential and isopycnal, and comparing the respective climatologies to each other. To build geopotential or isopycnal climatologies, the data are binned either over a range of geopotentials (constant depth surfaces) or a range of isopycnals (constant density surfaces). As water tends to flow along isopycnals rather than isobars, isopycnal climatology (ISO, hereinafter) gives superior results to the geopotential climatology (GEO, hereinafter). A discussion of the differences and similarities between the two climatologies is presented in *Chapter 3*. A comparison of diagnostically calculated velocities and transport rates, obtained from the newly-compiled climatologies and earlier climatologies, is also given in *Chapter* 3.

The seasonal variability of water mass properties and ocean processes is discussed in *Chapter* 4. A climatology for each of the four seasons (following the convention described in *Chapter* 2) is compiled by combining all the data collected in a particular season between the years 1910 and 2000. Seasonal variability is the most
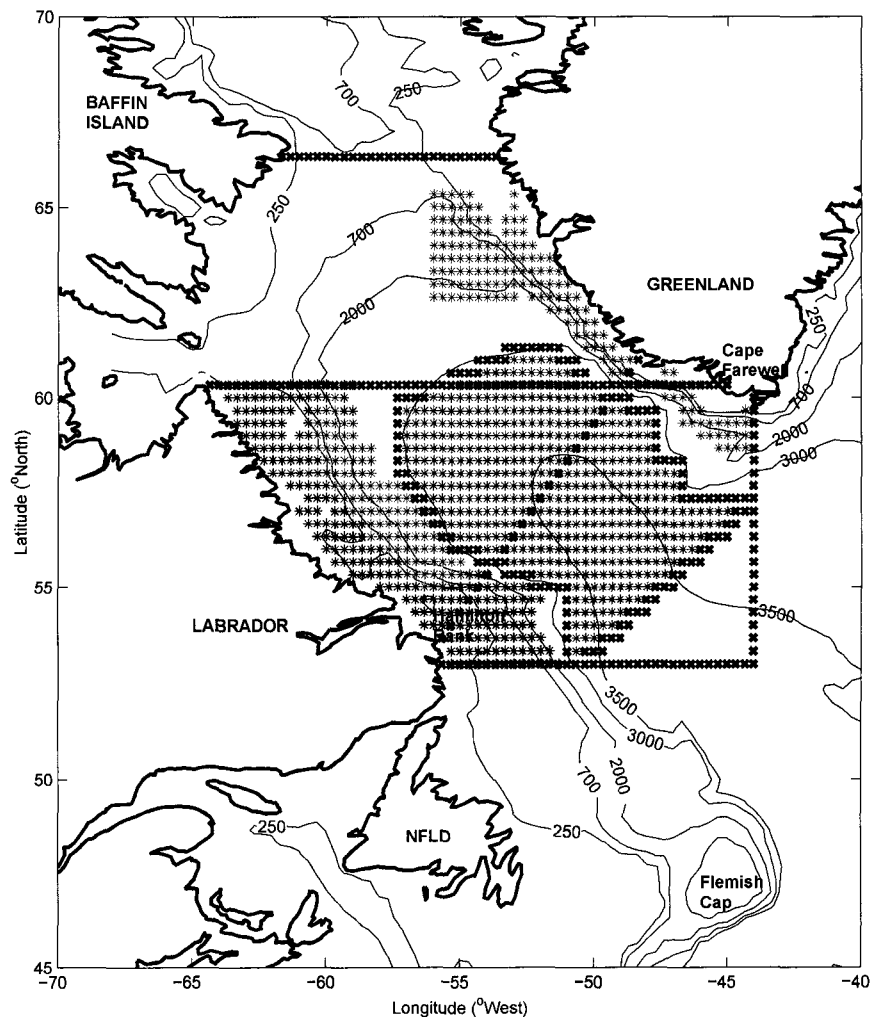
Figure 1.2: Map of the Labrador Sea study area. The lines formed by black crosses show the positions of the grid points used in the discussion of results along vertical cross-sections. The southernmost cross-section stretches zonally along 52.7°N from the Labrador Coast out to the Labrador Sea. The middle zonal line is drawn from the tip of Labrador to the tip of Greenland, along 60.3°N. The northernmost line is drawn between Baffin Island and Greenland, along 66.3°N. The meridional line is plotted from Cape Farewell down to 52.7°N along 44°E. The diagonal line which joins southern Labrador to Greenland is coincident with the AR7W line of repeated surveys of the World Ocean Circulation Experiment (WOCE) project. The closed line, which follows the 3000m isobath except for the opening of the Labrador Sea to the northern North Atlantic, is defined as the front between boundary currents and the interior Labrador Sea. The area within the closed line indicated by red stars represents the interior Labrador Sea. The green pluses represent the WGC, while the purple pluses identify the slope region. The combination of the blue and purple pluses define the LC.

basic form of intra-annual variability as it is maintained by the changes in solar heating. For example, the intensive cooling of the surface waters in winter can lead to convective overturning in the Labrador Sea. Accordingly, the winter properties are found to be the most distinctive.

After establishing the fact that the isopycnal climatology gives more favourable results, this method was chosen to calculate three-year running means (i.e. triads) of temperature and salinity fields *Chapter* 5. Each triad represents the year in its center, providing us with a 51-year time series of salinity, temperature and parameters derived from them. It is very difficult to have systematic, ship-based observations in a region such as the Labrador Sea. Therefore, temporal and spatial biases in the original data sets are vigorously removed from the data used in this study, allowing only the best representative values to be included in the calculation of the climatology and time-series. As a result, the quality of this newly-produced isopycnal climatology is believed to be high, as evidenced by the satisfactory level of agreement between our climatology and triads, and the observational and modelling studies cited in the literature.

The time-series obtained from triads are used to calculate some of the key components of the convective overturning, such as the freshwater flux into the interior Labrador Sea. Among the two boundary currents encircling the Labrador Sea, the WGC and LC, the WGC is found to be the major freshwater source. The cross-

boundary freshwater flux and other results obtained from the triad analysis are also discussed in *Chapter* 5.

The last two chapters are papers written based on the climatologies built in this study. *Chapter* 6 investigates the links between the freshwater content of the Labrador Sea and the evaporation-precipitation (E-P) budget (Myers et al., 2007a). *Chapter* 7 is a study of the IW variability near Cape Farewell (Myers et al., 2007b). These chapters illustrate some of the ways triad climatology can be used. These investigations were made possible as a result of the time-series produced during the Ph.D. studies of Nilgün Kulan. The *Chapters* 6 and 7 resulted from collaborative studies; hence, they are included in this dissertation with the consent of all collaborators.

Finally, the conclusions are stated in *Chapter* 8.

1.7   Statement of originality and contributions

The motivation for this study stemmed from the need to develop a climatology that is consistent with the dynamics of the Labrador Sea. This is achieved by improving the method of objective analysis in two ways. First modification is to include bathymetric information during the iterations. The second is to employ isopycnal coordinates in the vertical. Even though the first modification was applied to build a summer Labrador Sea climatology by Reynaud et al. (1995), the two approaches described in this dissertation were never combined before.

The use of isopycnal coordinates has been shown to improve hydrographic analysis of large ocean basins (Lozier et al., 1995). However, a detailed comparison of the vertical coordinates, i.e. the geopotential and isopycnal coordinates, by using the same database was not performed. This study represents a careful analysis of the strengths and weaknesses of the two coordinates.

Building a time-series by applying an advanced objective analysis method over shorter time windows is another novel approach used in this study. The property time-series produced here provides a robust tool to analyze inter-annual variability in the Labrador Sea. The climatologies and time-series developed in this study will make it possible for scientists to study the links between the MOC and the Labrador Sea hydrography and dynamics further.

The list below summarizes the major outcomes of the research which are detailed in the last chapter.

[i] A high resolution, regional climatology of the Labrador Sea, which may be used in numerical studies and to specify the mean state of the Labrador Sea over much of the 20th century has been constructed.

[ii] The first Labrador Sea climatology based on isopycnal surfaces has been developed.

[iii] A unique comparison of the use of geopotential versus isopycnal coordinates in

objective analysis has been provided.

[iv] Seasonal climatologies of water mass properties (temperature and salinity) as well as a mixed layer depth (MLD) climatology have been produced.

[v] The improved objective analysis scheme has been used as a novel tool to create a time-series of oceanic parameters, in order to study variability in the Labrador Sea from inter-annual to inter-decadal scales.

[vi] A diagnostic ocean model has been employed to calculate current velocities, and hence the transport rates of mass, heat and freshwater from the density field derived from temperature and salinity climatologies.

[vii] Formation sites, advection pathways and types of LSW have been re-evaluated.

[viii] The mean freshwater exchange between the boundary currents and interior Labrador Sea, and the relative importance of WGC versus LC has been studied.

Chapter 2

Data and Methodology

2.1 Data

2.1.1 Area of interest, data source and distribution

All the temperature and salinity data used in this study were extracted from an extensive hydrographic database maintained by the Bedford Institute of Oceanography (BIO). The Climate Database incorporates temperature and salinity data collected using various instruments including hydrographic bottles, CTDs, batfish tows, and bathythermographs.

Marine Environmental Data Service (MEDS), which is the national data centre for the Department of Fisheries and Oceans - Canada, gathers all the temperature and salinity data. After the initial quality controls applied by the original institute

or organization, the data are validated by the MEDS according to the procedures described in the Intergovernmental Oceanographic Commission (IOC) publication (Manuals and Guides 22: GTSPP real-time quality control manual[1]). The additional quality control procedures include location and identification tests, density inversion tests for profile data, climatological tests against known climatologies, and visual inspection of the data.

The Climate Database at BIO assembles all temperature and salinity data collected in the North Atlantic Ocean between 42 to 100°W and 35 to 80°N. After the data are extracted from the MEDS, they are subjected to another set of quality control tests, mainly to remove duplicate profiles before they are added to the Climate Database. A duplicate profile is defined by the BIO Climate Database as any profile recorded within 30 minutes time, and 0.02 °latitude and 0.03 °longitude distance of another profile. The Climate Database is updated monthly and the data can be downloaded from their internet site[2] by filling out an enquiry form that provides options for downloading the relevant data.

For this study, only observations with both temperature and salinity measurements collected over an area bounded by the 40 to 70 °W longitudes and 45 to 70 °N latitudes, and during the period from 1910 to 2000 were used to compile a new

---

[1]A copy of this manual can be obtained from the URL:
http://www.nodc.noaa.gov/GTSPP/document/qcmans/mg22/guide22.htm

[2]The details about the contents of the database and how to access the data through a query system can be obtained from the URL:
http://www.mar.dfo-mpo.gc.ca/science/ocean/database/climapp.html

climatology of the Labrador Sea. A total of 997,408 individual observations satisfied these criteria. An individual observation is defined as a single observation taken at a fixed depth, or each record in a property (temperature/salinity) versus depth profile. The data distribution at the surface (all observations recorded from 0 to 5 metres) is shown in Figure 2.1a. However, assessing the data density by just looking at the surface data distribution would be misleading since the surface layer has the highest data density among all depth levels. The data density for the density surfaces between $\sigma_\theta =$ 27.74 and 27.80, which corresponds to the classical LSW density class, is shown in Figure 2.1b. There is a noticeable decrease in the data density in this mid-depth water mass.

More detail about the vertical data distribution after the quality control and bias removal processes for the geopotential and isopycnal surfaces can be found in Table 2.1 and 2.2 respectively. The GEO (ISO) climatology has 44 standard isobaric levels (density surfaces) in the vertical between the surface and $4600m$ ($\sigma_\theta =$ 18.95 and 27.98). The vertical resolution of the GEO and ISO climatologies is the highest among widely-used global and regional climatologies. The vertical resolution in some of those climatologies are:

- 33 geopotential levels in the top $5500m$ of the water column in Levitus (1982); World Ocean Atlas 1994 (Levitus, 1994) (WOA-94, hereafter); World Ocean Atlas 2001 (Stephens et al., 2002; Boyer et al., 2002) (WOA-01, hereafter); and
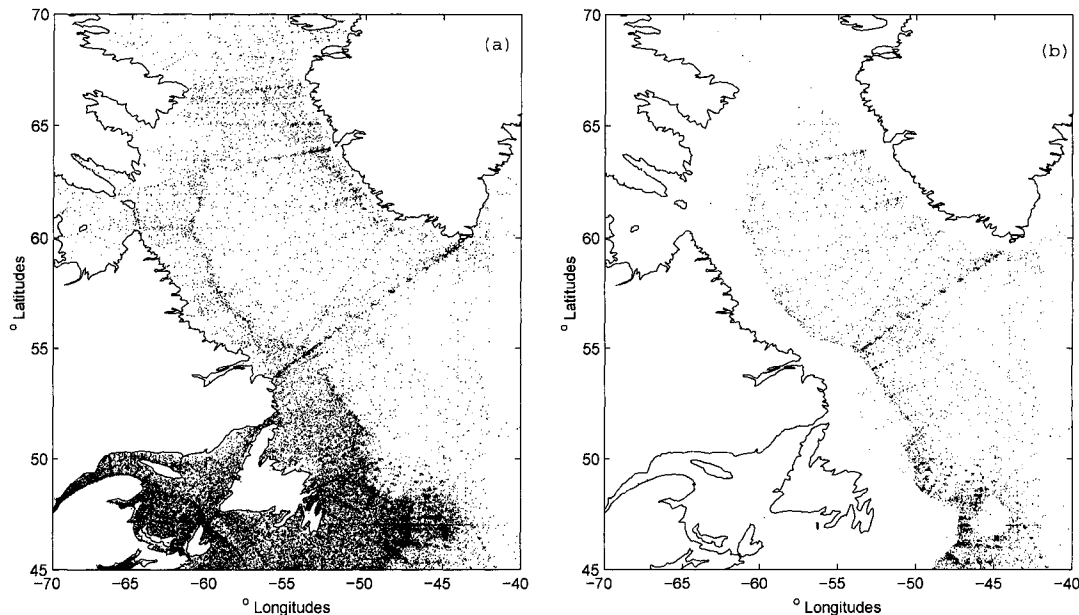
Figure 2.1: Original data density distribution on a particular layer used for the calculation of GEO and ISO climatologies. The surfaces shown here are: (a) The surface level ($z = 0$ to 5 db) of the geopotential, (b) LSW density surface (σ_θ= 27.74 to 27.80) of the isopycnal climatology. Every dot represents an observation made at the location. Coastal areas are highly sampled as these regions can be more easily accessed than open ocean regions. Also, frequently visited stations and lines, such as the OWS-Bravo and AR7W are noticeable from the data density distribution in both subplots.

World Ocean Atlas 2005 (Boyer et al., 2005) (WOA-05, hereafter)

- 37 geopotential levels in the top $4500m$ in Reynaud et al. (1995)

- 12 isopycnal levels between $\sigma_0 = 26.50$ and $\sigma_4 = 45.90$ in Lozier et al. (1995)

The total number of observations used in the compilation of the GEO climatology is 643,966; it is 620,992 for the ISO climatology. The slight difference in the total number of observations between the GEO and ISO climatologies stems from

the fact that after the initial clean-up statistical QC tests are performed on different coordinates (geopotential vs. isopycnal) in the vertical.

Table 2.1: Standard geopotential levels, their depth range, and the number of observations that fall on each level after bias removal and QC checks.

Depth Level	Range (m) $\leq x <$	Number of Data	Depth Level	Range (m) $\leq x <$	Number of Data
1	0-5	70879	23	1050-1150	1415
2	5-15	54094	24	1150-1250	2196
3	15-25	54245	25	1250-1350	1031
4	25-35	57696	26	1350-1450	1172
5	35-45	28497	27	1450-1550	2092
6	45-55	54704	28	1550-1650	593
7	55-70	26758	29	1650-1750	363
8	70-90	46376	30	1750-1850	497
9	90-110	43862	31	1850-1950	416
10	110-130	21400	32	1950-2100	1260
11	130-150	20721	33	2100-2300	448
12	150-180	31512	34	2300-2500	550
13	180-220	29683	35	2500-2700	471
14	220-275	20932	36	2700-2900	359
15	275-350	20557	37	2900-3100	441
16	350-450	13859	38	3100-3300	274
17	450-550	9329	39	3300-3500	268
18	550-650	7698	40	3500-3700	180
19	650-750	3323	41	3700-3900	62
20	750-850	6103	42	3900-4125	45
21	850-950	2617	43	4125-4375	26
22	950-1050	4947	44	4375-4825	15

Although the database is almost a century long, the number of observations available prior to the second half of the 20th century is very limited, and those obser-

Table 2.2: Standard isopycnal surfaces, their density range, and the number of observations that fall on each surface after bias removal and QC checks.

Density Surface	Range $\leq \sigma_\theta <$	Number of Data	Density Surface	Range $\leq \sigma_\theta <$	Number of Data
1	17.95-19.95	2820	23	26.89-26.98	18400
2	19.95-20.95	5376	24	26.98-27.05	16545
3	20.95-20.95	9620	25	27.05-27.12	16106
4	21.95-22.95	14107	26	27.12-27.19	16253
5	22.95-23.45	12955	27	27.19-27.26	15688
6	23.45-23.95	15668	28	27.26-27.33	15644
7	23.95-24.45	18554	29	27.33-27.40	15127
8	24.45-24.75	17230	30	27.40-27.45	12601
9	24.75-25.05	19938	31	27.45-27.50	12411
10	25.05-25.35	22726	32	27.50-27.55	12537
11	25.35-25.55	20845	33	27.55-27.60	13004
12	25.55-25.75	23048	34	27.60-27.65	12433
13	25.75-25.90	22725	35	27.65-27.70	11686
14	25.90-25.90	24560	36	27.70-27.74	9356
15	26.05-26.20	25724	37	27.74-27.77	6662
16	26.20-26.35	26087	38	27.77-27.80	4163
17	26.35-26.44	21543	39	27.80-27.83	2083
18	26.44-26.53	21591	40	27.83-27.86	1241
19	26.53-26.62	21621	41	27.86-27.89	826
20	26.62-26.71	21230	42	27.89-27.92	651
21	26.71-26.80	19912	43	27.92-27.95	500
22	26.80-26.89	19034	44	27.95-28.00	161

vations have larger error bounds due to the measurement methods. However, in the analysis, pre-1950 data was not totally excluded, because the aim was to build a climatology over the longest possible timescale. Also, by including the entire period, we partially avoid biasing the climatology to the conditions associated with an extended period of positive NAO index (Hurrell, 1995), during most of the 1980s and 1990s.

There has been an exponential increase in the available data since World War II; the largest data accumulation rate occurred in the 1990s (Figure 2.2a). This bias towards the present day conditions must be taken into consideration when interpreting the results. Besides this long-term trend in the data availability, another bias towards the warmer months of the year is also evident (Figure 2.2b). Unlike the long-term bias, this monthly bias is partially removed by assigning differential weights to each month. The monthly weights are determined by dividing the number of observations collected in a particular month to the total number of observations.

Apart from the temporal bias, the data contain spatial biases. For example, Ocean Weather Station Bravo (OWS-Bravo), which was located at about 56°30' N, 51°00' W, provided oceanographic data between 1964 and 1974 with an unparalleled resolution. The high density of observations at this location, as well as some other frequently visited stations and transect lines, such as the Station-27 and the transect line AR7W of the WOCE program can easily be seen in Figure 2.1a. The high concentration of observations centred around OWS-Bravo is capable of strongly biasing the results towards the oceanographic conditions of a period during which deep convection was brought to a halt due to restratification of the Labrador Sea.

An earlier version of the GEO climatology was compiled without down-sampling the data from the OWS-Bravo. The results were severely biased, especially in the deep Labrador Sea (approximately $1000m$). The observations made in the deep, central
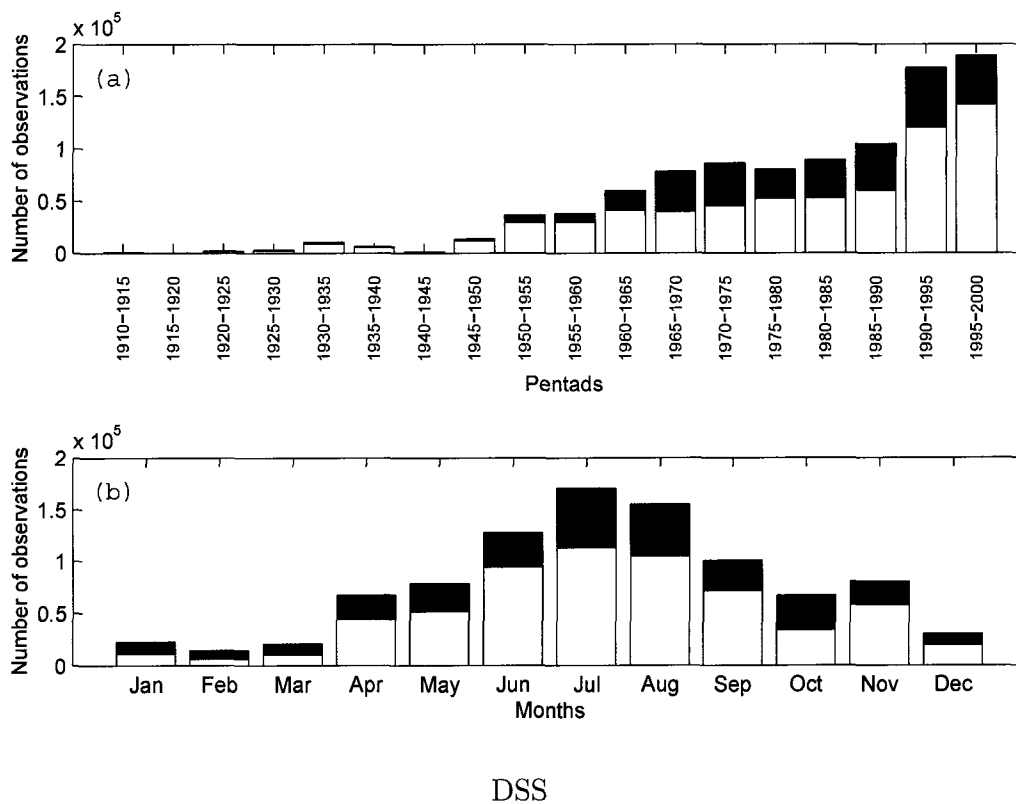
Figure 2.2: The number of observations recorded in (a) pentads (in groups of five years), (b) months. The darker shade represents the portion of data rejected due to QC cleaning processes and spatial and temporal bias removal.

Labrador Sea during the OWS-Bravo era greatly outnumber any other period. Deep convection in the Labrador Sea was limited to near surface waters or non-existent over most of the period OWS-Bravo was operational; hence, the deep waters became warmer and saltier than usual (Lazier, 1980). Therefore, the property maps produced

from the climatology which included all the OWS-Bravo data had patches of warm and high salinity waters located in the deep, central Labrador Sea (figures not shown). This early result showed that OWS-Bravo data must be down-sampled. The down-sampling is done in a way to include approximately one OWS-Bravo datum per season at a particular depth level or isopycnal surface. This is achieved by allowing only about 1% of the original observations from the OWS-Bravo to be included in the climatology database. It should be noted that long-term, coordinated measurements such as OWS-Bravo and repeated lines and stations provide valuable information even though they are not appropriate for a climatological study such as this one.

In other regions, temporal bias is removed by allowing only three data values collected on the same cruise to be included in the climatology, if the data collected on a particular cruise contributed more than 20% of the total number of observations. The data are assumed to be collected in the same cruise if they are collected within the same month and fall into the same geographical bin (2.5°x 2.5°or 5°x 5°squares). The 20% criterion to invoke the down-sampling is implemented in order to have a standard rule for down-sampling that is applicable to a wide range of cases, from data sparse geographical areas to densely sampled ocean weather stations.

Over-representation of a specific era should be avoided in a climatological study such as this. However, due to data availability limitations, this may be challenging to achieve; hence, the results should be interpreted prudently. The subject of bias

removal and data limitations is discussed in more detail in *Chapter* 4, where seasonal climatologies are examined.

Topographic data are extracted from the National Geophysical Data Center's 5-minute resolution ocean floor dataset (NOAA, 1988). It is, then, interpolated onto $1/3° \times 1/3°$ grids for the Labrador Sea region, from 45°N to 70°N and from 40°W to 70°W.

2.1.2 Quality control (QC)

Although we found that the quality of the data obtained from the hydrographic database was high, before continuing with the objective analysis, the original data were subjected to further QC tests. As reported by a number of scientists who have worked with raw data (e.g. see Levitus, 1982, for a detailed discussion on this topic), the choice of a proper quality control procedure is a difficult problem in climatological studies. The criteria for passing a QC test cannot be set without considering the type of study, region, data density and so on. The quality control procedures applied in this study are detailed below together with reasons for choosing them and possible effects on the analysis.

The first procedure was to define broad ranges for the property values in order to eliminate grossly erroneous values. The range for salinity was set from 10 to 37, while for temperature the range was set from -1.8°C (freezing temperature for most

oceanic water masses) to 25°C. It should be noted that this procedure targets errors that might have been caused by the sampling instrument, such as a CTD taking its first record before being submerged. The same temperature and salinity limits were applied throughout the water column without taking into account depth as a factor. Therefore these large ranges were chosen with rounded values, in order to speed the first elimination process. Only 1731 individual observations were eliminated by this method out of a total of 997,408. Most of the rejected values came from the near surface measurements in the upper Gulf of Saint Lawrence and in the Hudson Bay area. Most of these points were excluded for bearing a low salinity value, which does not mean that those values were unrealistic for the location at which they were recorded. However, these regions are not meant to be the focus of this study. Since pairs of temperature and salinity are required in order to calculate density, if either a temperature or a salinity value is rejected, the other one is also eliminated.

For the profile data, another QC test to check the static stability of the water column was applied. For this test the density profile is calculated from the temperature, salinity and pressure profiles. If the vertical density gradient had two or more density inversions, with a denser water parcel lying above a less dense water parcel, both the temperature and the salinity profiles are rejected. Any profile containing a single density inversion is processed to remove the pair of temperature and salinity values that caused the density inversion, and the remainder of the profile is kept in

the database.

After preliminary checks were applied to remove gross errors and outliers, the statistical methods explained below were used on vertically-binned data to meet the QC standards. The QC standards employed in this study are adopted from the recommendations made in the Intergovernmental Oceanographic Commission of UNESCO's QC manual annex-C, and Boyer and Levitus (1994). Two different coordinates in the vertical, geopotential and isopycnal, were used to bin the data. One of the goals of this study is to explore the influence of the choice of vertical coordinates on climatological results. The procedures explained below are applied to every geopotential and isopycnal surface equally.

Once the gross errors and outliers were removed as described above, the data were sorted into 12 groups according to the month (January – December) in which they were collected. Then, geographically they were binned into $5° \times 5°$ squares in the northern part of the domain (between the 60°N and 70°N latitudes), where the data density is low, and into $2.5° \times 2.5°$ squares in the southern part of the domain (between the 45°N and 60°N latitudes). Next, the data in each vertical bin were examined to determine whether a single cruise contributed more than 1/5 of all the observations taken in a $2.5° \times 2.5°$ or $5° \times 5°$ box. If so, all but three data values from this cruise were rejected before the statistical means and standard variations were calculated. During this first statistical test, binned data were subjected to a

± 3 standard deviation (σ) criterion, in such a way that a property value deviating more than three standard deviations from the mean calculated for a particular box and month was rejected. A $\pm 3\sigma$ criterion is stiffer than that used in some other climatological studies (e.g. MacDonald et al., 2001). The choice of a narrower window in our case is justified due to the shorter time scale over which the data is binned (i.e. one month). In addition to the natural variability being narrower within a one month period, natural variability $> \pm 3\sigma$ is mostly limited to coastal areas (Boyer and Levitus, 1994, e.g.).

Following this preliminary statistical clean up, another statistical test which had a different spatial and temporal scale was applied. For this test, the data were grouped into four seasons: winter (January, February, March), spring (April, May June), summer (July, August, September), fall (October, November, December). Then, seasonal means and standard deviations were calculated by using a search radius of 150 km, the smallest radius of influence employed in the objective analysis (discussed in more detail in Section 2.2), at each grid point. The depth dependence factor of the objective analysis scheme was also switched on in the calculation of the mean and the standard deviation at a grid point. Following the same $\pm 3\sigma$ criterion as the first statistical check, data points that fell outside the $\pm 3\sigma$ window around the mean were excluded from the database.

Approximately 35% of all the data extracted from the climatology database at

the BIO was rejected as a result of QC tests and bias-removal procedures. As the data had already been subjected to QC checks before being incorporated into the BIO climatology database, most of the data rejected in this study was not due to the additional QC test but rather the bias removal procedures.

2.2 Methodology

The method of analysis used here was originally developed for the spatial analysis of meteorological data, and later introduced into oceanographic problems by Bretherton et al. (1976). While these early studies were focused on developing better error estimates, the interest has shifted towards producing an analyzed value from the observations by suppressing the observational noise as much as possible and maximizing the signal (e.g. Levitus, 1982; deYoung et al., 1994). The next section is aimed at introducing the method of successive correction from this point of view. For a more comprehensive introduction to the subject, the reader is referred to Daley (1991).

2.2.1 Objective Analysis (OA)

The observations over a domain are unevenly distributed along cruise tracks, moorings and stations; however, numerical models require the input data to be specified on a regular grid. The same is true for the comparison of variables, and for

plotting the property fields. Therefore, interpolation of data from irregularly distributed observations onto regular grids is a common procedure, known as objective analysis.

There is no unique way to perform an objective analysis. The choice of an OA scheme is determined by the specifics of the problem, such as the data distribution, grid spacing, and geographical location. A variety of iterative OA schemes has been used in the North Atlantic. These studies include:

- The application of the original iterative difference-correction scheme employed in the Climatological Atlas of the World Ocean (Levitus, 1982; Levitus, 1994; Stephens et al., 2002; Boyer et al., 2002).

- Iterative difference-correction method with directionality (deYoung et al., 1994).

- Iterative difference-correction method with depth dependence (Reynaud et al., 1995).

In this study an iterative difference-correction OA scheme with depth dependence similar to Reynaud et al. (1995) is employed. The iterative difference-correction scheme with varying search radii was first developed by Cressman (1959). It starts with a first-guess field generated for every grid point. Then, the initial guess is corrected by the weighted mean of the differences between the guess value and all measurements within the radius of influence. The corrected value is then used as the

first-guess field for the next iteration. This whole process is repeated several times, decreasing the radius of influence with each iteration.

Starting with a large radius of influence and going towards smaller radii of influence enables gaps in the property fields to be filled progressively, by assigning large-scale averages to data-deficient grid points, and then adding small-scale details to them by decreasing the radius of influence.

A general formulation for this scheme is:

$$G_{i,j} = S_{guess_{i,j}} + C_{i,j} \tag{2.1}$$

where $G_{i,j}$ is the analyzed value, $S_{guess_{i,j}}$ is the first–guess, and $C_{i,j}$ is the correction value (weighted sum of observation increments):

$$C_{i,j} = \frac{\sum W_s Q_s}{\sum W_s} \tag{2.2}$$

where

$$Q_s = S_{guess} - S_i \tag{2.3}$$

and

$$W_s = 0 \qquad r > R \tag{2.4}$$

$$W_s = e^{-4(r^2/R^2)} \qquad r \leq R \qquad\qquad (2.5)$$

where r is the distance between the observation S_i and the grid point. The initial

guess, S_{guess}, is corrected by the weighted mean of the differences between that value

and all measurements S_i within the radius of influence, R. The form of the weighting

function used here was originally developed by Barnes (1964); it is iteration dependant

since it includes the search radius which is reduced progressively.

The iterations were repeated three times with radii of influence of 500 km, 300

km, and 150 km (except for the series of three-year long climatologies (triads) as

discussed in *Chapter* 5). The number of iterations and the radii of influence are

constrained by the data density and the horizontal grid resolution. The number of

observations available for this study is significantly larger than in previous Labrador

Sea climatologies; this explains the smaller radii of influence chosen here than in the

earlier studies (e.g. $R_1 = 1541$ km, $R_2 = 1211$ km, $R_3 = 881$ km, $R_4 = 771$ km in

Levitus (1982); $R_1 = 800$ km, $R_2 = 500$ km, $R_3 = 200$ km in Reynaud et al. (1995);

and $R_1 = 892$ km, $R_2 = 669$ km, $R_3 = 446$ km in World Ocean Atlas 2001 (Stephens

et al., 2002; Boyer et al., 2002).

Since the objective analysis scheme introduces a certain smoothing, no other

smoothing technique is applied between the iterations, except following the last it-

eration. Smoothing of the final product is carried out in a way consistent with the

modified objective analysis scheme; it was necessary to remove small-scale observational noise which would otherwise disturb the robustness of the climatological property fields.

The most commonly used approach to smoothing is to smooth the gridded data with the data from neighboring grid boxes. (Levitus, 1982; Lozier et al., 1995; Boyer et al., 2005). In this study, particular attention is given to directionality of the flow i.e. the tendency of the flow to follow constant f/h lines, where f is the Coriolis parameter and h is the total depth of the water column. This is not contradictory to using isopycnal coordinates in the vertical. A water parcel's position in the water column is determined by its density ($\sigma_\theta = \sigma(S, \theta, 0)$). By binning the data according to their density distribution in the vertical, an artificial mixing between different water masses is avoided. Topographic steering, on the other hand, influences the general circulation pattern and controls the water mass distribution in the lateral direction. Therefore, smoothing is performed preferentially along isobaths rather than across isobaths. This is achieved by invoking the depth-dependence criteria explained below.

The original iterative difference-correction method assumes that the problem is isotropic, and hence the radius of influence is the same in every direction. However, isotropy is not a valid assumption in this region. In reality, strong boundary currents and interior waters have very different temperature and salinity characteristics. Using information from different water masses in the calculation of a variable at a grid point

introduces unnecessary smoothing of that property. Avoiding this kind of "artificial" smoothing in an objective analysis scheme is important, in order to produce realistic representation of fronts and boundary currents. This can be achieved by including information from waters that have similar properties and by rejecting others.

There exists a strong relationship between water mass distribution and bathymetry; hence, an additional search criterion to include data only from a range of isobaths is suggested by Reynaud et al. (1995). Therefore, the spatial distance r is redefined as:

$$r = d + R\delta \tag{2.6}$$

where d is the real spatial distance between the observation and the grid point at a particular vertical level, and δ is defined by

$$\delta = 0 \quad if \quad |H - H_{obs}| \leq \Delta h \tag{2.7}$$

$$\delta = 1 \quad if \quad |H - H_{obs}| > \Delta h \tag{2.8}$$

where H is the ocean depth at the grid point and H_{obs} is the ocean depth at the data location.

The functional form of Δh has little significance compared to the values imposed by the depth criterion. Therefore, instead of the Gaussian function used in the

Reynaud (1994) study, a tailored polynomial function is used to define the range of

allowed depths for calculating the property values at a grid point:

$$\Delta h = 33x^3 + 90x^2 + 130x + 300 \qquad (2.9)$$

where x is defined as

$$x = \frac{H - 2000}{1200} \qquad (2.10)$$

The third-order polynomial function used to specify the depth-dependence cri-

terion (Δh) implies a larger value ($\sim$ 900 m) in the deep ocean and a smaller value ($\sim$

250 m) in coastal regions. The advantage of the new definition is that a larger range

of isobaths is allowed in the calculation of the correction term in deeper waters, where

data are scarce, compared to coastal regions, where the range of isobaths allowed in

the calculation is set to be narrower (Figure 2.3).
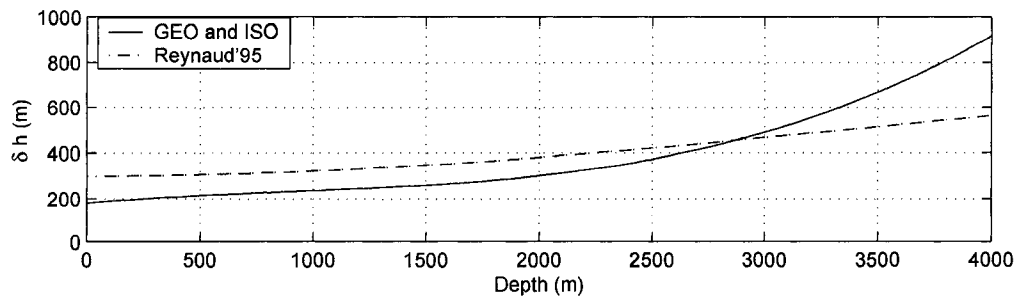
Figure 2.3: The functional form of the depth criterion used in our study versus Reynaud et al. (1995)

2.2.2 Diagnostic Calculations

The model used in the diagnostic calculations[3] is a version of the SPOM model developed by Myers (2002) to study ocean processes and ocean - climate interactions of the sub-polar north Atlantic ocean. The SPOM code is based on MOMA (Modular Ocean Model - Array), a variation of the (MOM) mode reconstructed to make use of array architecture (Webb, 1993).

The SPOM model is based on geopotential coordinates with 36 levels in the vertical. The bottom-most cell is partially filled following the work of Adcroft et al. (1997), which improves the representation of topography in the model. The horizontal resolution of the model is $1/3° \times 1/3°$, the same as in the climatology. Therefore, interpolation is not needed in the horizontal, but it is required in the vertical, where a simple linear interpolation scheme is used to deduce 36 vertical levels of model climatology from the original 44 geopotential levels.

The isopycnal climatology is converted, first, to 44 geopotential levels by using the pressure data, which were objectively mapped onto isopycnal surfaces, just as was done with the temperature and salinity data. This first interpolation is necessary in order to compare the two climatologies derived from almost the same data but on different vertical coordinates. The second step is to linearly interpolate the isopycnal

---

[3]The term "diagnostic calculation" refers to the case where the velocity field is calculated from the density field by an ocean general circulation model

climatology (which had been interpolated onto geopotential climate levels) onto 36 vertical model levels.

The SPOM model is set up for the whole North Atlantic region from 38° N to 70° N latitudes and from 67° W to the 0th meridian. However, the new climatologies cover only the northwestern portion of the North Atlantic, from 45°N to 70°N latitudes and from 70°W to 40°W longitudes. For the diagnostic runs, the newly compiled climatologies are merged with a climatology that covers the whole model domain. The temperature and salinity fields obtained from the GEO replaces the WOA-94 (Levitus, 1994) values in the northwestern North Atlantic. Similarly, the ISO replaces a modified version of the Lozier et al. (1995) climatology (Grey and Haines, 1999) within our study domain. The merge creates a discontinuity of temperature and salinity values at the boundaries of the study area, across 45°N latitude and 40°W longitude.

A few different methods have been tried for the merging of the two climatologies: GEO with WOA-94 climatology, which was originally compiled on geopotential surfaces; and ISO with the isopycnally-compiled Lozier et al. (1995) climatology. It is concluded that the data mismatch at the merge line did not affect the velocity calculations further than three grid points away from this line. Therefore, for the diagnostic calculations, it was deemed sufficient to replace all temperature and salinity values with the ones calculated from the GEO and ISO climatologies within our

study domain.

In the diagnostic mode of SPOM, the salinity and temperature fields, which are used to calculate density, are not allowed to evolve; instead, the salinity and temperature fields are set back to the climatological values after each time step. The diagnostic runs start from an ocean-at-rest. Horizontal velocities, $\vec{u}$ and $\vec{v}$, and surface pressure are integrated at every time step. The winds are turned off during the diagnostic runs as their effect on the water column is indirectly included in the climatological temperature and salinity distributions based on observations.

When the model is run in the diagnostic mode, the total energy reaches a quasi-steady state in about one month. The diagnostic runs use two time steps, one to resolve fast surface gravity waves ($30s$) and another for the baroclinic part ($1800s$) as in the prognostic mode.

Chapter 3

Climatology

The following discussion is aimed at providing a basis for the evaluation of the newly built climatologies. First, an overview of the Labrador Sea hydrography as obtained from the ISO climatology is presented (*Section* 3.1). The ISO climatology is the preferred climatology since it preserves a higher degree of detail in property maps. It also produces more realistic flow fields when used in diagnostic calculations, as compared to the GEO climatology. The foundation for favouring the ISO over GEO is set through the discussion of hydrographic and diagnostic results in *Section* 3.2. The conclusion is reached in *Section* 3.3, after a thorough investigation of the strengths and weaknesses of ISO and GEO. In *Section* 3.4, ISO and GEO are compared to some of the existing climatologies in order to highlight the improvements achieved in these new climatologies.

The key points covered in this chapter are:

[i] The effects of including topographic information in the objective analysis process

[ii] The advantage of isopycnal surfaces over geopotential levels

[iii] The use of a diagnostic tool to calculate dynamic properties of the basin from a climatology.

Most importantly, the yearly climatology discussed here provides the groundwork for the interpretation of seasonal and inter-annual variability in the following chapters.

3.1 Labrador Sea Climatology (1910-2000)

Climatological temperature[1] and salinity fields were compiled by mapping the data collected between 1910 and 2000 with a depth-dependent iterative correction scheme on isopycnal surfaces (ISO). In this section, the results from the ISO climatology are discussed. The vertical cross-sections of temperature and salinity along a frequently visited oceanic line, AR7W of the WOCE program, are presented in Figure

---

[1]all temperatures reported in this chapter and following chapters are "potential temperatures", unless otherwise noted.

3.1. This line traverses the Labrador Sea diagonally from the Labrador coast to the Greenland coast (*see* Figure 1.2 for its location).

In the central Labrador Sea density surfaces located in the vicinity of the sea surface are domed upwards, in accordance with the large-scale requirement for deep convection (Clarke and Gascard, 1983). This basin-scale cyclonic circulation is set up by the large scale wind field and hence it is associated with the surface Ekman forcing.

Beneath the surface waters, there is a thick lens of water with weak stratification, roughly between the 27.65 and 27.80 σ_θ density surfaces, part of which is filled with the convectively formed LSW ($27.74 \leq \sigma_\theta < 27.80$). The two density classes, which are found below the LSW, are the GFZW and the DSOW. They are formed in other parts of the North Atlantic. They enter the basin from the East, circulate cyclonically around the basin and exit from the Southeast.

There is a strong relationship between the flow structure and property distributions over the Labrador Sea. The basic elements of the Labrador Sea circulation, such as its boundary currents (fresh and cold) near the surface, weakly stratified LSW (relatively warmer and saltier), and DWBC at depth are distinguished by their temperature and salinity signatures in Figure 3.1.

The surface boundary currents, the WGC on the Greenland side and the LC on the Labrador side, form sharp fronts with the denser water masses of the central
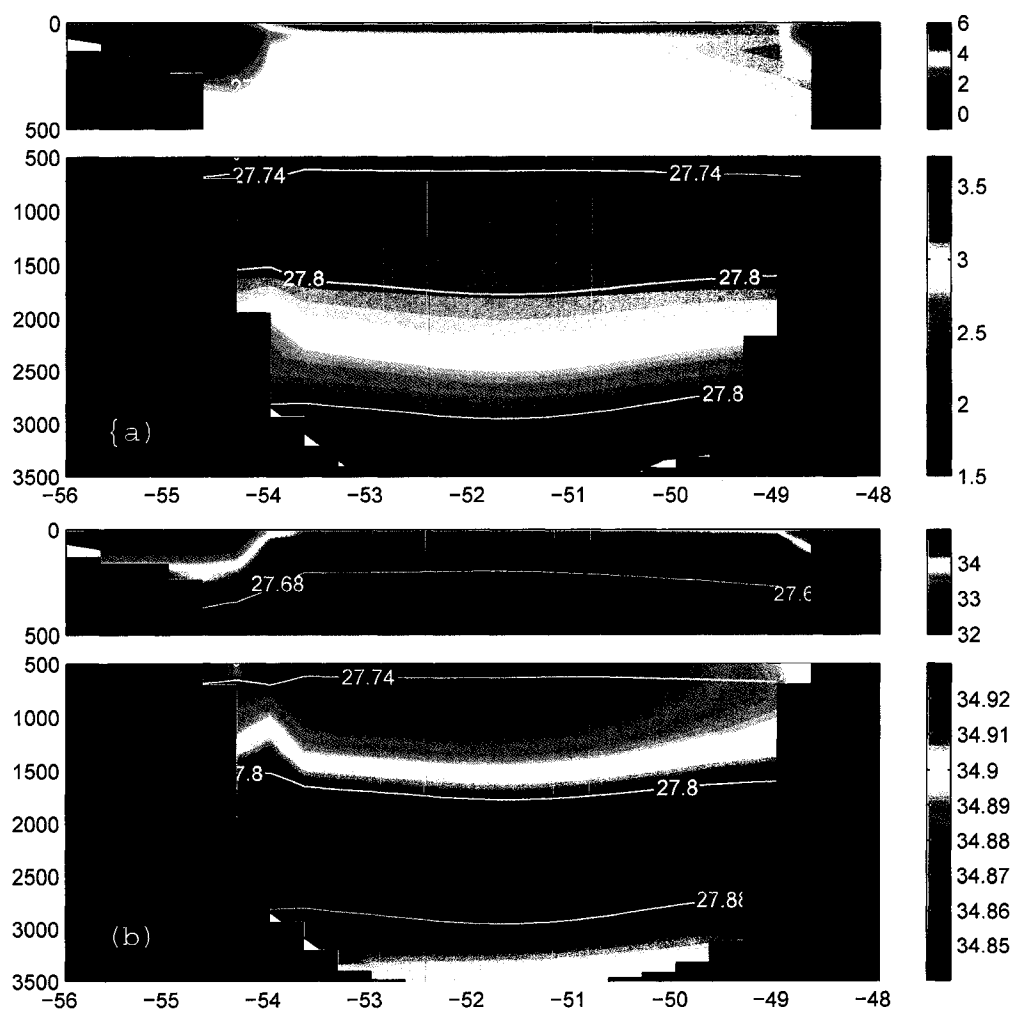
Figure 3.1: A high resolution map of (a) temperature and (b) salinity fields along the AR7W cross-section. Labrador is on the left and Greenland is on the right hand side of the figure. White contour lines are the σ_θ surfaces that separate the major water masses, uLSW, cLSW, GFZW, and DSOW. Note that the top $500m$ of the water column exhibits large temperature and salinity gradients in the lateral direction, hence drawn in a separate panel. The temperature and salinity range decreases as depth increases. However, since the GEO and ISO climatologies achieve high spatial resolution, various deep water masses can be visually identified in these figures. Also see Table 3.1 for temperature and salinity records taken from this figure.

Labrador Sea, which can be identified by the strong temperature and salinity gradients in the top $500m$. The DWBC is identified by a salinity maximum at about $2400m$ off Labrador. High salinity water around this depth can be identified as the GFZW and the fresher water underneath as the DSOW. The GFZW and DSOW make up the lower part of DWBC, while a portion of LSW forms the upper limb of the DWBC, as these three water masses are advected further south. Climatological temperature and salinity of some the major water masses are listed in Table 3.1.

Table 3.1: Climatological temperature and salinity values for frequently-cited water masses at various locations along the AR7W diagonal transect in the Labrador Sea. Please note that the values given in the table are chosen to represent not the mean temperature and salinity of a specific water mass but their local extremes at a certain depth.

Water Mass	T ($°C$)	S
WGC (at $30m$)	1.16	32.36
LC[1] (at $80m$)	-0.80	32.98
LC[2] (at $80m$)	-0.43	33.18
IW (off Greenland at $140m$)	4.21	34.82
IW (off Labrador at $500m$)	3.69	34.84
LSW (central Labrador Sea at $1300m$)	3.20	34.89
GFZW (off Greenland at $2300m$)	2.67	34.93[3]
GFZW (off Labrador at $2400m$)	2.82	34.93[3]
DSOW (off Greenland at $3400m$)	1.36	34.90[4]
DSOW (off Labrador at $3400m$)	1.58	34.90[4]

[1]Inside the subsurface cold-layer
[2]Offshore of the subsurface cold-layer
[3]The salinity difference between off Greenland and off Labrador is 8 per thousand.
[4]The salinity difference between off Greenland and off Labrador is 4 per thousand.

As the water masses are advected in and out of the Labrador Sea they are mixed with ambient water masses with varying temperature and salinity characteristics. The differences in water properties between the Greenland and Labrador side of the basin (Table 3.1) are due to the diffusion and mixing that these transient water masses experience along their trajectories.

3.2 Combined Results: Hydrography and Dynamics

So far, only the hydrography of the Labrador Sea as obtained from the ISO climatology has been presented. In the following sections, links between the hydrography and circulation are investigated. Current velocities are calculated from the climatological density fields using a diagnostic model. The results are discussed in two vertical levels: surface and intermediate to deep water masses. In addition, the volume, heat and freshwater exchanges between the Arctic Ocean and the Labrador Sea through the Canadian Archipelago are discussed. Hydrographic and dynamic results from the GEO climatology are included as well as the ISO climatology, wherever relevant, in order to compare the two methods.

3.2.1   Surface and Near-Surface Waters

The salinity and temperature fields at 30 metres (Figure 3.2) represent the near surface water mass distribution. The EGC is only partially resolved in this study; however, its climatological salinity and temperature near the southern tip of Greenland are ~32.2 and ~1°C, respectively. The low salinity and temperature of the EGC create a strong gradient with the higher salinity (>34.8) and temperature of the (>5°C) IW offshore.

To the west of Cape Farewell, the boundary current that flows northwestward along the western bank of Greenland is called the WGC. The WGC is described as a mixture of the EGC and IW that has slightly higher salinity and temperature properties than those of the EGC (Clarke, 1984). In this analysis, the mean annual salinity and temperature properties of the EGC and the WGC are found to be almost the same (~32.3 and ~1.2°C for WGC). These salinity and temperature values are less than the ones reported in the Reynaud climatology (Reynaud, 1994) and closer to the observed values in Clarke (1984). The WGC seems to be getting saltier and warmer as it progresses northwestward, with a salinity of ~33 and a temperature of ~2.5°C at ~65°N. However this increase is more likely to be caused by the bias towards summertime observations than by physical effects.

An area of significant exchange between the WGC and the interior Labrador Sea water masses is evident from the temperature field (Figure 3.2) between the latitudes
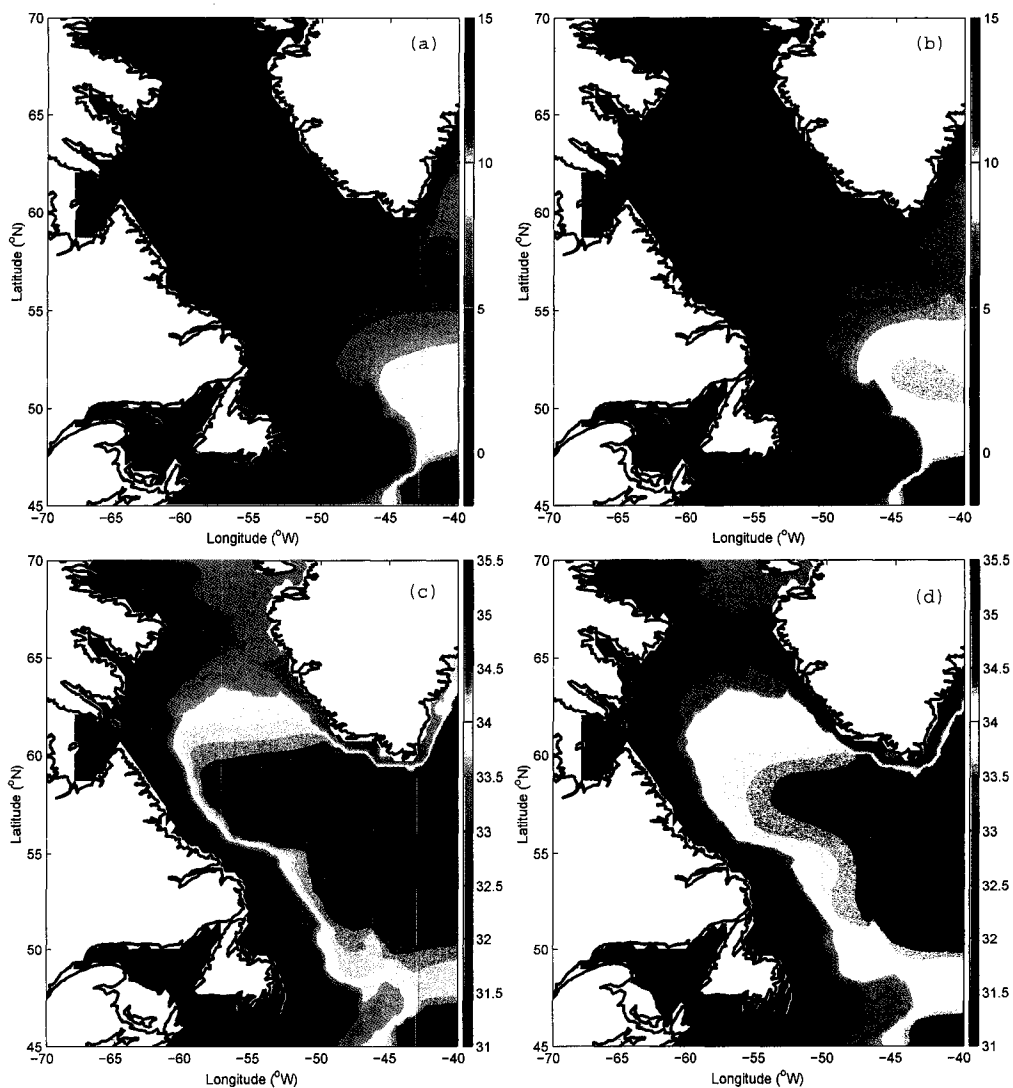
Figure 3.2: Temperature (a,b) and salinity (c,d) fields at 30 metres as computed from the GEO (a,c) and ISO (b,d) climatology.

of 61°N and 63°N, where persistent eddy activity is reported (e.g. Cuny et al., 2002; Eden and Böning, 2002; Fratantoni, 2001). A climatology can not represent an eddy

field; however, when proper measures are taken to avoid over-smoothing and the elimination of the natural variability, as in this case, one would expect the results of intense mixing to be preserved in the climatology.

A salinity and temperature cross section along 60.3°N (Figure 3.3) reveals the vertical flow structure and the steep density gradient that exist between the cold/fresh WGC and the adjacent warm/salty IW, which are brought into the region by the IC. The density gradient between the two water masses is maintained during the objective mapping due to two factors, each of which avoids excessive smoothing. The first factor is the smaller range of depths over which the correction term is calculated. This separates the relatively warmer and saltier waters offshore from the cold and fresh WGC, which flows over the continental shelf and slope. The second factor is the use of isopycnal coordinates in the vertical, which is discussed in more detail in *Section 3.4*.

It is well documented in the literature (e.g. Clarke, 1984; Cuny et al., 2002) that IW enters the Labrador Sea from the East and exits to the south after circulating around the basin cyclonically. This subsurface circulation can be seen in Figures 3.1a and 3.3 as a temperature maximum ($> 4°C$) at $\sim 150m$, on the Greenland side when it enters the Labrador Sea, and at $\sim 200m$, on the Labrador side, as it deepens along its path in order to maintain its neutral density surface in the water column. In Figure 3.3, the upper bound of this water mass coincides with the 27.6 σ_θ surface in

the interior Labrador Sea and it becomes slightly less (more) dense on the Greenland

(Labrador) side. Further south (around 55 °N, on the Labrador side), the subsurface

temperature maximum associated with the IW is found roughly between the 27.68

and 27.74 σ_θ surfaces at about $\sim 400m$ (Figure 3.1a). Changes in the properties of

the IW suggest mixing along its path.

The maximum current velocities are found over the offshore end of the steepest

topography and, coincidentally, next to the steepest lateral density gradients near the

surface (e.g. Figures 3.4, 3.5, and 3.6). Recent studies (e.g. Lilly et al., 2003; Straneo,

2006) on the heat balance of the interior Labrador Sea have shown the importance of

the IW as a heat source. Straneo (2006) showed that without the lateral heat supply,

it would be impossible to sustain the deep convection. Since the deep convection is

initiated by a large heat exchange between the ocean and the atmosphere (Marshall

and Schott, 1999), it requires an additional heat source for the restratification of the

water column, soon after an episode of convective mixing.

Lilly et al. (2003) showed that the Greenland eddies might be responsible for the

speedy restratification of the water column. Eddies have been observed around Cape

Desolation where the topographic slope changes rapidly. Interactions between high-

speed currents (approaching $30cm/s$ in Figure 3.4b near the Greenland coast) and

the rapidly changing topographic slope create boundary current instabilities leading

to the shedding of eddies (e.g. Katsman et al., 2004; Spall, 2004). While the warm
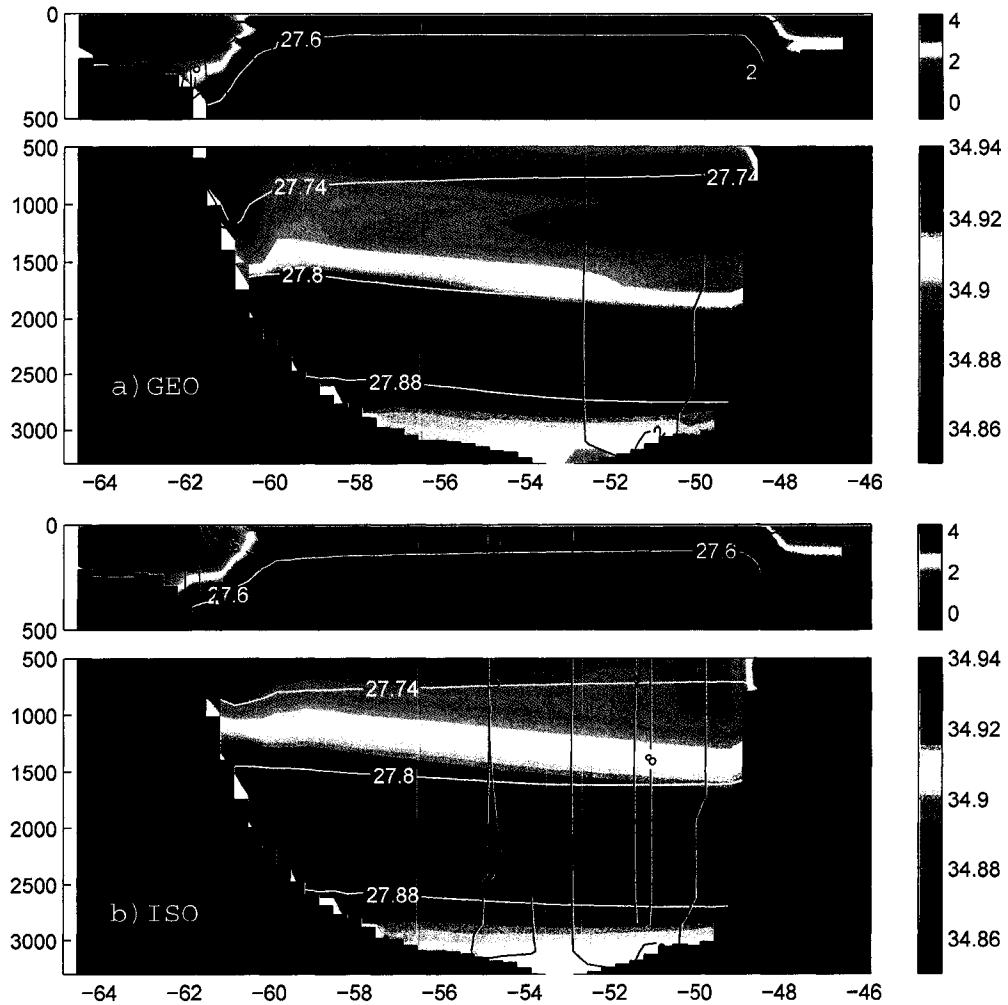
Figure 3.3: Property maps along 60.3°N line overlaid with the potential density contours (white) and velocity contours across this transect (black). (a) for GEO, and (b) for ISO climatology.

IW just below the surface (150 − 700m in Cuny et al. (2002); Lazier et al. (2002); and as seen in Figure 3.1a) is the primary source of heat for the interior Labrador Sea after a deep convection episode (Straneo, 2006), cold and fresh surface waters of the

WGC and LC control the freshening and cooling of the interior waters, as discussed

in Lazier (1980). In this study, the robustness of the freshwater and heat budgets of

the interior depends strongly on the accuracy of the property distribution obtained

from the climatology and the current velocities calculated from it.
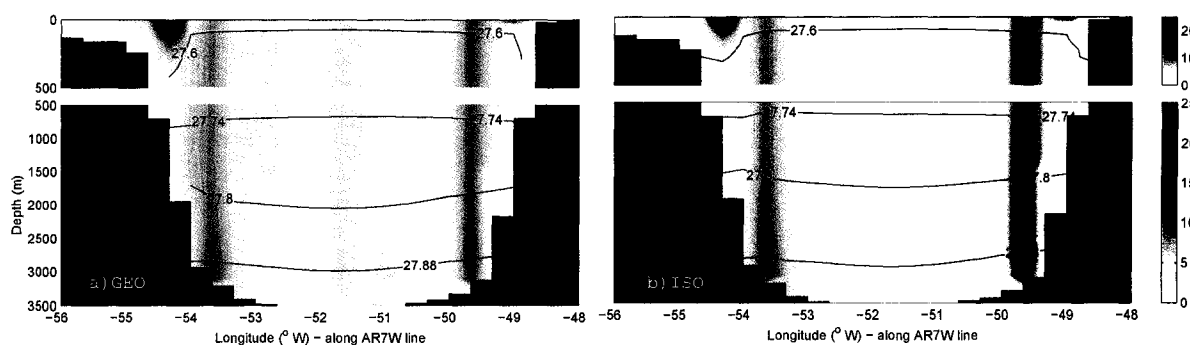
Figure 3.4: Current speeds across the AR7W line calculated from the (a) GEO and (b) ISO climatology. Black contours are the selected potential density surfaces.

Intense mixing between inshore and offshore water masses around Cape Deso-

lation is evident in the temperature and salinity maps obtained from the ISO clima-

tology (Figure 3.2b and d); this location agrees well with the map of eddy kinetic

energy deduced from the surface drifters in Cuny et al. (2002) (their Figure 7). Al-

though the spatial and temporal resolution of this study is not adequate to resolve

heat flux to the interior by the IW eddies, high-speed currents calculated from the

GEO and ISO climatologies near Cape Desolation (Figure 3.4) are in agreement with

the aforementioned studies.
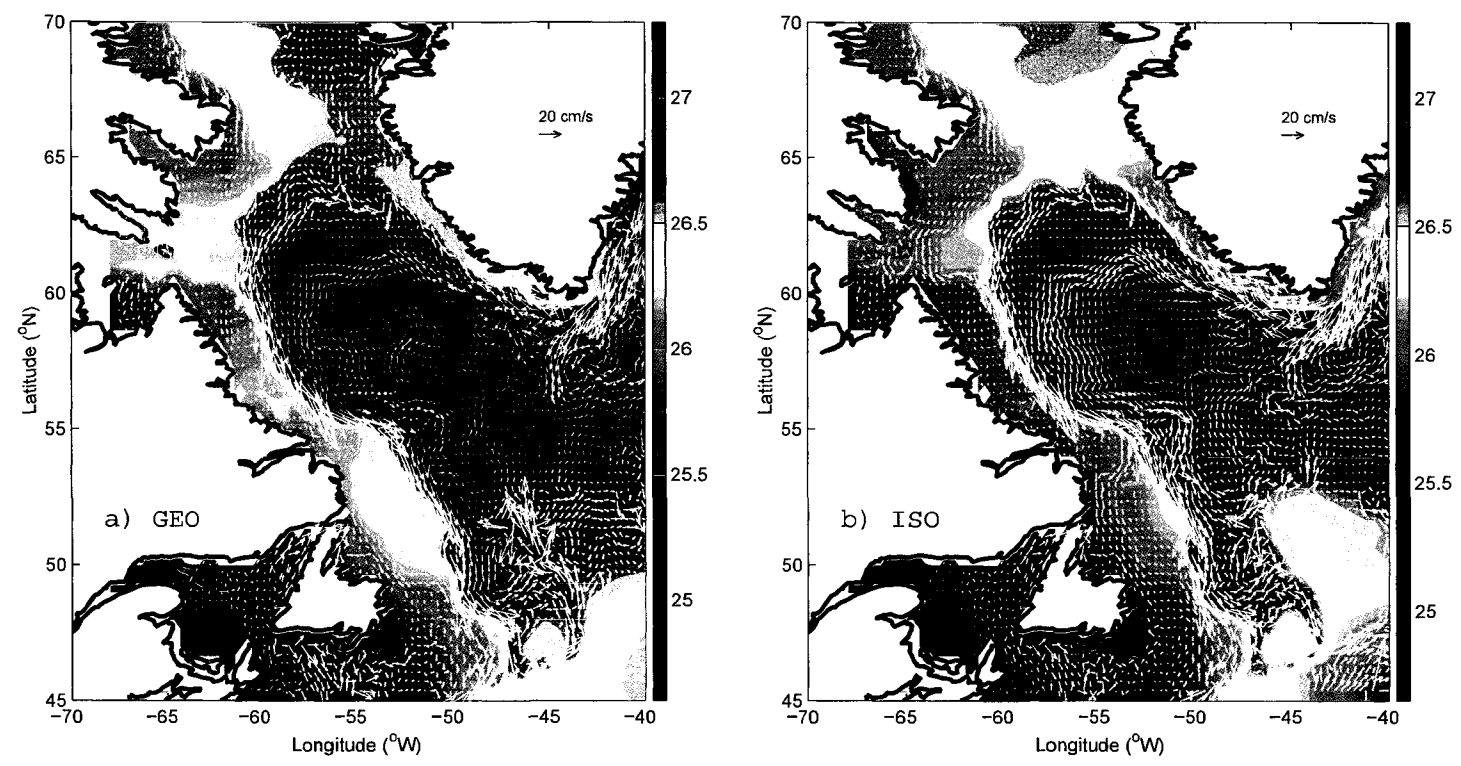
Figure 3.5: Density field obtained from the (a) GEO and (b) ISO climatologies at $30m$, overlaid with velocity vectors calculated from the diagnostic model.

Figure 3.5 shows the velocity vectors overlaid on the density field at $30m$. The bifurcation of the WGC around 60°N, near Cape Desolation, is one of the features well captured by the diagnostic calculations. Even though the diagnostic velocities calculated from the GEO and ISO climatology show good agreement on the fundamentals of the flow field, there are some subtle but important differences between the two methods, which are discussed later on in this chapter. Here is a list of near-surface (at $30m$) flow characteristics, which are adequately demonstrated by the current climatologies:

[i] The WGC and LC represented as narrow boundary currents circulating cyclonically around the Labrador Sea, concentrated over the strong density gradient created between the fresh and cold shelf waters and the warmer and saltier interior waters.

[ii] Bifurcation of the WGC at about 60 °N.

[iii] Separation of the LC to the south of Hamilton Bank.

[iv] Evidence of the NAC and IW influencing the interior Labrador Sea (better represented with the ISO based results than with GEO)

The southernmost cross-sectional property map along 52.7°N (Figure 3.6b) shows a subsurface temperature minimum at $\approx 80m$, with a temperature of $\approx$ -1.2°C, whereas the minimum temperature for the LC along the northern transect is

~0.5°C. The subsurface minimum-temperature layer along the Labrador current and its north-south polarity are linked to local sea-ice formation and melting processes, which are discussed in detail by Colbourne and Mertz (1998).
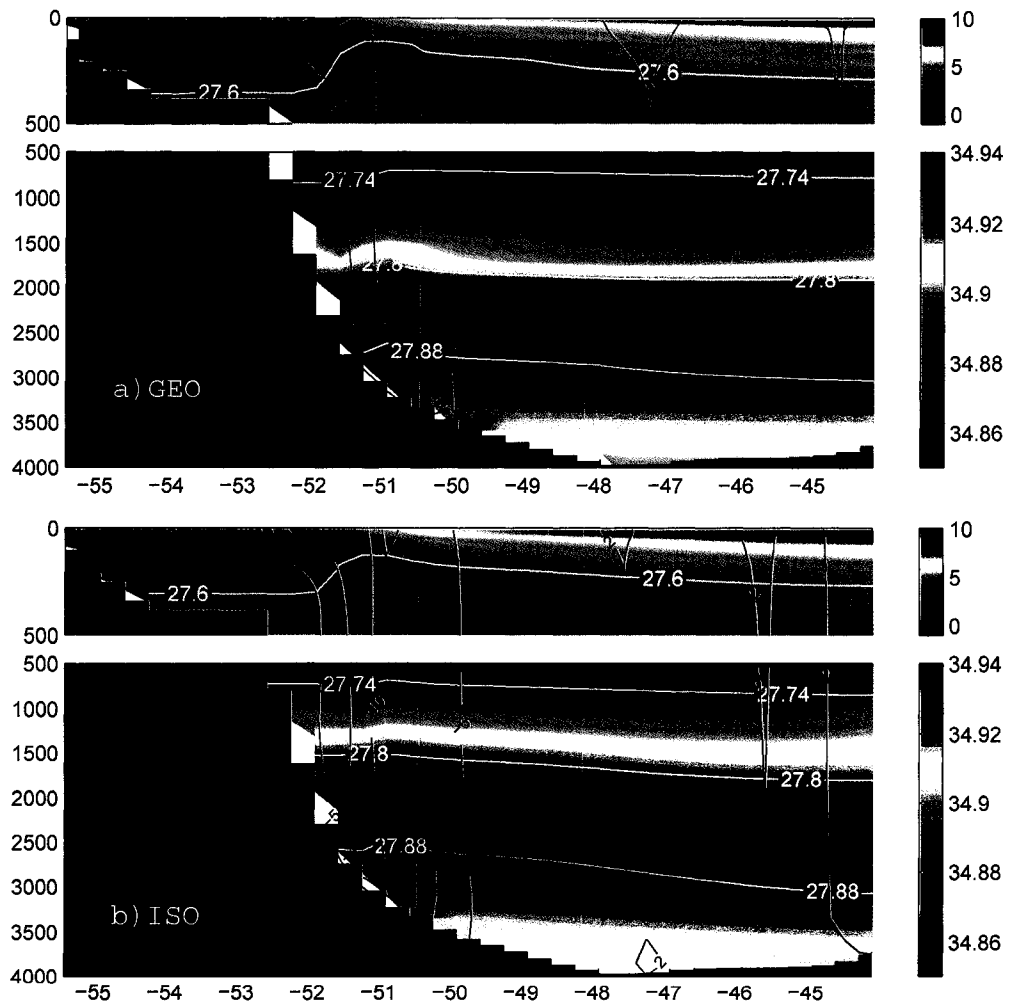
Figure 3.6: Property maps along 52.7°N line overlaid with the potential density contours (white) and velocity contours across this transect (black): (a) for GEO, and (b) for ISO climatology.

The two branches of the LC to the south of Hamilton Bank are described by Lazier and Wright (1993) and can be identified in Figure 3.6. The offshore branch is mainly barotropic, with an average southward velocity of $10cm/s$ throughout the water column and centred over the $2500m$ isobath as described by Lazier and Wright (1993). The baroclinic component of the LC is concentrated in the top $200m$ or so and is located inshore of the barotropic component.

The mean salinity of the LC (≈ 33.7) is slightly less than that of the WGC (≈ 34.2). Because of the wider continental shelf over which it flows, the LC carries a larger volume of freshwater. Mean water properties of the LC and WGC, including their freshwater and heat contents are summarized in section 3.4 Table 3.3 and 3.4. Below this fresh and cold boundary current, a salinity maximum is observed centred at around $450m$. This maximum is caused by the IW that enters the Labrador basin from the east on the Greenland side at $\approx 150m$, crosses 60°N southward at $\approx 200m$, and is found at $\approx 500m$ at 55°N (and 54.5°W, in Figure 3.1). The IW can be seen as a subsurface temperature maximum in the cross-sectional plots.

3.2.2 Intermediate to Deep Waters

Intermediate depths of the Labrador Sea are filled primarily by the LSW. Mean temperature and salinity values for the LSW are found to be $\approx 3.2°C$ and ≈ 34.89 from ISO; between the potential density surfaces of 27.74 and 27.80 (Figure 3.1). These

property values compare well with the range of salinity and temperature properties attributed to the LSW over the years (e.g. 3.4°C and 34.89 by Lazier, 1973 and 2.8°C and 34.89 by Clarke and Gascard, 1983).

By limiting the LSW to waters with potential densities less than 27.80, the climatological maximum of the LSW depth appears to be approximately 1700m. This lower limit for the LSW depth provides an adequate estimate for and agrees well with the average depth of deep convection noted in Lilly et al. (1999). Direct observations performed in the first half of the 1990s suggest that, when conditions are favourable, deep convection can reach depths greater than 2000m (Lazier et al., 2002, e.g.). On the other hand, weak convection episodes (Lazier, 1980, e.g.) are also included in the climatology, bringing the climatological mean of the maximum depth of deep convection to an intermediate value.

As shown by Talley and McCartney (1982) Potential Vorticity (PV), which is defined as

$$PV = \frac{f}{\rho} \frac{\Delta\rho}{\Delta z} \tag{3.1}$$

can be used as a dynamical tracer to follow the dispersal of the LSW. The LSW causes a minimum in the potential vorticity of the water column due to its weak stratification. The depth at which the potential vorticity minimum is observed seems to be $\approx 1800m$ in the Labrador Sea, with depths exceeding 1800m near the centre of

the formation region (Figure 3.7). These values agree well with the range given by

Talley and McCartney (1982) (500 − 2000m).
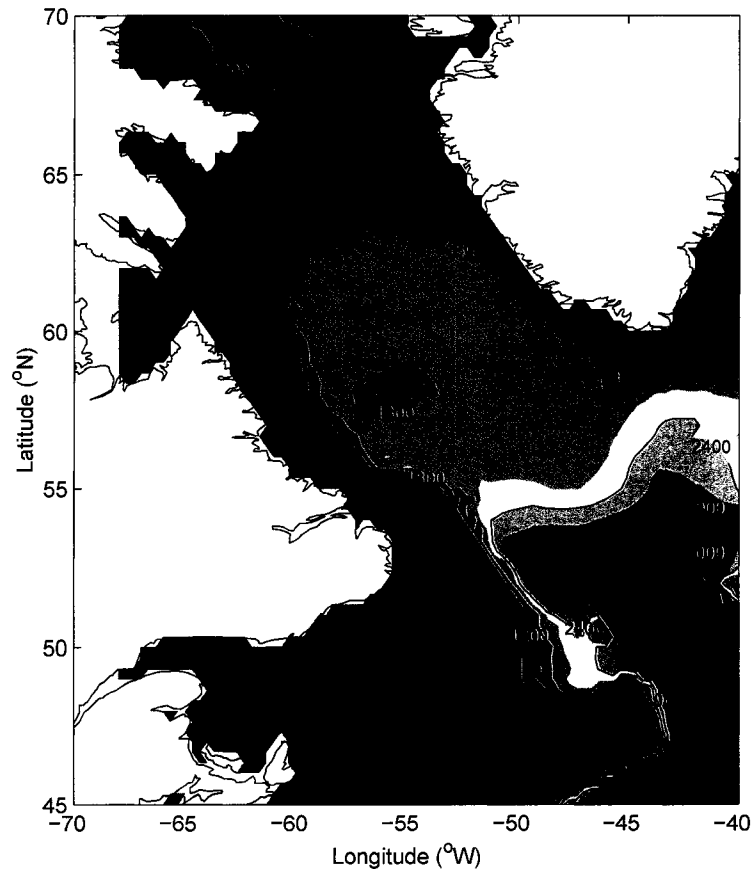
Figure 3.7: A contour map of the depth at which the minimum in PV (potential vorticity) is found. Black contours represent: 1200, 1800, 2400, and 3000m.

The advection of the LSW to the south via the DWBC occurs in a very narrow

channel (Figure 3.7). The eastern pathway which links the LSW to the eastern North

Atlantic directly is also visible in this figure. However the third pathway to the south first and then east under the NAC, as mentioned in Talley and McCartney (1982), is obscured by the inflow of NAC at the northwest corner and further north.

Another way of tracing the LSW is to look at the property distribution on its associated potential density surface, $\sigma_\theta = 27.77$, which can be presumed to be the climatological core density. The isopycnal averaging prevents unrealistic mixing of different water masses and their salinity and temperature characteristics; therefore, one can expect that the pathways of the LSW should be seen on the property maps plotted on this density surface (Figure 3.8).

The climatological property maps along the AR7W (Figure 3.1) line show that the interior basin below 1700 m is filled with waters that originate in the northeastern Atlantic Ocean. The GFZW, the lighter component of DWBC, enters the Labrador Sea at a depth slightly shallower ($2300m$) than the depth at which it exits ($2400m$). The salinity maximum caused by the GFZW at this depth can be seen hugging the Labrador rise and extending towards the interior with a salinity of ≈ 34.93 (Figure 3.6b).

The DSOW ($\sigma_\theta > 27.88$), the denser component of the DWBC, is found to be fresher (34.91) but colder (1.7°C) than the GFZW and fills the bottom of the Labrador Sea (Figure 3.1 and 3.6). A freshening trend in both of the GFZW and DSOW, which make up the lower limb of the DWBC has been observed for the period between the
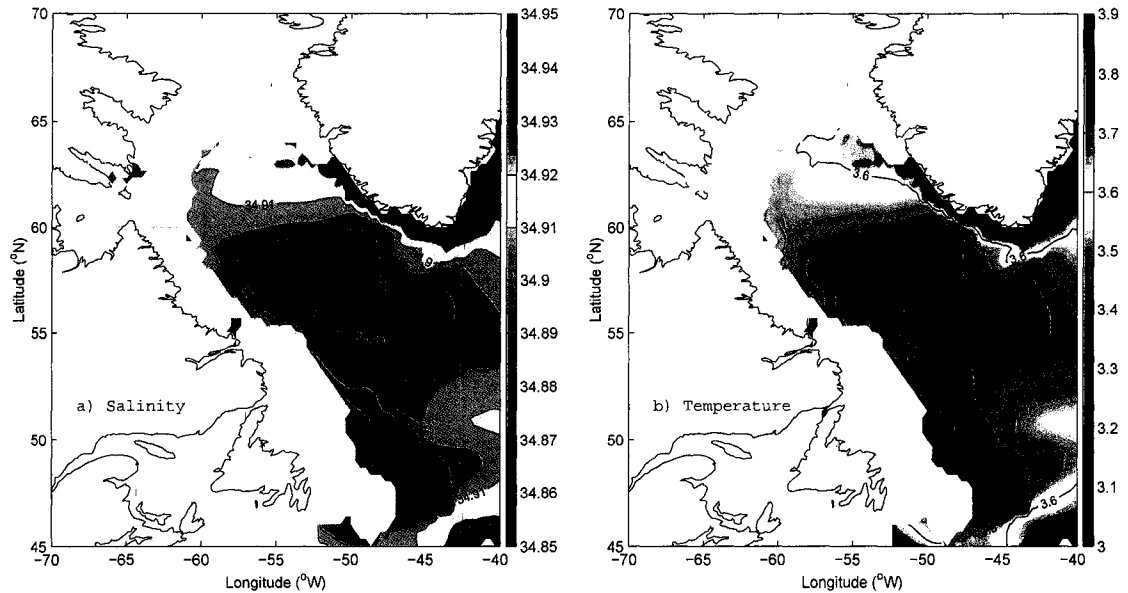
Figure 3.8: (a) Salinity and (b) temperature field plotted directly from the ISO climatology. The property maps shown here are the average of isopycnal surfaces 37 $(\sigma_\theta = 27.74 - 27.77)$ and 38 $(\sigma_\theta = = 27.77 - 27.80)$ from the Table 2.2. These surfaces correspond to the uLSW and cLSW, respectively.

early 1960s and the late 1990s (Dickson et al., 2002). The salinity of the deep water masses in the Labrador Sea fluctuated between 34.95 and 34.90 for the GFZW, and between 34.91 and 34.88 for the DSOW over this period.

The climatological salinity of deeper water masses (GEO and ISO) is in better agreement with the salinity observed before the recent freshening of deep water masses. The freshening of deeper water masses in the latter half of the 20th century seems to be a significant deviation from the 91-year mean (see Chapter 5 for further discussion on inter-annual variability).

The cyclonic circulation of the DWBC at $2400m$ as calculated from the diagnostic density field (σ_θ referenced to $0m$) is shown in Figure 3.9. The flow field calculated from the GEO and the ISO climatologies depicts the flow of DWBC, concentrated over the $3000m$ isobath, through the Labrador basin reasonably well. However, the DWBC is stronger ($\approx 20cm/s$) and the density is lighter ($\Delta\ \sigma_\theta \approx 0.03$) in the ISO case than the GEO. Differences such as these are discussed in *Section* 3.3, where the strengths and weaknesses of the ISO and GEO methods are discussed.
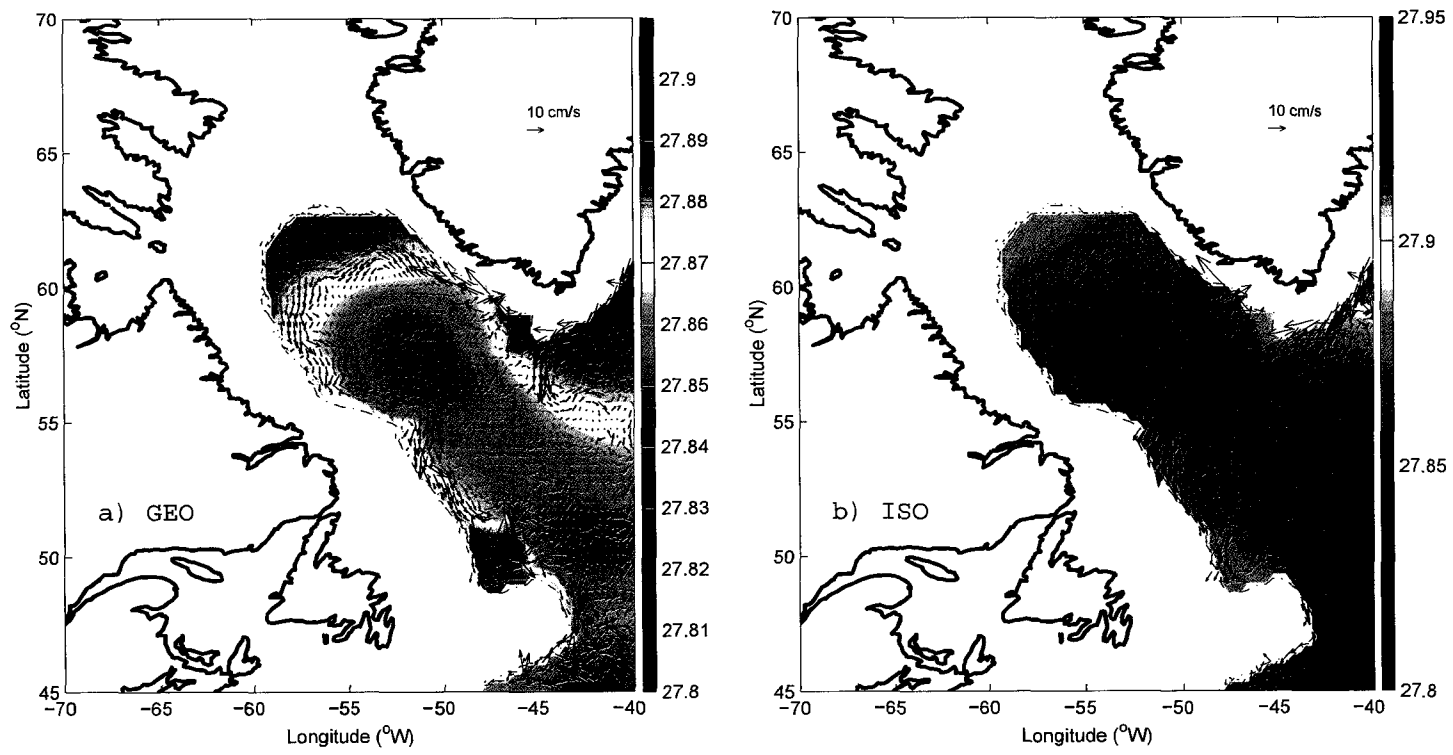
Figure 3.9: Density field obtained from the (a) GEO and (b) ISO climatologies at $2400m$, overlaid with velocity vectors calculated from the diagnostic model.

3.2.3 Northern Labrador Sea

To the north, the Labrador Sea is connected to the Arctic through the relatively

narrow and shallow Davis Strait, which provides a limited exchange of sea ice and

freshwater. Here, only the climatological properties of the waters crossing the Davis

channel and the current velocities at its southern exit are examined (Figure 3.10).
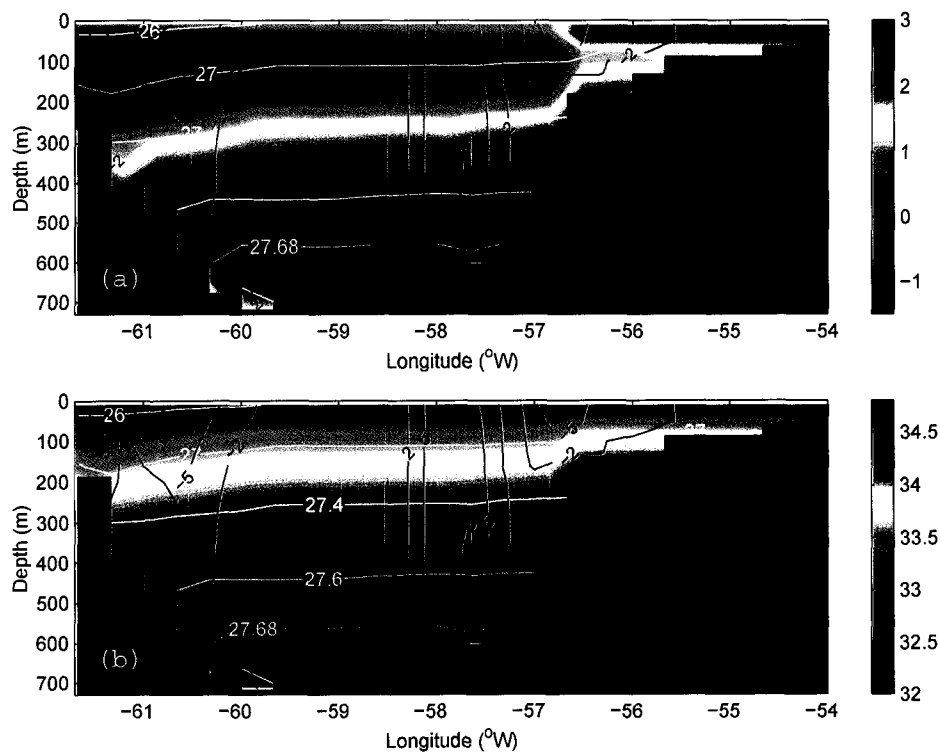
Figure 3.10: (a) Temperature and (b) salinity cross-section along 66.3°N line from the ISO climatology with black contours showing the diagnostic velocity calculation. Velocity contours shown are: -5, -2, 2, 5, and $8cm/s$.

The surface waters off Baffin Island are fresher ($\approx$ 32.5) and colder ($-1.4°$C) as their origin is the Arctic Ocean. They flow southwards towards the Labrador Sea through the Canadian Archipelago with velocities of up to $10cm/s$ at $66.3°$N (Figure 3.10).

The continental shelf is much wider on the Greenland side, extending about $150km$ offshore. This shallow area is covered by ice during most of the year, as is the rest of Davis Strait, which is about $700m$ deep at its deepest point. However, over the continental shelf, only a very short period in summer is suitable for ship-based observations; therefore, the data are unavoidably biased towards summer temperature and salinity values. Unexpectedly high temperatures ($\approx$ 2.5 °C) seen over the continental shelf next to the Greenland coast (between 54 and 57 °W longitudes in Figure 3.10a) are due to this bias. The front created between the slope and summer-biased shelf observations results in a strong southward flow, which is not realistic.

On the other hand, the diagnostic velocity calculations represent the northward branch of the WGC, which can be observed as the deep-reaching northerly flow between 57 and 58°30' W longitudes in Figure 3.10. The climatological speed of the northern branch of the WGC reaches up to $8cm/s$ around $57.7°$W and $66.3°$N. Higher WGC velocities are found closer to the bottom than the surface, in agreement with an ice-covered, stagnant, near-surface layer during most of the year.

The long-term mean volume, heat, and freshwater exchange between the Arctic

Ocean and the Labrador Sea through Davis Strait is summarized in Table 3.2. The heat and freshwater fluxes across a vertical cross-section are calculated according to Equations 3.2 and 3.3, respectively. The integration is carried out from the surface down to a depth of z.

$$Q_H = c_p \rho_o \int_0^z (T - T_r) \vec{v} \cdot d\vec{A} \tag{3.2}$$

where c_p=4000J/kg°C is the specific heat of water; ρ=1000 kgm^{-3} is the reference density; A is the surface area of the grid cell; v is the velocity at that grid cell calculated from the diagnostic model; T is the climatological temperature; and T_r=0°C is the reference temperature.

$$Q_{FW} = \int_0^z (\frac{S_r - S}{S_r}) \vec{v} \cdot d\vec{A} \tag{3.3}$$

where A is surface area of the grid cell along the vertical transect; v is the velocity at that grid cell calculated from the diagnostic model; S is the climatological salinity; and S_r=35 is the reference salinity.

The reference salinity is set to 35, a value greater than the salinity of all water masses in the Labrador Sea. This choice assures that the sign of the freshwater flux is determined only by the directionality of the flow.

Following the Cartesian coordinate sign convention, northward (y), eastward (x), and upward (z) fluxes are positive. According to Table 3.2, the total volume

flux is to the south in the top $300m$ of the water column, and to the north when the volume flux is integrated over the entire water column. This is because of the strong northerly WGC found near the bottom of the channel off the Greenland shelf. The high velocities calculated by the diagnostic model are probably due to the narrowing of the channel at this location (Figure 3.10).

Depth Range (m)	Volume Flux (mSv)	FW Flux (mSv)	Heat Flux(GW)
0-300 m	-485.0 (-399.2)	-36.2 (-31.9)	1,810 (2,516)
Entire	21.2 (107.0)	-31.7 (-27.4)	7,720 (8.426)

Table 3.2: Volume, freshwater, and heat fluxes across the 66.3°N line. The numbers in bracket indicate the fluxes obtained by excluding the large continental shelf off the Greenland Coast. Reference salinity is set to 35 and reference temperature is set 0°C in freshwater flux and heat flux calculations, respectively.

3.3 Justification of the choice of the isopycnal climatology over the geopotential climatology

In this section, the results from GEO and ISO are compared to each other, and their relative strengths and weaknesses are discussed. To allow a common base between the climatologies, the ISO climatology is converted into geopotential coordinates first. This conversion is also necessary since the diagnostic model employs geopotential coordinates in the vertical. The conversion from isopycnals to isobars is

carried out by interpolating temperature and salinity in the vertical with the help of the pressure field, which has been objectively mapped on isopycnal surfaces. At every grid point, the vertical profiles of temperature and salinity are linearly interpolated onto the isobaric levels used in GEO to make the two climatologies compatible for the comparison.

To begin the comparison, some of the important water properties averaged over the three key regions (see the map in Figure 1.2 for the location of the LC, WGC, and Interior) are presented in Table 3.3 and 3.4. In these tables, the heat and freshwater content of the water column from the surface of the ocean down to a depth of "z" is calculated according to the following formulae:

$$H = c_p \rho_o \int_0^z (T - T_r)dV \qquad (3.4)$$

where c_p=4000J/kg°C is the specific heat of water; ρ=1000 kgm^{-3} is the reference density; V is the volume; T is the climatological temperature; and T_r=0°C is the reference temperature.

$$FW = \int_0^z \frac{S_r - S}{S_r}dV \qquad (3.5)$$

where V is the volume; S is the climatological salinity; and S_r=35 is the reference salinity.

In ISO, the average water temperatures (salinities) are slightly higher (lower)

Depth Range (m)	Region	S_{mean}	T_{mean} (°C)	σ_θ	$\Sigma FW(m^3)$	$\Sigma H(GJ)$
0-300	LC	33.84	1.61	27.07	2.1×10^{12}	4.1×10^{11}
	WGC	34.31	3.17	27.31	6.4×10^{11}	4.1×10^{11}
	Interior	34.75	3.77	27.61	8.2×10^{11}	1.8×10^{12}
0-1500	LC	34.43	2.71	27.44	2.4×10^{12}	1.6×10^{12}
	WGC	34.71	3.64	27.59	8.0×10^{11}	1.4×10^{12}
	Interior	34.85	3.45	27.72	2.3×10^{12}	7.1×10^{12}
0-3000	LC	34.52	2.76	27.51	2.5×10^{12}	2.0×10^{12}
	WGC	34.74	3.51	27.63	8.4×10^{11}	1.6×10^{12}
	Interior	34.88	3.13	27.78	3.5×10^{12}	1.3×10^{13}
0-> 3000	Interior	34.88	2.98	27.79	3.8×10^{12}	1.4×10^{13}

Table 3.3: A list of mean water properties and total freshwater and heat content for the three key regions of the Labrador Sea. Values derived from the GEO climatology.

Depth Range (m)	Region	S_{mean}	T_{mean} (°C)	σ_θ	$\Sigma FW(m^3)$	$\Sigma H(GJ)$
0-300	LC	33.74	1.89	26.96	2.3×10^{12}	4.8×10^{11}
	WGC	34.22	3.30	27.23	7.2×10^{11}	4.3×10^{11}
	Interior	34.70	4.00	27.54	1.0×10^{12}	1.9×10^{12}
0-1500	LC	34.38	2.80	27.40	2.6×10^{12}	1.6×10^{12}
	WGC	34.67	3.65	27.56	8.8×10^{11}	1.4×10^{12}
	Interior	34.84	3.51	27.71	2.4×10^{12}	7.2×10^{12}
0-3000	LC	34.48	2.82	27.48	2.6×10^{12}	2.0×10^{12}
	WGC	34.72	3.51	27.61	9.1×10^{11}	1.6×10^{12}
	Interior	34.88	3.16	27.77	3.5×10^{12}	1.3×10^{13}
0-> 3000	Interior	34.88	3.02	27.79	3.8×10^{12}	1.4×10^{13}

Table 3.4: A list of mean water properties and total freshwater and heat content for the three key regions of the Labrador Sea. Values derived from the ISO climatology.

for all three regions. The differences between the ISO and GEO climatologies are more significant in the upper parts of the ocean and in the boundary current. For example, on average, a temperature difference of 0.2°C is observed between ISO and GEO in the upper $300m$ as compared to a 0.03°C difference when the top $3000m$ of

the water column is considered. The lower layers of the ocean are not subjected to as much variability as the surface ocean; therefore, the integrated and mean properties calculated from the two climatologies are expected to converge in deeper waters as shown in Tables 3.3 and 3.4.

The boundary current properties also show a larger deviation between the ISO and GEO results. The LC and WGC salinities are, on average, 0.1 fresher in the top $300m$ in ISO than in GEO. The reason for this deviation must be related primarily to the different coordinates used in the vertical. The ISO climatology avoids the smearing of shelf-break fronts by analyzing data isopycnally over steep isopycnal slopes, such as those that exist between the boundary currents and the interior of the Labrador Sea.

In addition, the ISO climatology has finer resolution of the near surface waters, which may enable it to better represent solar heating. Higher temperatures seen near the top of the water column, in many transects plotted from the ISO climatology (e.g. Figure 3.6), are in agreement with this explanation. However, it can only partially account for the differences between the ISO and GEO climatologies. Although the two climatologies made use of the same database, the data were binned differently in the vertical. Differences in the data composition could effect which points are statistically identified as outliers.

Warmer and fresher water properties found in the ISO climatology result in

lower densities (calculated according to the Fofonoff and Millard (1983) formulation) in all three regions. However, a more important aspect of the climatologies is how well they preserve the gradients of density between different water masses, since one of the aims of this study is to construct the flow field diagnostically, from the density distribution. As briefly discussed earlier in section 3.2.1, Figure 3.5, the density field obtained from the ISO climatology has stronger lateral gradients and the near-surface flow field calculated from this density field is more realistic. Here, further discussion is provided in support of this statement.

The diagnostic velocities, calculated from the climatological density fields, are overlaid on a cross-sectional property map plotted along the 52.7°N transect, just to the south of Hamilton Bank (Figure 3.6). The two branches of the LC can be identified from the high current velocities near the surface. The surface velocities in the inshore (baroclinic) branch of the LC calculated from ISO climatology are approximately $20cm/s$. Even though the GEO velocities are comparable with the ISO velocities near the surface, they decay rapidly with depth. This leads to ISO velocities in mid-to-deep waters being nearly twice as high as the GEO velocities.

As a result, the volume of water carried by the boundary current system across the southern transect is almost doubled in ISO (Figure 3.11). Total volume transport is 46.6 Sv in ISO, compared to 26.1 Sv in GEO. The ISO-based transport value is consistent with previous diagnostic estimates for the sub-polar gyre, such as those of

Reynaud (1994), Reynaud et al. (1995) and Myers et al. (1996). In Reynaud (1994), the maximum transport at 53°N was $45 - 50$ Sv in the cold season (December-May) and 40 Sv in the warm season (June-November). The ISO is a yearly climatology; therefore, the ISO-based transport value is intermediate to the seasonal transports found in Reynaud (1994).

Point-wise volume transports (Figure 3.11) pinpoint the location at which the two branches of the LC crosses the 52.7°N transect (at 51.3°W and 50.3°W). They also indicate that the largest transport deviations between the climatologies occur around these points. The GEO simulations also show only only a weak and broad northward flow around 44°W, while in ISO this feature is stronger and better defined.

Furthermore, consistent with the barotropic nature of the offshore branch, the sea surface height (ssh) calculated from the diagnostic model (Figure 3.12) predicts a larger ssh gradient across this branch. The broadening of the jet and associated weakening of the transport can be clearly seen from this figure.

Another important difference between the two climatologies is the location of the deep salinity maximum along the 52.7°N transect. The ISO climatology gives a sharper DWBC signal at a depth of $\sim$ 2400 m and centred around 49.5°W longitude (Figure 3.6b), whereas the salinity maximum in GEO is broader and its peak is shifted towards the east ($\sim$44 W, Figure 3.6a). Since both climatologies use the same depth-dependence criterion, this difference must be a consequence of the vertical averaging
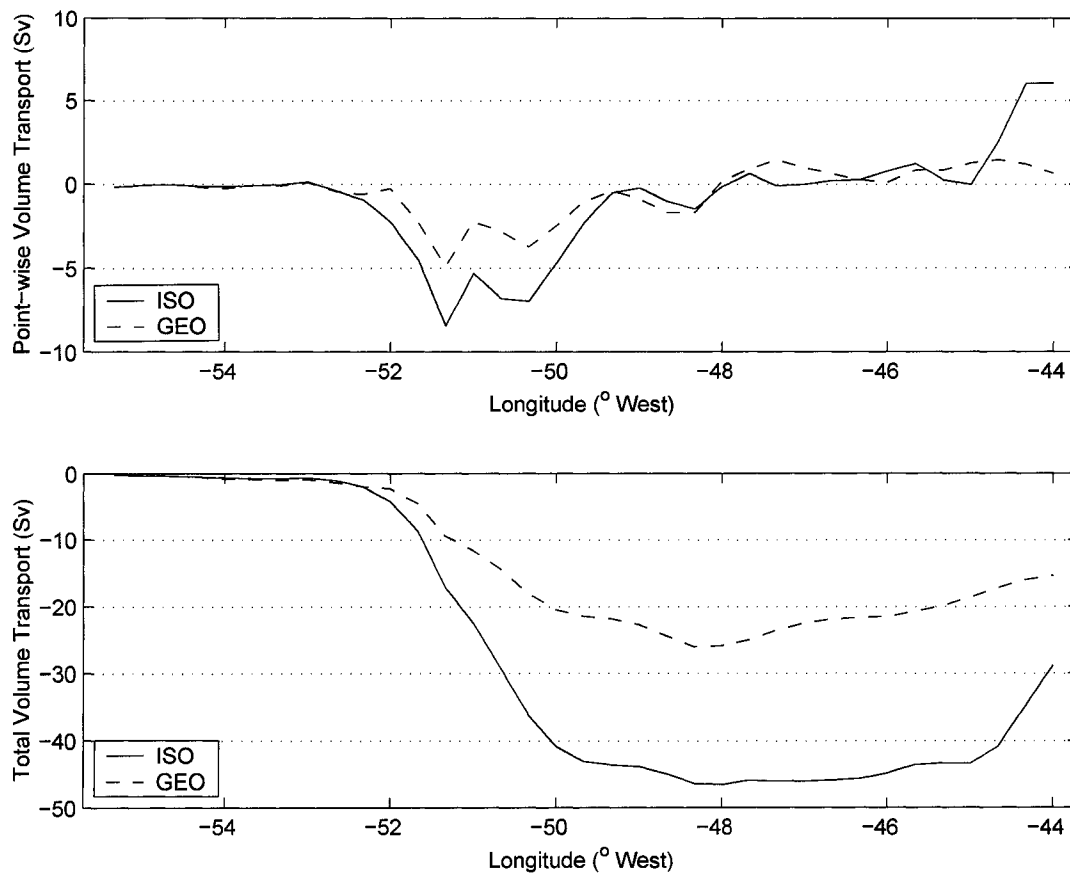
Figure 3.11: Point-wise and total volume transport across the 52.7°N line calculated diagnostically by the GEO and ISO climatologies.

method, i.e. the use of geopotential vs. isopycnal coordinates in the vertical. Since the baroclinic nature of the DWBC is not well preserved in the GEO, the current velocities and volume fluxes calculated from this climatology are underestimated. The northern transect (Figure 3.3) shows similar velocity differences between the two climatologies.
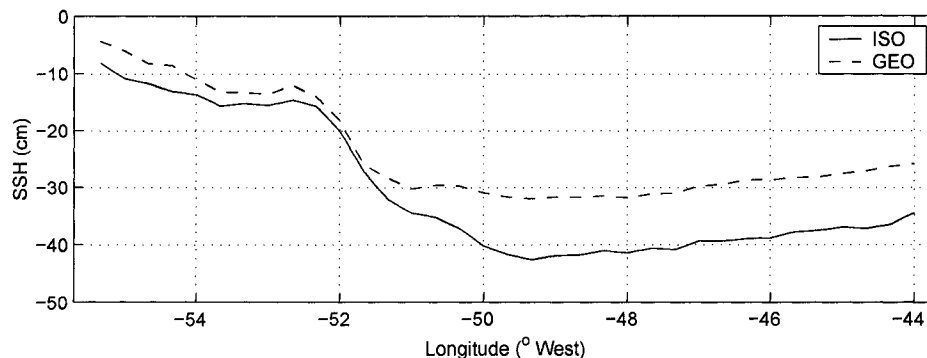
Figure 3.12: Sea surface height along the 52.7°N line calculated from the diagnostic model by the GEO and ISO climatologies.

Perhaps the most striking difference between the ISO and GEO property fields is the location of the DWBC. The salinity maximum associated with the DWBC hugs the Labrador slope at $\sim 2000 - 2500m$ in the ISO, whereas the salinity maximum in the GEO is displaced to the east, and hence away from the topography (Figure 3.6). Since both climatologies employ very similar data and methods, except in the vertical, this difference must be a consequence of the vertical averaging method. The use of geopotential vs isopycnal coordinates in the vertical determines how well the baroclinicity of the deep waters ie represented. A comparison between the results of this study and some direct observations indicates that the current velocities and volume fluxes calculated from the ISO climatology are more realistic.

A comparison between ISO- and GEO-based volume fluxes and Fischer et al.'s (2004) LADCP (Lowered Acoustic Doppler Current Profiler) based flux estimates is

given in Table 3.5. Considering the differences in the period covered in this study (1910-1999) and Fischer et al. (2004) (1996-2001), in transect alignment, and in measurement methods, the agreement between the ISO volume fluxes and LADCP measurements is remarkable. On the other hand, GEO consistently underestimates the volume fluxes by about a factor of two for all the water masses examined here. The agreement between the ISO and LADCP measurements is clear evidence of the advantage of using isopycnal coordinates in the vertical, especially in places where the baroclinicity of the flow needs to be represented accurately.

Table 3.5: Volume fluxes calculated from the GEO and ISO climatologies are compared to the LADCP-based fluxes reported by Fischer et al. (2004). The potential density ranges in the first column correspond to LSW, GFZW, and DSOW. Volume transports are in Sverdrup.

Density Range	GEO	ISO	LADCP [1]
$\sigma_\theta < 27.74$	-6.1	-13.5	-12.3
$27.74 \leq \sigma_\theta < 27.80$	-3.8	-15.3	-10.7
$27.80 \leq \sigma_\theta < 27.88$	-5.2	-7.2	-9.4
$\sigma_\theta > 27.88$	-3.7	-7.4	-5.3

[1]taken from Fischer et al. (2004) Figure 5.

3.4 Comparison of the new climatology with the existing climatologies

One of the aims of this study was to build an improved climatology for the Labrador Sea. The increased data density in the Labrador Sea region since the 1990s allowed the climatology to be computed over a finer grid both in the vertical (see Table 2.1 for the vertical bin ranges used in the ISO and GEO climatologies) and in the horizontal ($1/3° \times 1/3°$). When the resolution is increased, the water mass distribution and characteristics are determined more precisely. For example, the higher vertical resolution of the GEO and ISO climatologies is instrumental in capturing the DWBC signal (e.g. Figure 3.3). In addition, the dynamical features of the flow field that are calculated based on this high resolution climatological hydrography also have more detail and precision.

In addition to the increased resolution, the results are improved by the use of a more natural coordinate system in the vertical. Here, two large-scale ocean climatologies, one based on geopotential (Levitus, 1994) and the other based on isopycnal (Lozier et al., 1995) coordinates are compared with the GEO and ISO climatologies presented here.

Increased horizontal and vertical resolution, smaller search radii in the iterations, and the application of a depth-dependant OA scheme employed in this study

have successfully preserved the shelf-break fronts (Figure 3.13). The differences between the larger scale climatologies and the current ones are remarkable, especially near the fronts.

Figure 3.13 shows the salinity field at $30m$ as mapped from four climatologies: GEO, ISO, WOA-05 and Lozier et al. (1995). WOA-05 is the most up-to-date version of the $1°$resolution World Ocean Atlas. WOA-05 has more detail in many areas of the world's ocean due to increased data volume; hence, smaller search radii were used in iterations. However, the differences between the WOA-94 and WOA-05 are insignificant, when compared to the differences between the new climatological hydrography of the Labrador Sea (GEO/ISO) and that of WOA-94, which is used in the diagnostic model calculations, or the WOA-05 whose salinity field is plotted in Figure 3.13.

The coarser resolution of the WOA-05 and Lozier et al. (1995) climatologies is only one of the factors that distinguishes GEO and ISO from them. The tightness of the fronts between the interior and shelf waters found in the GEO and ISO climatological fields (Figure 3.13-a, -d) is missing, even in the 0.25 degree resolution version of the WOA-05 climatology (figure not shown). The improved representation of the fronts in the GEO and ISO is primarily due to the modified objective analysis scheme, which makes use of the topographic information, as explained in Section 2.2.1.

Although the topography-dependent OA scheme is successful in capturing the fronts and boundary currents, the northwest corner of the NAC needs to be better
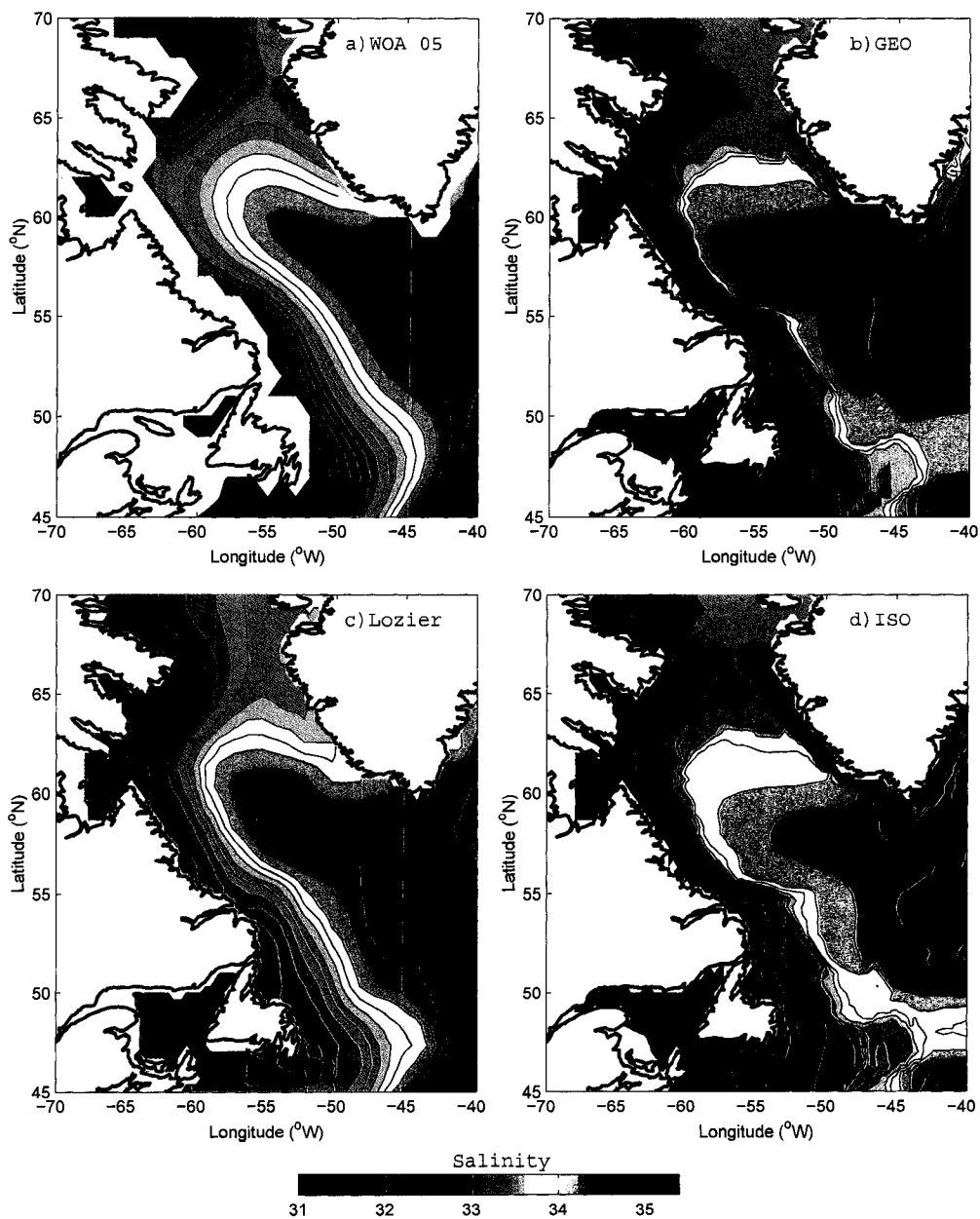
Figure 3.13: Salinity field at $30m$ from (a) WOA-05, (b) GEO, (c) Lozier et al. (1995), and (d) ISO climatologies.

resolved in the GEO and ISO climatologies. The discrepancy between observations, WOA-05, Lozier et al. (1995), and GEO/ISO is heightened because the northwest corner is located very close to the southeast boundary of the study domain and to the Flemish Cap. The northwest corner lies over the deeper part (3000m) of the Labrador Sea, and hence, the grid points in this area have larger depth ranges ($\delta H \sim 900m$), causing data from shallow parts to be included in the analysis. Since the northwest corner is located near the boundary of the study area, the database has a limited number of data points in its depth range. Therefore, some of the observations taken over the slope area are unavoidably included and it is possible that they dominated the calculations over the northwest corner. This results in the misleading appearance of the NAC, which is discontinued in the southeastern corner of the study domain (Figure 3.13-a and -d). To ensure that this discrepancy does not influence the discussions, none of the transects or regions includes the northwest corner.

The differences in the resolution, OA scheme, vertical coordinates, and time period of the four climatologies (GEO, ISO, WOA-94, and Lozier et al. (1995)) lead to variations in the property fields and velocity calculations based on them. For example, in Figures 3.14 and 3.15, the eastward export of all the water masses, including the LSW, to the eastern basin is noticeable roughly between 55 and 56.5°N latitudes, in all climatologies except the WOA-94. Furthermore, the LSW does not have a

strong salinity signature in the WOA-94. This is probably due to the fact that the WOA-94 includes the fewest observation from the 1990s, when a freshening of all mid-depth waters has been observed. This is partially true for the Lozier et al. (1995) climatology, which has a very similar time coverage to the WOA-94. Even though the eastward flow of the LSW at the mid-depths of the Labrador Sea is better resolved in the Lozier et al. (1995) climatology than in the WOA-94, its salinity signature and eastward velocity is not as pronounced as in the GEO and ISO climatologies.

The GEO climatology gives somewhat discontinuous temperature and salinity variations throughout the water column; this seems to be the case, to a lesser extent, in the WOA-94 as well. The discontinuity in the GEO might have been intensified due to the increased vertical resolution as compared to the WOA-94. Interpolating data in the vertical in advance of the vertical binning, or after compiling a geopotential climatology can be a solution. Since the conversion from the isopycnal surfaces to the geopotential levels requires interpolation in the vertical, this problem is solved naturally in the ISO.

The point-wise and total volume transport values calculated from the four climatologies are shown in Figures 3.16 and 3.17. The lack of eastward transport across the 44°E between 55 and 56°N in the WOA-94 based calculation is clearly seen in the point-wise transport calculations. The other three climatologies indicate that approximately $5Sv$ of water crosses the 44°E line eastward at these latitudes. Among these
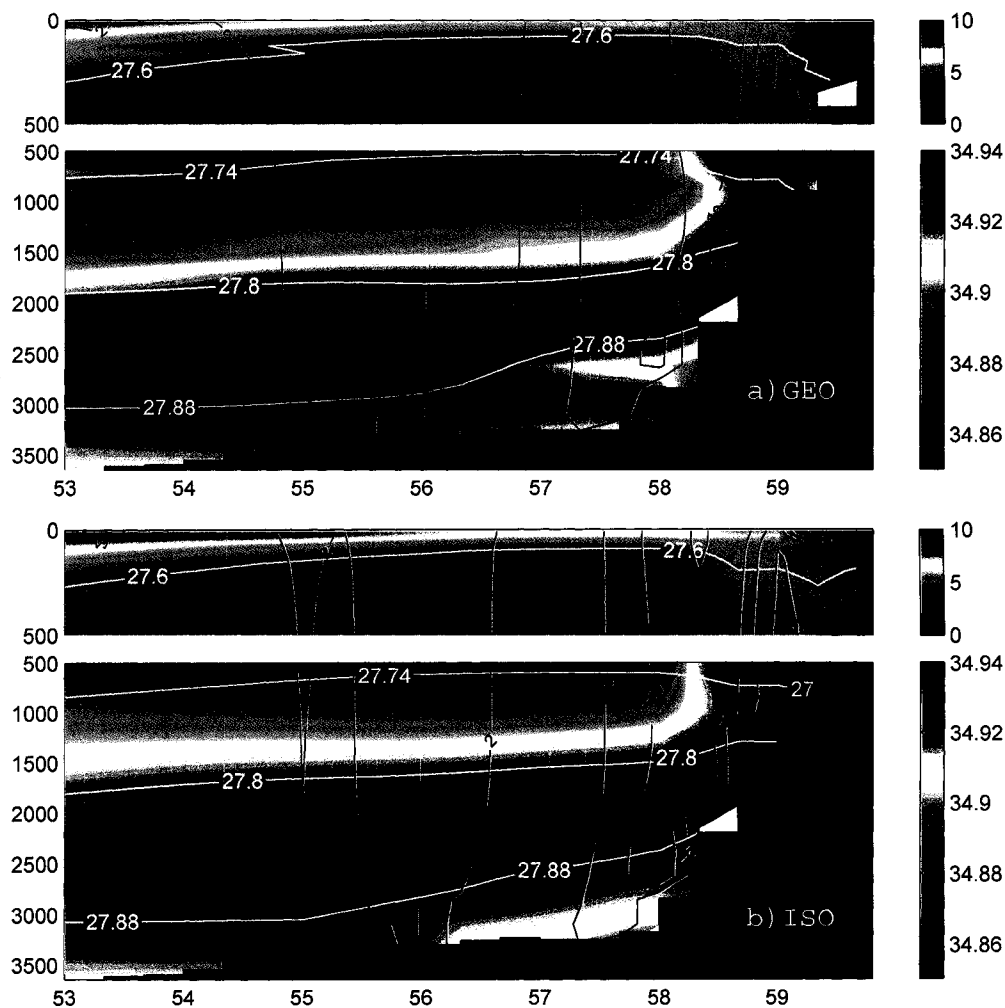
Figure 3.14: Property maps along 44°W line overlaid with the potential density contours (white) and velocity contours across this transect (black). (a) for GEO, and (b) for ISO climatology.

three climatologies, ISO yields the highest volume flux at this location. In terms of

the total volume fluxes, ISO also gives the highest value with $-42.0Sv$. The total

volume fluxes calculated from the other climatologies are as follows: Lozier et al.
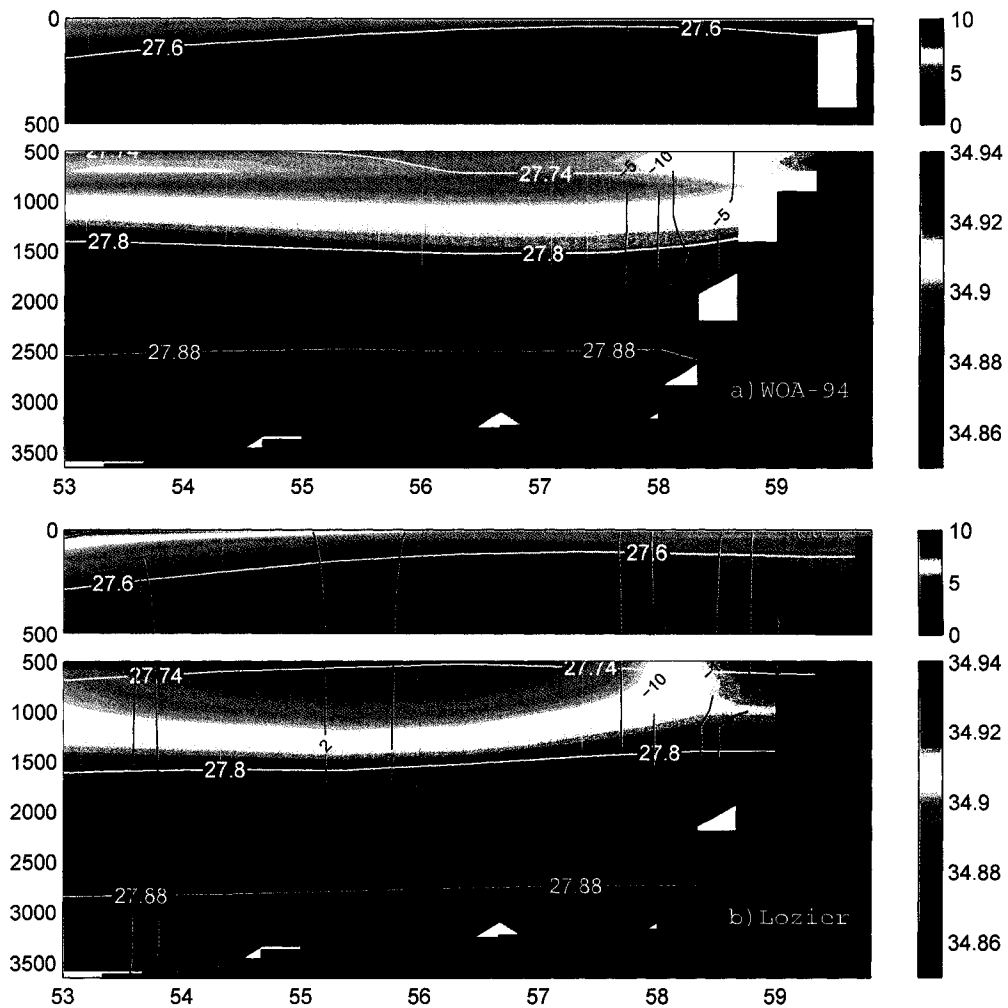
Figure 3.15: Property maps along 44°W line overlaid with the potential density contours (white) and velocity contours across this transect (black). (a) for WOA-94, and (b) for Lozier et al. (1995) climatology.

(1995) climatology $= -38.1Sv$; GEO $= -35.8Sv$; and WOA-94 $= -34.9Sv$. The volume fluxes calculated from all four climatologies (GEO, ISO, WOA-94, and Lozier et al. (1995)) are less than the total transport reported by Clarke (1984). However,

ISO-based total volume flux compares best with the results of Clarke (1984), which were based on direct observations.
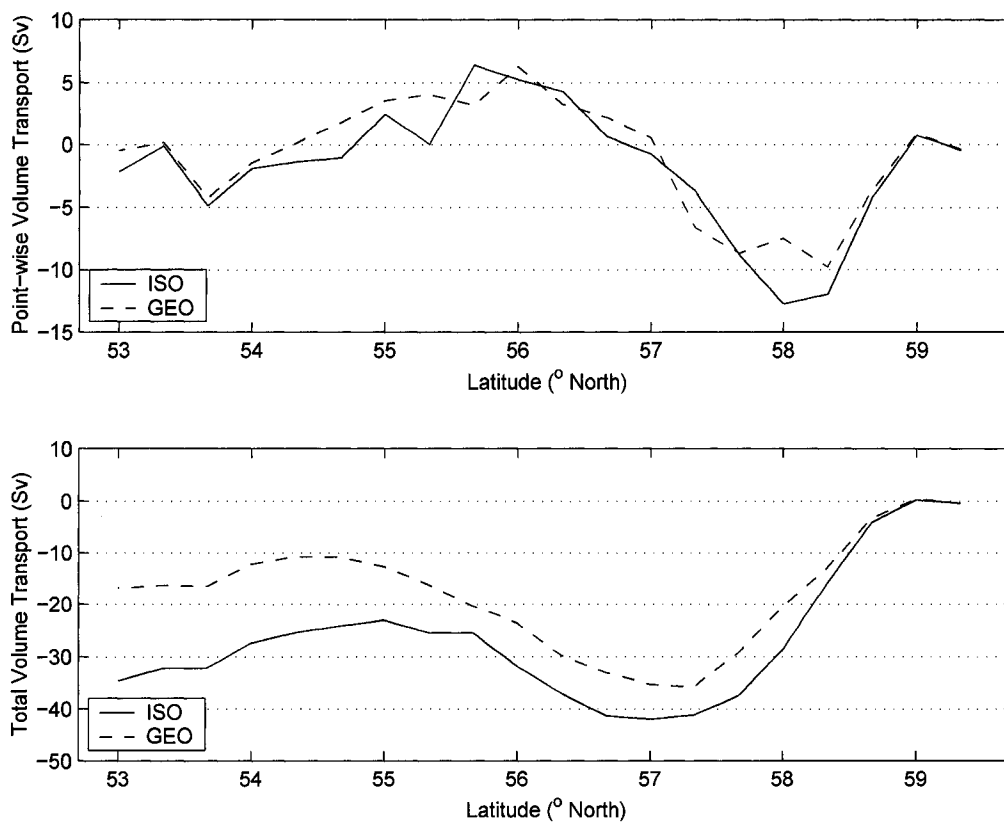
Figure 3.16: Point-wise and total volume transport across the 44°W line calculated diagnostically by the GEO and ISO climatologies.

Finally, to highlight the differences between the WOA-94/Lozier et al. (1995) and GEO/ISO climatologies (presented in Tables 3.3 and 3.4, earlier) the mean water properties obtained from the WOA-94 and Lozier et al. (1995) climatology are
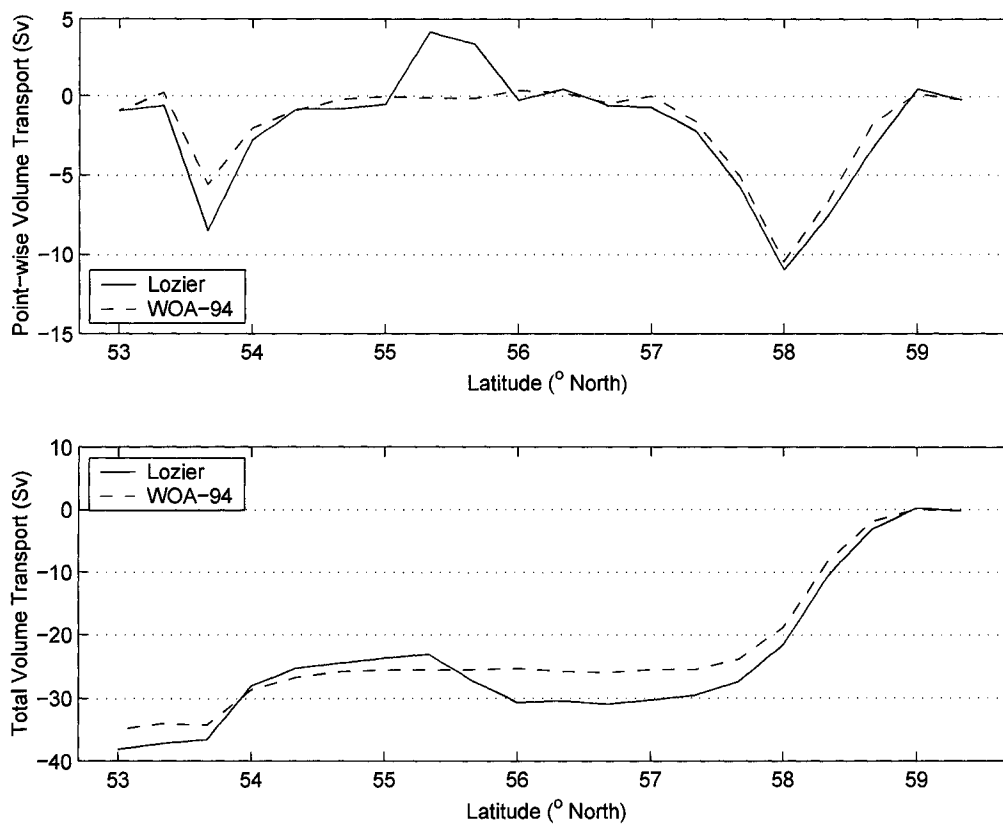
Figure 3.17: Point-wise and total volume transport across the 44°W line calculated diagnostically by the WOA-94 and Lozier et al. (1995) climatologies.

summarized in Tables 3.6 and 3.7, respectively.

Depth Range (m)	Region	S_{mean}	θ_{mean} (°C)	σ_θ	$\Sigma FW(m^3)$	$\Sigma H(GJ)$
0-300	LC	33.90	2.21	27.07	1.9×10^{12}	5.4×10^{11}
	WGC	34.57	3.04	27.53	2.9×10^{11}	2.8×10^{11}
	Interior	34.56	3.09	27.52	1.4×10^{12}	1.3×10^{12}
0-1500	LC	34.55	3.01	27.52	2.4×10^{12}	2.2×10^{12}
	WGC	34.80	3.48	27.68	4.2×10^{11}	1.0×10^{12}
	Interior	34.82	3.38	27.71	2.7×10^{12}	7.3×10^{12}
0-3000	LC	34.64	2.96	27.60	2.5×10^{12}	2.9×10^{12}
	WGC	34.82	3.41	27.70	4.4×10^{11}	1.1×10^{12}
	Interior	34.88	2.95	27.79	3.8×10^{12}	1.3×10^{13}
0-> 3000	Interior	34.88	2.85	27.80	4.1×10^{12}	1.3×10^{13}

Table 3.6: A list of mean water properties and total freshwater and heat content for the three key regions of the Labrador Sea. Values derived from the WOA-94 climatology.

Depth Range (m)	Region	S_{mean}	θ_{mean} (°C)	σ_θ	$\Sigma FW(m^3)$	$\Sigma H(GJ)$
0-300	LC	34.07	2.21	27.20	1.9×10^{12}	6.2×10^{11}
	WGC	34.51	3.70	27.42	4.8×10^{11}	5.1×10^{11}
	Interior	34.73	3.93	27.58	8.3×10^{11}	1.7×10^{12}
0-1500	LC	34.64	3.10	27.58	2.5×10^{12}	3.0×10^{12}
	WGC	34.82	3.74	27.67	7.4×10^{11}	2.1×10^{12}
	Interior	34.86	3.52	27.72	2.2×10^{12}	7.6×10^{12}
0-3000	LC	34.70	3.05	27.64	2.7×10^{12}	3.8×10^{12}
	WGC	34.84	3.58	27.70	8.1×10^{11}	2.5×10^{12}
	Interior	34.89	3.11	27.79	3.3×10^{12}	1.3×10^{13}
0-> 3000	Interior	34.89	3.00	27.80	3.6×10^{12}	1.4×10^{13}

Table 3.7: A list of mean water properties and total freshwater and heat content for the three key regions of the Labrador Sea. Values derived from the Lozier et al. (1995) climatology.

Chapter 4

Seasonal Variability

Seasonal variability is the fundamental mode of variability in the ocean-atmosphere system. The Labrador Sea undergoes remarkable changes in its freshwater and heat content, which regulate winter convection and restratification. A major question to be addressed in the Labrador Sea is the role of freshwater and heat transport from the boundary currents to the interior, where classical LSW is formed during winter convection (Lab. Sea Group, 1998).

This chapter is dedicated to the intra-annual variability of the freshwater and heat budgets of the Labrador Sea interior, WGC and LC system. In addition to the seasonal hydrography of these three key regions, cross-boundary transports of freshwater and heat are also discussed. As suggested by recent studies (e.g. Lilly et al., 2003; Katsman et al., 2004; Spall, 2004), the lateral exchange of heat and

freshwater between the boundary currents and the interior is an important process in marginal seas, such as the Labrador Sea.

The temporal distribution of the seasonal observations should be considered carefully in a study such as this one, which makes use of data collected over a long period (between 1910 and 2000 in this study). Some seasonal data might be strongly biased towards a particular period when the conditions were extraordinary (such as during a GSA event or when the convective overturning was shut down). Therefore, a discussion of the effects of temporal bias on the seasonal analysis and decadal distributions of the seasonal data is also included in this chapter.

4.1 Heat and Freshwater Budgets

4.1.1 The Boundary Current System: WGC and LC

The two boundary currents, the WGC and LC are the main sources of freshwater for the Labrador Sea. In this analysis, these two current systems are defined as the waters located off the coast of western Greenland and the Labrador coast, respectively, roughly between the 100 and 2500 m isobaths (Figure 1.2). Hence, they include the slope water and part of the deep boundary current, as well the coastal waters and surface boundary currents. The mean and total heat and freshwater contents are tabulated in three depth classes in order to distinguish intermediate to deep water

masses from the near surface waters.

The heat and freshwater content of the near surface waters ($< 300m$) show greater seasonal variability than the deeper waters. As the surface waters are in close contact with the atmosphere, they show the greatest response to atmospheric heating/cooling and precipitation/evaporation, in addition to freshwater run-off and the melting of sea-ice. Some of these processes are more prominent in coastal regions than in the Labrador Sea interior. Therefore, the seasonal variations in freshwater and heat content near the coastal areas, i.e. in the boundary current system, are greater than in the interior Labrador Sea (Tables 4.1 - 4.4). The interior heat and freshwater budgets are discussed in the next subsection. The cross-shelf freshwater exchange, which is particularly important for the Labrador Sea winter convection (Straneo, 2006, e.g.), is discussed in *Section* 4.2.

It is evident from the mean freshwater contents that the LC carries 3 to 5 times the total freshwater content of the WGC, with respect to a reference salinity of 35 (Tables 4.1 - 4.4). The LC freshwater content shows an increase from spring to fall and stays relatively constant between fall and winter, in all depth ranges shown in Tables 4.1 - 4.4. A large increase in salinity is observed between winter and spring. The area defined as the LC is mostly covered by ice in winter and spring. Therefore the increase in salinity during this period is most likely due to the arrival of saltier waters, such as the IW, and perhaps inclusion of some of the interior Labrador Sea

Depth Range (m)	Region	S_{mean}	θ_{mean} (°C)	σ_θ	$\Sigma FW(m^3)$	$\Sigma H(GJ)$
	LC	33.96	1.56	27.16	1.88×10^{12}	3.96×10^{11}
0-300	WGC	34.30	2.72	27.35	6.39×10^{11}	3.49×10^{11}
	Interior	34.67	3.53	27.57	1.10×10^{12}	1.64×10^{12}
	LC	34.49	2.60	27.50	2.12×10^{12}	1.51×10^{12}
0-1500	WGC	34.71	3.43	27.61	7.83×10^{11}	1.28×10^{12}
	Interior	34.84	3.39	27.72	2.39×10^{12}	7.00×10^{12}
	LC	34.67	2.66	27.56	2.19×10^{12}	1.89×10^{12}
0-3000	WGC	34.75	3.34	27.65	8.18×10^{11}	1.51×10^{12}
	Interior	34.88	3.08	27.78	3.52×10^{12}	12.71×10^{12}
0-> 3000	Interior	34.88	2.96	27.79	3.80×10^{12}	13.47×10^{12}

Table 4.1: A list of mean water properties, and total freshwater and heat contents for the three key regions of the Labrador Sea in spring.

Depth Range (m)	Region	S_{mean}	θ_{mean} (°C)	σ_θ	$\Sigma FW(m^3)$	$\Sigma H(GJ)$
	LC	33.75	1.86	26.97	2.29×10^{12}	4.73×10^{11}
0-300	WGC	34.17	3.28	27.19	7.59×10^{11}	4.19×10^{11}
	Interior	34.68	4.04	27.53	1.07×10^{12}	1.88×10^{12}
	LC	34.38	2.75	27.40	2.53×10^{12}	1.56×10^{12}
0-1500	WGC	34.66	3.59	27.56	9.10×10^{11}	1.35×10^{12}
	Interior	34.84	3.50	27.71	2.41×10^{12}	7.24×10^{12}
	LC	34.48	2.77	27.48	2.60×10^{12}	1.94×10^{12}
0-3000	WGC	34.71	3.46	27.60	9.48×10^{11}	1.56×10^{12}
	Interior	34.88	3.14	27.77	3.61×10^{12}	12.94×10^{12}
0-> 3000	Interior	34.88	3.00	27.79	3.91×10^{12}	13.68×10^{12}

Table 4.2: A list of mean water properties, and total freshwater and heat contents for the three key regions of the Labrador Sea in summer.

water masses, in the spring climatology of the LC.

Meanwhile, the WGC area gains more freshwater from winter to summer as a result of melting sea-ice and increased run-off from Greenland caused by warmer air temperatures. This is followed by a decrease in the freshwater content of the WGC

Depth Range (m)	Region	S_{mean}	θ_{mean} (°C)	σ_θ	$\Sigma FW(m^3)$	$\Sigma H(GJ)$
0-300	LC	33.43	2.13	26.70	2.83×10^{12}	5.38×10^{11}
	WGC	34.22	3.77	27.18	7.09×10^{11}	4.79×10^{11}
	Interior	34.60	4.11	27.46	1.32×10^{12}	1.91×10^{12}
0-1500	LC	34.25	2.96	27.28	3.12×10^{12}	1.73×10^{12}
	WGC	34.68	3.84	27.54	8.53×10^{11}	1.43×10^{12}
	Interior	34.82	3.58	27.68	2.66×10^{12}	7.40×10^{12}
0-3000	LC	34.38	2.96	27.38	3.19×10^{12}	2.12×10^{12}
	WGC	34.72	3.67	27.59	8.93×10^{11}	1.63×10^{12}
	Interior	34.87	3.16	27.76	3.86×10^{12}	13.02×10^{12}
0-> 3000	Interior	34.87	3.07	27.77	4.07×10^{12}	13.41×10^{12}

Table 4.3: A list of mean water properties, and total freshwater and heat contents for the three key regions of the Labrador Sea in fall.

Depth Range (m)	Region	S_{mean}	θ_{mean} (°C)	σ_θ	$\Sigma FW(m^3)$	$\Sigma H(GJ)$
0-300	LC	33.46	1.30	26.77	2.78×10^{12}	3.29×10^{11}
	WGC	34.30	2.44	27.37	6.27×10^{11}	3.08×10^{11}
	Interior	34.68	3.31	27.60	1.06×10^{12}	1.55×10^{12}
0-1500	LC	34.23	2.43	27.31	3.12×10^{12}	1.39×10^{12}
	WGC	34.69	3.35	27.60	7.63×10^{11}	1.16×10^{12}
	Interior	34.83	3.38	27.71	2.47×10^{12}	6.99×10^{12}
0-3000	LC	34.37	2.53	27.41	3.18×10^{12}	1.78×10^{12}
	WGC	34.74	3.27	27.64	7.98×10^{11}	1.38×10^{12}
	Interior	34.88	3.12	27.78	3.50×10^{12}	12.85×10^{12}
0-> 3000	Interior	34.88	2.99	27.79	3.77×10^{12}	13.58×10^{12}

Table 4.4: A list of mean water properties, and total freshwater and heat contents for the three key regions of the Labrador Sea in winter.

from summer to winter months. Even though the WGC and LC are inter-connected, they have differing freshwater sources, which are linked to the variability observed in GSA advection patterns (Belkin et al., 1998, e.g.). According to the seasonal climatologies, there seems to be a one-season shift between the periods when freshwater

content of the WGC and LC exhibit either an increasing or decreasing trend. The LC freshwater content lags one season behind the WGC freshwater changes. This shift is probably related to the additional freshwater sources, such as the arctic-origin waters reaching the LC through the Canadian Archipelago and Baffin Bay.

For example, a recent year-round mooring study (Straneo and Saucier, 2007) suggests that the maximum freshwater output from the Hudson Strait into the Labrador Sea occurs in November and December. According to the seasonal definitions used in this study, November and December are fall months. These seasonal climatology results are in agreement with freshwater content of the LC reaching its maximum in fall and staying high during winter. On the other hand, the WGC freshwater content reaches its peak in summer and starts to decrease by fall.

There is greater synchronicity between the heat content of the WGC and LC. They both gain heat from winter to fall, with a large drop in heat content occurring between fall and winter, as would be expected. As in the freshwater content, seasonal variability of the heat content of the WGC is not as pronounced as the LC (Tables 4.1 - 4.4).

The heat content of the whole water column $(0 - 2500m)$ increases from $1.8 \times 10^{12}GJ$, in winter to $2.1 \times 10^{12}GJ$, in fall for the WGC, and from 1.8×10^{12} to $2.1 \times 10^{12}GJ$, during the same period for the LC. Depth versus temperature and salinity plots for the WGC region (Figure 4.1) show that the maximum temperature

in the water column is located at $370 \pm 120m$. The temperature maximum shifts upwards in the water column in fall ($\approx 250m$) and lower in winter ($\approx 390m$). Wintertime deepening of the thermocline is expected due to increased storminess and mixing. The shallowing of the thermocline in fall, after months of increased solar heating, is also expected.
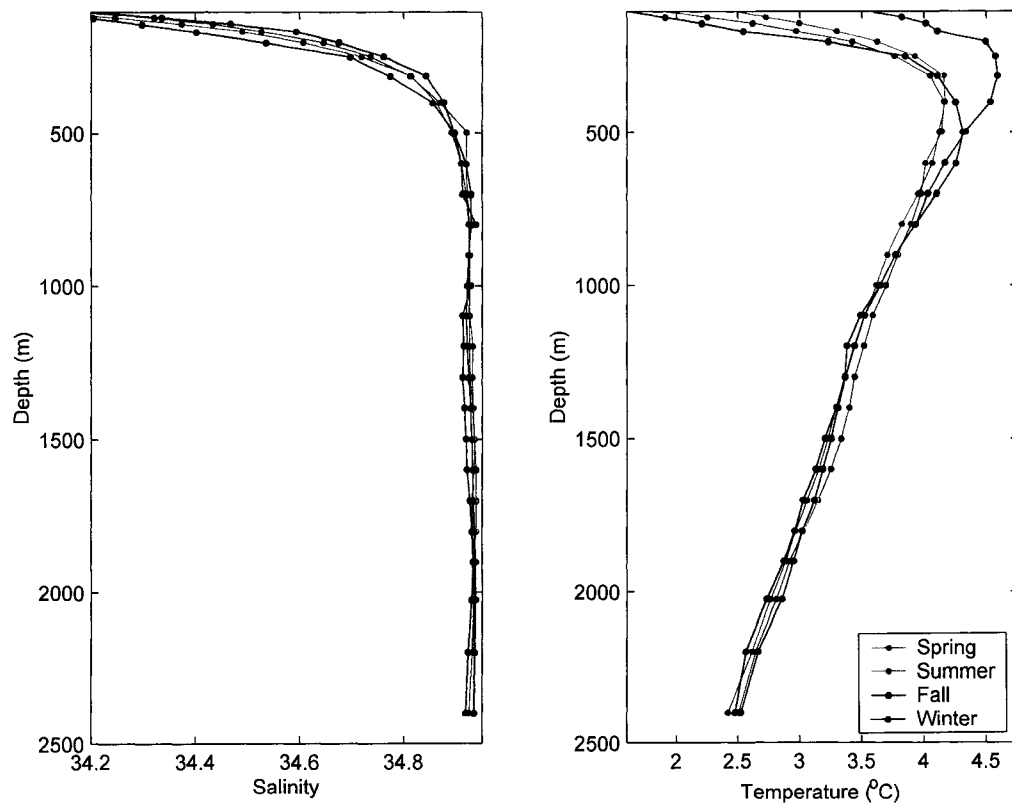
Figure 4.1: Vertical profiles of temperature and salinity for the WGC region between 100 and 2500 meters for four seasons.
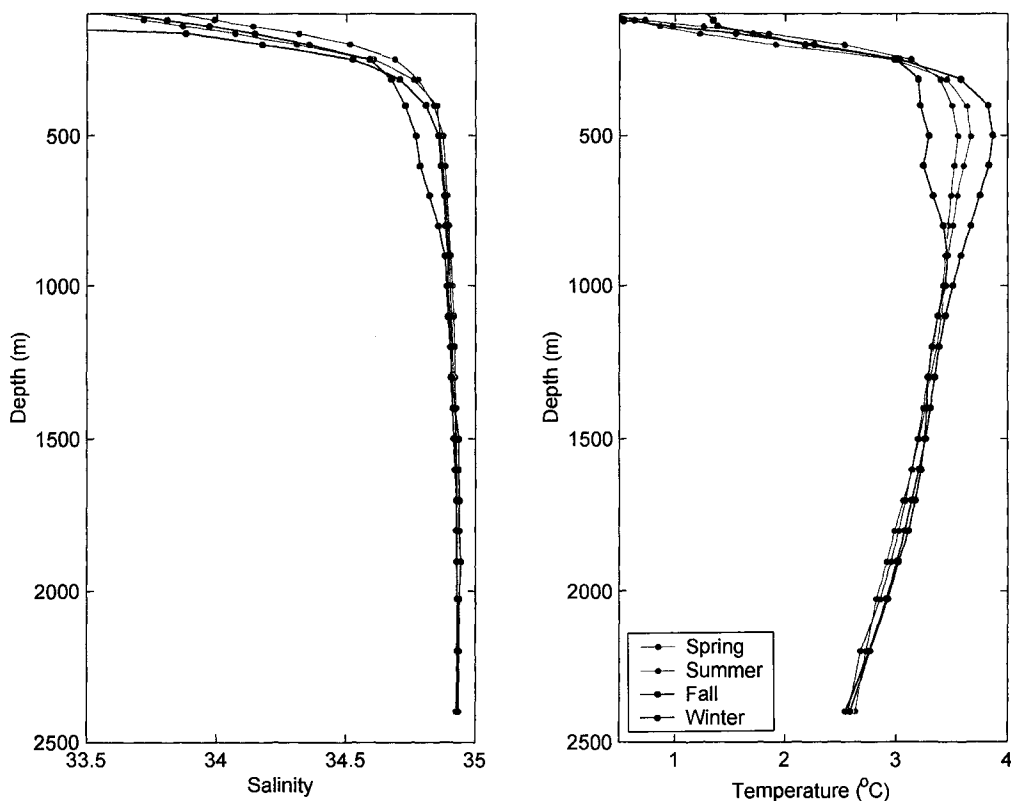
Figure 4.2: Vertical profiles of temperature and salinity for the LC region between 100 and 2500 meters for four seasons.

In the LC region, the maximum temperature is located $\approx 450m$ in all seasons, except winter (Figure 4.2). The deepening of the temperature maximum on the Labrador side is probably related to the deepening of the IW along its cyclonic path. There are two local temperature maxima recorded in winter, one at $\approx 500m$ and another at $\approx 900m$. This bilateral temperature structure is absent in other seasons and in the WGC region. Since having a warm water source at this depth is not

realistic, there must be another explanation, based on either how the climatology was compiled or an ocean process that can change the vertical distribution of heat in the ocean. Vertical distributions of both the mean temperature and salinity (Figure 4.2) indicate that the water column becomes more homogeneous in winter. These are several indications that this is due to oceanic processes rather than data processing:

[i] The definition of the boundary current region is set to cover a large area, between the 100 and 2500 m isobaths. Boundary currents do not always occupy such a large area, especially deeper in the water column, where slope waters and sometimes the DWBC are included. However, the variations in the temperature profile (also in the salinity profile) in Figure 4.2 are located in the top $\approx 1000m$ of the water column, above the level of influence of these water masses.

[ii] Another possibility would be that the interior water masses are included in the horizontal averaging during the compilation of the climatology. If this were the case, a similar anomaly would be expected in the mean WGC temperature and salinity profiles; perhaps more significantly than in the LC since the topographic gradient is sharper on the Greenland side, making the WGC more susceptible to these kinds of artificial mixing. Besides, if the interior waters were, in fact, included in the LC region, an increase in temperature of waters around $500m$ would be expected, as the interior waters have higher temperatures.

[iii] The magnitude of the temperature maximum of the WGC at the base of the thermocline is not lowered like that of the LC. To lower the water temperature at this depth, either a new cold (and fresh) water mass should be added to the LC in the top $1000m$ or the cooler (and fresher) surface waters must be brought down by an ocean process such as deep convection.

[iv] Below 1000 m, the LC region temperature and salinity profiles do not present any anomalies, just the seasonal cycle expected of these parameters in deeper water masses.

[v] The concept of boundary convection, i.e. that deep convection may be occurring inside the boundary current in the LC, is relatively new. There is growing experimental and theoretical (e.g. Pickart et al., 1997; Lab. Sea Group, 1998; Stramma et al., 2004) evidence as to its existence, even though the mechanism and robustness of the boundary convection is not well understood.

In conclusion, it is proposed that the winter convection is the mechanism that brings cold and fresh surface waters to mid-depths, modifying the heat and fresh-water content inside the LC water column. The frequency and magnitude of winter convection in the LC must be significant enough to have this signal present in the climatology, but this might be a result of temporal bias.

It should also be noted that the boundary convection product is neither as dense

as the classical LSW, nor does it reach as great depths, i.e. 2400 m, as the interior deep convection. However, it is still an important mechanism affecting how convection works in the boundary current system, whether or not this lighter convective product makes its way into the DWBC, and how this lighter LSW would affect the large scale thermohaline circulation. It is also important to understand whether there is any relation between the "boundary convection" and "interior convection" and how one influences or is influenced by the other.

Apart from sharing the same origin, the Arctic Ocean, the two inter-connected boundary currents, the LC and WGC, undergo different processes and experience different forcing along their paths. For example, the narrow continental shelf and abrupt topographic slope changes force barotropic instability in the WGC, causing it to separate from the western flank of the Greenland and shed eddies (Katsman et al., 2004, e.g.). On the other hand, the LC flows over a smoother and wider topography and follows the f/H lines along its path without much perturbation. As a result, the large amount of freshwater (nearly twice as much as the WGC, after normalizing for the total volume difference between the LC and WGC) accumulated in the LC has limited contact with the interior Labrador Sea waters. The cross-shelf exchange of freshwater is further discussed in *Section* 4.2.

4.1.2 Interior Labrador Sea

The interior Labrador Sea defined in this study (Figure 1.2) includes the region where the classical LSW is formed and its surroundings. It has long been known that deep convection takes place in small patches offshore of the $3000m$ isobath (e.g. Lazier, 1980; Gascard and Clarke, 1983). Once the LSW is formed by deep convection, it spreads out and fills the intermediate to deep parts of the basin, hence the larger interior Labrador Sea definition used in this study to examine LSW properties.

Deep convection acts to homogenize the water column by redistributing freshwater and heat vertically. It exposes the deep layers of the Labrador Sea, which are normally not in contact with the atmosphere, enhancing the heat exchange between the Labrador Sea and atmosphere (Straneo, 2006). Deep convection also facilitates the communication of surface freshwater anomalies to greater depths (Houghton and Visbeck, 2002), occasionally exceeding $2000m$ (Lazier et al., 2002).

The LSW has long been recognized by its thick vertical pycnostad[1] . The result of this vertical redistribution of heat and salt can be seen in the interior Labrador Sea TS-diagram (Figure 4.3). The gradients of salinity and temperature are smallest within the LSW density range ($\sigma_\theta \approx 27.74 - 27.80$) . Also the seasonal variability in the LSW layer is more subtle than in the waters above and below it.

Below the LSW, between the potential densities of 27.80 and 27.88, the GFZW

---

[1]Pycnostad: A layer where the vertical density gradient of seawater is very small.
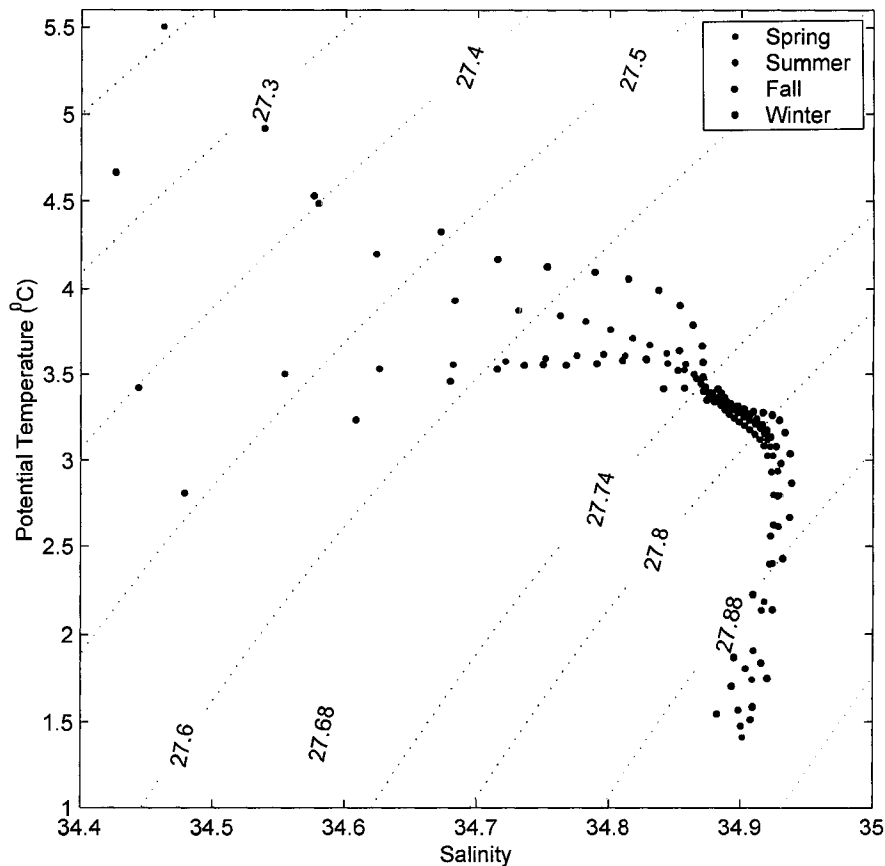
Figure 4.3: TS diagram for the interior Labrador Sea for four seasons.

can be identified by its salinity maximum (Figure 4.3). As a result, the freshwater

content reaches a deep minimum at $\approx 2400m$, the core depth of the GFZW layer

(figure not shown). Below this depth, the freshwater content continues to rise because

DSOW has an intermediate salinity to the LSW and GFZW. The reason DSOW is

found below the GFZW is that it has a lower temperature than the GFZW and density

is controlled primarily by temperature rather than salinity away from the surface.

The magnitude of freshwater and heat storage in the central Labrador Sea undergoes substantial changes throughout the year. Tables 4.1 to 4.4 list the total freshwater and heat content, and the mean temperature, salinity and density of the top 300, 1500, 3000m, and $> 3000m$ for the interior Labrador Sea. The total freshwater content of the interior Labrador Sea, in all four depth classes, reaches its maximum in the fall. As seen in the discussion of the boundary current regions (*Section* 4.1.1), the LC region also reaches its maximum freshwater content in the fall, while WGC freshwater content peaks earlier, in the summer, and starts to drop towards fall.

In winter, the total freshwater content of the interior Labrador Sea waters decreases, probably due to reduced inflow of freshwater from the continental boundaries, and limited exchange between ice-covered boundary currents and the ice-free interior. Freshwater content stays relatively constant for the rest of the year in the interior Labrador Sea. The source of freshwater for the interior is the boundary current system. Therefore, the freshwater flux into the interior from the boundaries of the Labrador Sea plays an important role in governing the freshwater content and its seasonality as discussed in *Section* 4.2.

4.1.2.1 Decadal bias vs. natural variability

The heat and freshwater contents of the interior Labrador Sea have similar patterns: an increase from winter to fall, reaching a maximum in fall, and a large decrease between fall and winter. This holds true for all the depth ranges, except when the integration is done over the entire water column. The heat content of the interior Labrador Sea over the entire water column show a seesaw structure with a spring minimum ($13.47 \times 10^{12} GJ$), summer maximum ($13.68 \times 10^{12} GJ$), fall minimum ($13.41 \times 10^{12} GJ$), and winter maximum ($13.58 \times 10^{12} GJ$) (values are taken from Tables 4.1 - 4.4).

Since the entire water column is the only depth range that includes the DSOW water, it can be concluded that the difference in its seasonal pattern is related to the DSOW, which is produced by deep convection, not in the Labrador Sea, but in the GIN Seas. Deep waters do not generally show great seasonal variability as they are not exposed to the atmosphere, unless they originated at the surface and sank to depths via deep convection, as would be the case for DSOW.

Here, it is argued that the apparent heat content minimum of the DSOW ($3.9 \times 10^{11} GJ$) in fall results from a decadal bias, not from natural seasonal variability.

Tables 4.5 to 4.8 give a decadal breakdown of the number of observations that were available in each of the five density classes (surface, uLSW, cLSW, GFZW, DSOW), in each season. A close examination of the data collected in the fall reveals

that the DSOW (and to a lesser extent the GFZW) was extensively sampled during the 1980s. Although an upward trend in data availability is seen in recent decades, there were almost three times as many observations in the 1980s as in the 1990s (i.e. 68 observations in DSOW in the 1980s compared to only 22 in the 1990s, Table 4.7). Therefore, the climatological properties of these two deep water masses are strongly biased towards their properties in the 1980s.

SPRING	Number of Observations				
Decades	Surface	uLSW	cLSW	GFZW	DSOW
1910s	310	3	0	0	0
1920s	641	823	47	28	11
1930s	3634	403	369	163	23
1940s	1898	192	159	39	14
1950s	14086	1398	841	90	42
1960s	17312	1866	1247	301	202
1970s	28173	1506	860	172	67
1980s	32747	1981	721	195	70
1990s	76793	1687	624	146	131

Table 4.5: Decadal break-down of spring data in five density classes: Surface, upper LSW, classical LSW, GFZW and DSOW

The significance of this bias lies in the conditions under which the DSOW was produced, and its temperature and salinity characteristics at the formation site. The early 1980s have a low NAO index, which is associated with higher than normal deep convection rates in the Nordic Seas (Dickson et al., 1996), while low or no deep convection in the Labrador Sea is observed. During the years with strong convection,

SUMMER	Number of Observations				
Decades	Surface	uLSW	cLSW	GFZW	DSOW
1910s	431	6	4	0	0
1920s	2173	132	80	29	5
1930s	4612	379	367	187	113
1940s	4157	261	171	88	74
1950s	21603	1374	875	369	251
1960s	24007	1252	669	203	129
1970s	32641	1072	432	93	49
1980s	38051	1486	671	304	251
1990s	148907	1093	380	53	70

Table 4.6: Decadal break-down of summer data in five density classes: Surface, upper LSW, classical LSW, GFZW and DSOW

FALL	Number of Observations				
Decades	Surface	uLSW	cLSW	GFZW	DSOW
1910s	63	0	0	0	0
1920s	49	8	6	7	4
1930s	342	1	0	0	0
1940s	831	1	1	0	0
1950s	3255	65	52	16	18
1960s	6344	319	164	52	13
1970s	9688	431	193	57	19
1980s	19804	1074	396	132	68
1990s	65969	1306	546	108	22

Table 4.7: Decadal break-down of fall data in five density classes: Surface, upper LSW, classical LSW, GFZW and DSOW

the resulting product, the DSOW in this case, becomes fresher and colder. Based on tracer data analysis, the transit time of the DSOW from its formation site to the central Labrador Sea is reported to be between 0.4 and 2.6 years (Smith et al., 2005). This atypical DSOW would, then, lead to freshwater and heat anomalies observed

WINTER	Number of Observations				
Decades	Surface	uLSW	cLSW	GFZW	DSOW
1910s	0	0	0	0	0
1920s	14	0	0	0	0
1930s	294	26	19	6	0
1940s	207	90	18	0	0
1950s	1200	40	37	14	2
1960s	3366	403	283	188	313
1970s	4962	386	230	127	145
1980s	5374	527	245	96	4
1990s	9732	262	118	41	28

Table 4.8: Decadal break-down of winter data in five density classes: Surface, upper LSW, classical LSW, GFZW and DSOW

below 2200 meters once it reaches the Labrador Sea.

The decadal bias in seasonal analysis, or the mismatch of the decadal data volumes between the seasons, is not unique to the fall. For example, there is abundant data from winter in the 1960s, especially from the mid-to-deep water masses. The high density of data is due to the ocean weather ship Bravo being operational in the area, between 1964 and 1974, another period when the Labrador Sea convection was severely reduced and brought to a halt. It is very important to have a continuous record of oceanic properties at depth, as the deep waters formed in the polar regions provide a link between the atmosphere and the ocean. The sinking of the surface waters of the North Atlantic ultimately form the deep branch of the MOC, which controls the world's climate as well as being influenced by it. Therefore, it is possible to infer climate change by following the climate signals ingrained in deep waters.

Having sustained and regular observations is crucial for the study of variability from seasonal to inter-annual and climate time scales. Since the decadal bias affects the seasonal results quite severely, the interpretations derived from the seasonal analysis in this chapter take that into account. In *Chapter* 5, a series of yearly climatologies from three-year running means of the data is prepared for study of the year-to-year variability in the Labrador Sea, with special attention being paid to the seasonal bias for similar reasons.

4.1.2.2 An estimate of seasonal ocean-to-atmosphere heat flux

Upper water properties are the least affected by the temporal bias as there is usually an adequate number of observations from every decade. Therefore, concentrating on the top ≈ 300 meters of the water column, an average ocean-to-atmosphere heat flux in the interior can be calculated from the seasonal heat content by assuming that the heat content change has resulted from a heat flux to the atmosphere.

Steffen and D'Asaro (2002) calculated the atmospheric heat flux during a convection event recorded by Lagrangian floats in February, 1997. Two temperature profiles, one taken before the convection started, and one just after the convection ceased are used in their calculation. They calculated the heat content change in the upper ocean, i.e. heat flux to the atmosphere, according to the following formula:

$$Q = \rho c_p \frac{\int (\theta_2 - \theta_1) dz}{\Delta t} \qquad (4.1)$$

where θ_1 and θ_2 are the two temperature profiles, Δt is the time interval between the two profiles, ρ is the density and c_p is the heat capacity of seawater.

In this study, instead of using individual temperature profiles, the climatological heat content of the top $300m$ of the water column is used. The heat content reaches its maximum in fall (before convection), and its minimum in winter (during and just after convection). Therefore, these two seasons are used to calculate the heat flux to the atmosphere . By using the total heat content of the top $300m$, a net heat flux of $\sim 136Wm^{-2}$ from the ocean to the atmosphere is calculated from the seasonal climatologies, as follows:

$$Q = \frac{Q_{H_{fall}} - Q_{H_{winter}}}{\Delta t \times A} \qquad (4.2)$$

where $Q_{H_{fall}}$ and $Q_{H_{winter}}$ are the heat content of the top $300m$ of the water column in fall and winter, respectively. Δt is the time interval and A is the surface area of the region defined as the "interior" Labrador Sea ($\approx 3.4 \times 10^5 km^2$).

Considering that this value represent the long-term mean heat flux over a large area, it is in good agreement with Steffen and D'Asaro's (2002) value of $\sim 175Wm^{-2}$, for the top 600 m of the water column, from a single profile taken directly inside a convection site.

4.1.2.3 An estimate of the LSW formation rate

A depth versus density plot (Figure 4.4) places the 27.74 and 27.80 potential density surfaces between the depths of $650 \pm 100m$ and $1750 \pm 100m$, respectively. This figure indicates that the LSW density surface deepens in winter, after deep convection occurs; it also shows that the rate of change of density with depth, which can be considered as a measure of density stratification, is greatest in fall, the season preceding deep convection. The density stratification has to be overcome for convection to occur. Immediately before and during the convection, stratification is disturbed by buoyancy loss to the atmosphere, whereas restratification occurs rapidly after the end of convective overturning.

Figure 4.4 shows that the upper bound of the LSW density surface is located at almost the same depth in winter and fall. The volume of newly produced LSW between these two seasons can be estimated by the deepening of the lower bound of the LSW density surface, which is at approximately $70m$. By multiplying the increase in depth by the surface area of the interior Labrador Sea, the additional LSW produced during convection is estimated to be $28,000 \ km^3$, which corresponds to a volume flux of $\approx 3.6Sv$.
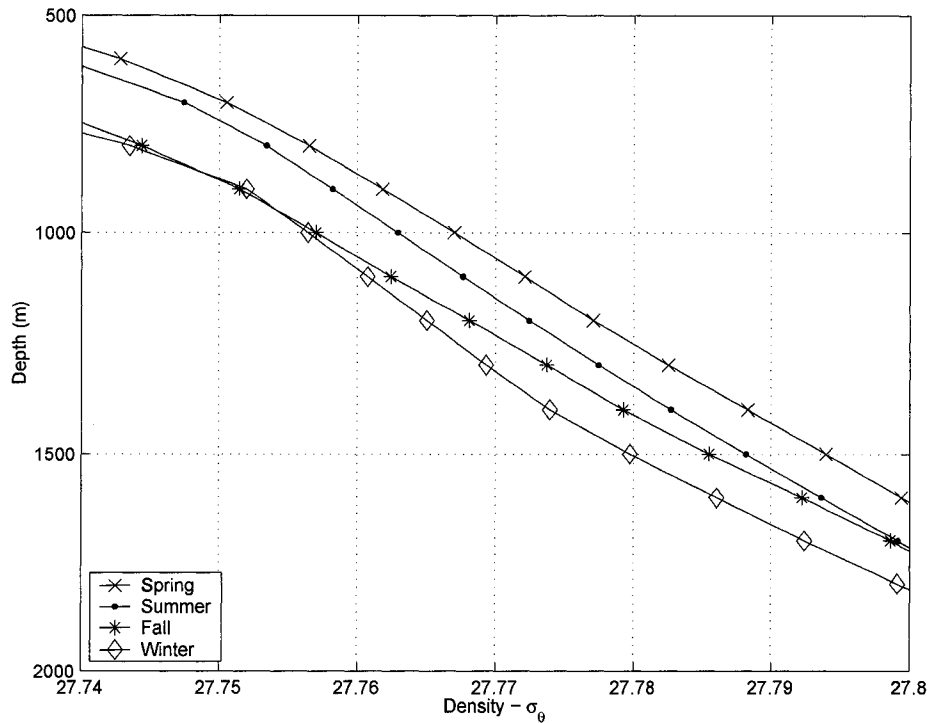
Figure 4.4: Density vs. depth plot between 500 and 2000 meters in all four seasons.

4.2 Freshwater Exchange Between the Shelf and Interior

A seasonal analysis of the freshwater exchange between the boundaries of the Labrador Sea and its interior is discussed in the following section from a steady-state point of view as the climatology does not include transient features such as eddies, and the velocities calculated from the diagnostic model are the mean velocity

components. However, the exercise of quantifying the freshwater pathways can shed light on the basic mechanisms by which the freshwater enters the interior Labrador Sea. The amount of freshwater present in the Labrador Sea is crucially important for the maintenance of the deep convection in this basin.

The line between the boundary currents and interior Labrador Sea is neither well-determined nor permanent. The boundary currents exhibit variations in their strength, and also their position between the coastline and the interior Labrador Sea changes. However, they generally stay onshore of the 3000 m isobath (Clarke and Gascard, 1983). Therefore, a line which approximates the 3000 m isobath, as shown in Figure 1.2, is chosen as the front between the boundary current system and the interior Labrador Sea.

Since the dividing line used in this study is an approximation to the natural boundary, and the diagnostic calculations are based on a B-grid model, where the salinity and velocity values are half a grid point away from each other, velocity values used in the freshwater flux calculations are the means of the velocities on either side of the salinity. The total freshwater flux at a point on this line is calculated according to formula 3.3. The integration is performed only for the top 2000 meters of the water column where most of the variability occurs.

The broken lines that surround the interior Labrador Sea start with a meridional section off the southern tip of Greenland and circulate counterclockwise around the
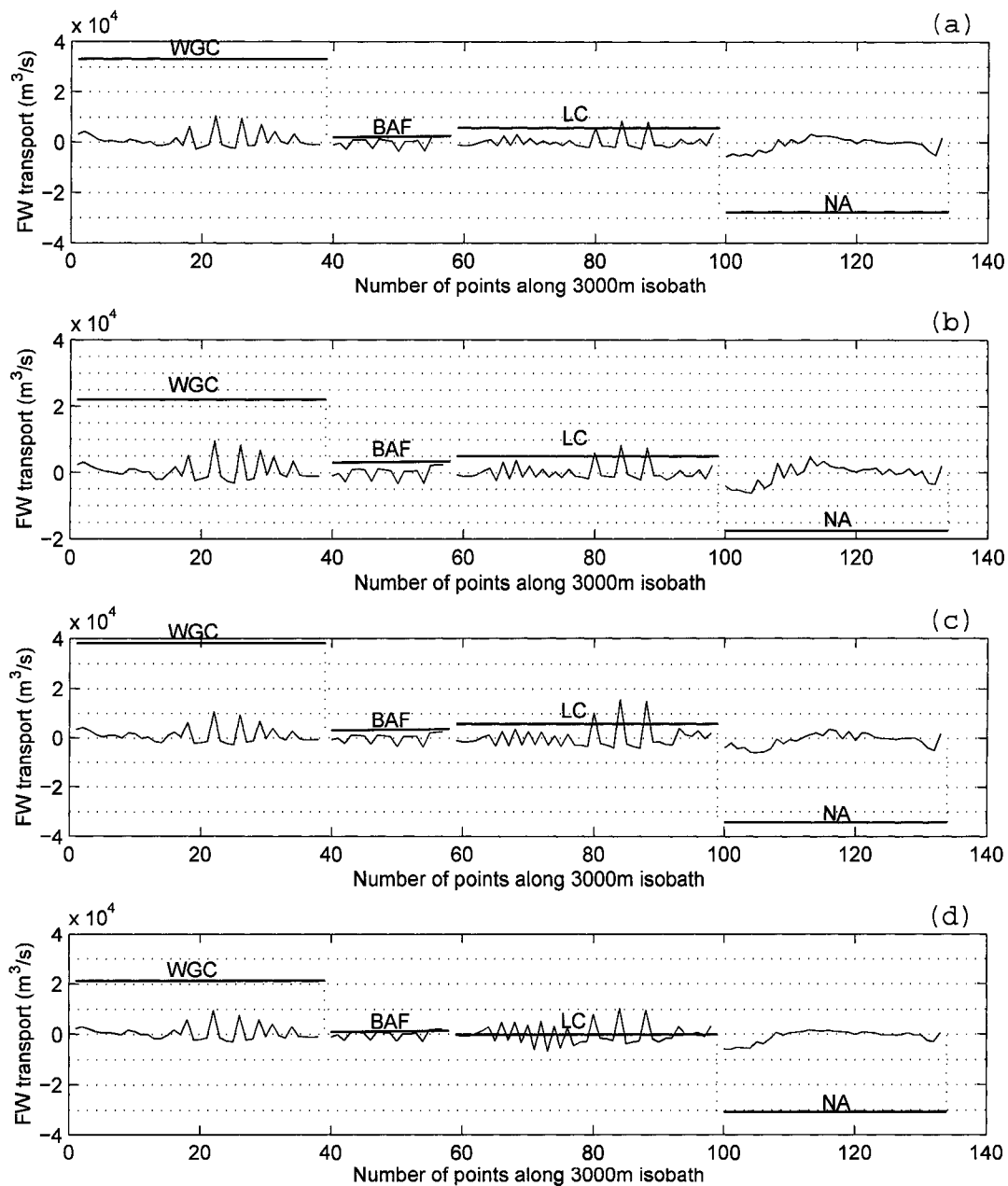
Figure 4.5: Freshwater flux between the boundary system and the interior Labrador Sea plotted along the 3000m isobath shown in Figure 1.2. Over-bars indicate the total freshwater flux originating from four regions: WGC, Baffin Island, LC, and North Atlantic. (a) Spring, (b) Summer, (c) Fall, (d) Winter.

Labrador Sea. The cross-sections are grouped according to the current system or the region to which they are related, starting with the cross-sections related to the WGC and hence the import of freshwater into the interior through this current system. The second region, indicated by black dots, is a transitional zone between the WGC and the LC; the third region is related to the LC, and the last region is located at the opening of the Labrador Sea interior into the North Atlantic.

For all seasons, the addition of freshwater into the interior is dominated by the WGC ($\approx 36mSv$) (Figure 4.5). The contribution of the LC to the interior Labrador Sea freshwater budget stays approximately between 0 and $8mSv$, depending on the season. It was shown earlier in *Chapter* 3 that the LC flows along isobaths and tends not to cross them to enter the interior; this is supported by the fact that the flow will follow f/H lines and the strongly barotropic component of the "deep" LC acts as a natural barrier between the fresh shelf waters and the interior. However, on the Greenland side, the narrow continental shelf, combined with the abruptly varying topography around Cape Desolation, causes the boundary current to separate from the coastline and mix more efficiently with interior waters. As can be seen from Figure 4.5, the largest freshwater import always occurs along the WGC.

4.3 Seasonal Variability of the Labrador Sea Water

Seasonal variability of the LSW is examined with the help of temperature and salinity fields constructed from the original isopycnal climatology (i.e. without being interpolated onto geopotential levels). The property maps shown in Figure 4.6 represent all water masses whose density range is defined as $27.74 \geq \sigma_\theta > 27.80$. The series of plots show the seasonal evolution of the LSW properties; it also hints at the advection path of the LSW out of the basin since these properties are deduced on neutral surfaces.
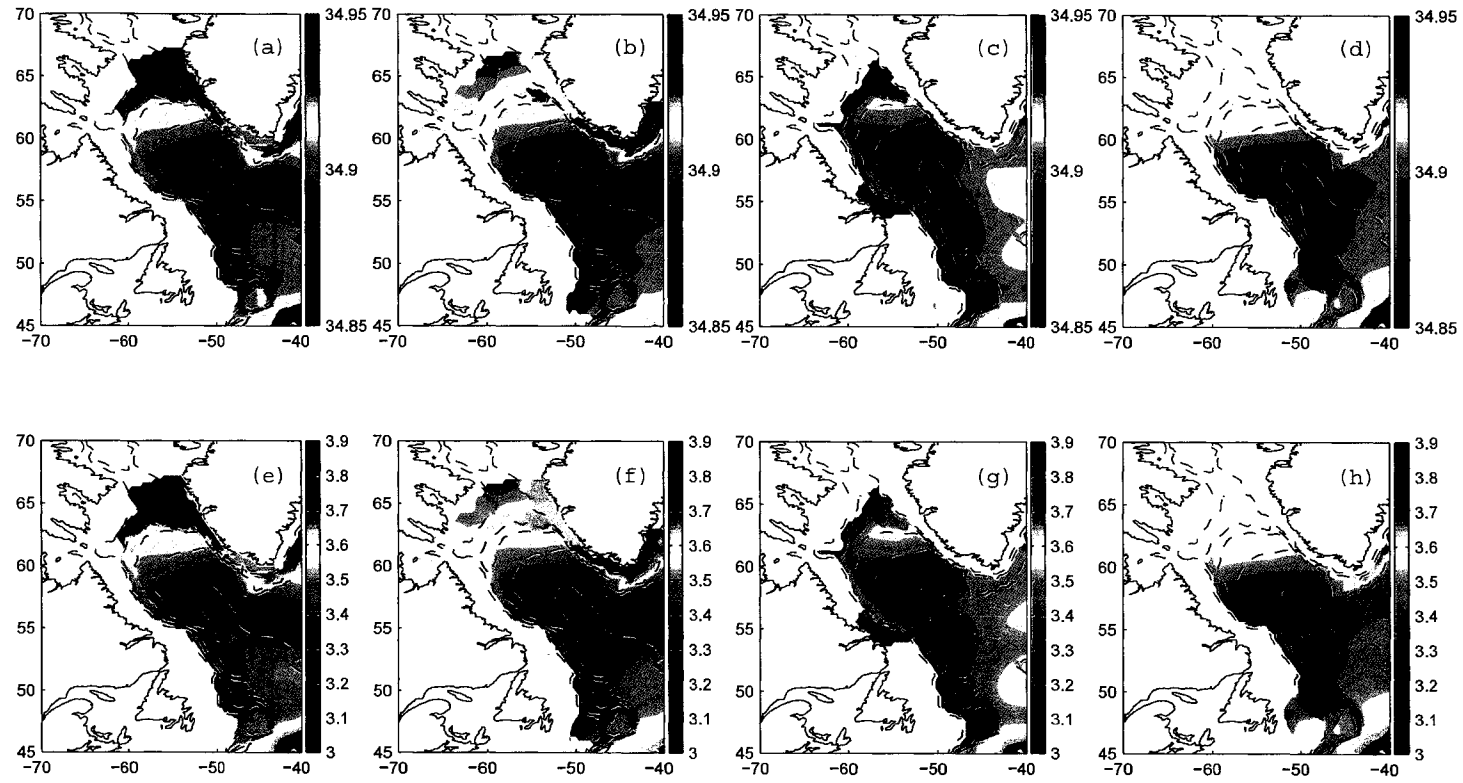
Figure 4.6: Salinity (upper panels) and temperature (lower panels) field obtained from the seasonal climatologies. (a,e) spring, (b,f) summer, (c,g) fall, (d,h) winter.

In winter, the freshest water is found just offshore of the $3000m$ isobath, a location at which deep convection is known to occur in most winters. The freshest and coldest waters were centred further offshore, to the east of this point in the fall. The position of the centre of the LSW in the interior Labrador Sea is most distinct in fall and winter. This occurs because, as already noted in the previous sections, deep convection is the source of sudden property changes in mid-to-deep water masses in the Labrador Sea. Even though the total water column budgets do not change much (Tables 4.1.2.1 - 4.1.2.1), heat and salt are redistributed vertically via deep convection to considerable depths. This causes intermediate to deep water mass properties to exhibit remarkable seasonal variability in the Labrador Sea (Figure 4.6).

Therefore, the magnitude of seasonal variability of the LSW is greater between the fall and winter, i.e. before and after the deep convection. LSW properties change more gradually during the rest of the year. For example, the centre of the freshest/coldest LSW continues its eastward progress following the winter convection as this new convective product fills the basins and flows into other parts of the North Atlantic (Figure 4.6). Eastward advection of LSW can be recognized in all seasonal property maps, but most profoundly in summer. This could be due to the high data density in summer months and hence the higher quality of the climatology for this season in particular. Nevertheless, such notable differences raise the question: do the advection pathways show a seasonal dependency or preference?

In order to further investigate seasonal variability, diagnostic velocities are calculated for various seasons. Cross-sectional velocity plots along the eastern section (Figure 4.7) indicate that the LSW advection rate to the eastern basin is lowest in winter and summer, and highest in spring and fall. In addition, the location and width of east-west flowing currents across the 44°W longitude are similar, not in consecutive but in alternate seasons; this points to a fairly high-frequency variability across the eastern transect. However, such high-frequency variability is not observed, for example, across the southern transect (figure not shown).
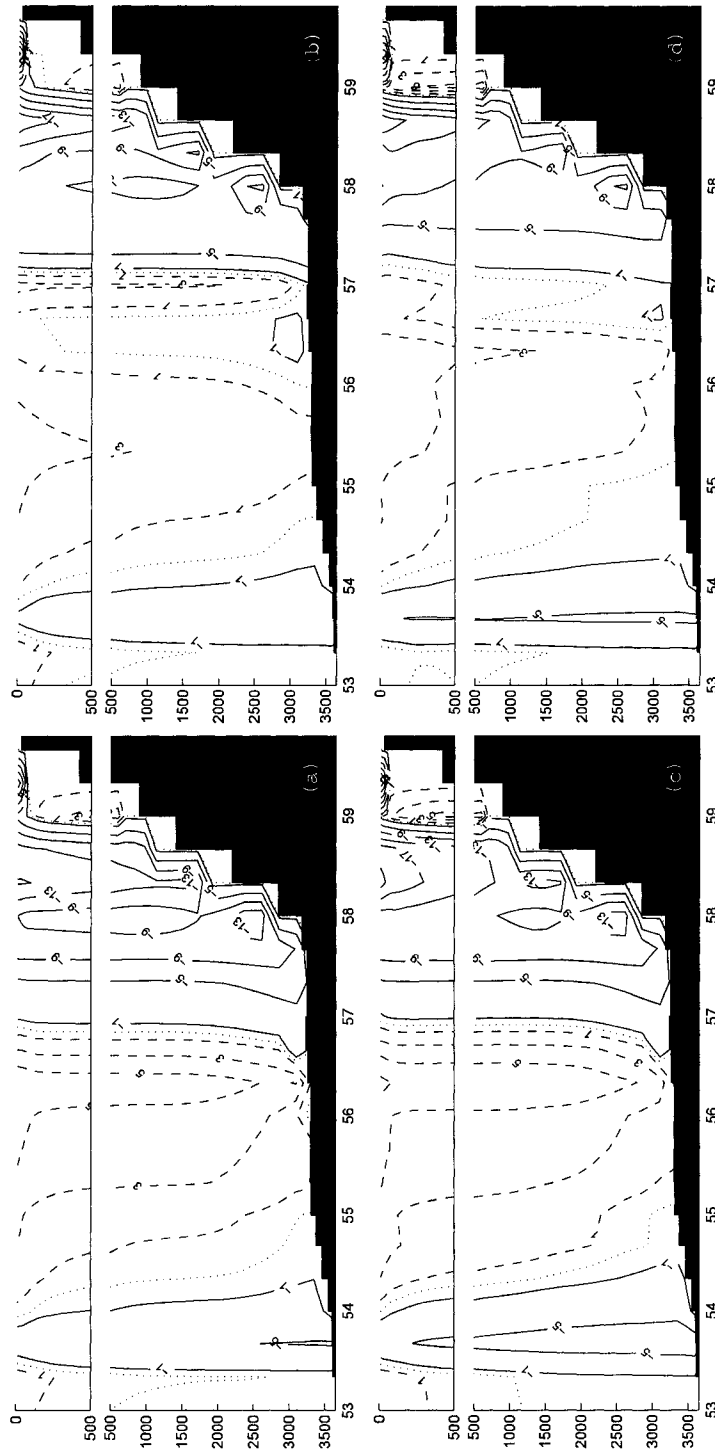
Figure 4.7: Seasonal velocity cross-section across 44°W longitude. (a) spring, (b) summer, (c) fall, (d) winter.

It should be noted here that the diagnostic velocity calculated from the model is a possible response, but not the absolute response of the flow field to the forcing and initial conditions imposed by the model inputs. The uncertainty about the advection of LSW out of the basin is great as there its production exhibits great variability from year to year. Increased use of Lagrangian floats provides valuable information about the mid-depth circulation in the Labrador Sea and its surroundings. However, questions such as how the LSW crosses the natural boundary formed by the NAC to the south still remain since the Lagrangian floats have failed to reveal the southern pathway of the LSW with clarity (Lavender et al., 2000). Seasonal to decadal variability of deep water pathways is considered a possibility and is being investigated (Straneo et al., 2003). The seasonal and yearly climatologies provide a way of examining the underlying mean flow structure in a highly variable environment.

Another contribution of Lagrangian floats is the discovery of a number of deep-reaching (at least including the LSW layer) recirculation cells (Lavender et al., 2002). Temperature and salinity fields plotted from the fall climatology on the LSW density surface (Figure 4.6) show an area, to the south of LSW formation site, with strong LSW-like properties. Its location coincides well with one of the recirculation cells presented in Lavender et al. (2002) (their Figure 4). If the LSW gets trapped in a recirculation cell, its advection rate would be moderated by that cell, causing a delay in spreading of the high-latitude freshwater and heat anomalies to the rest of the

world oceans. However, why the effects of the southern recirculation cell are only apparent in the fall climatology is not clear. A temporal bias does not seem to be the issue here since the seasonal data collected in the LSW density surface has a fairly uniform decadal distribution (Tables 4.1.2.1 - 4.1.2.1). In that case, a possible explanation might be that the southern recirculation cell is stronger in fall, perhaps due to the seasonal variability of the local forcing. Considering the implications of the spreading of LSW on the climate, the recirculation cells and their role are worth further investigation, perhaps in a future study.

4.4   Seasonal Variability of the Mixed Layer Depth (MLD)

The mixed layer depth is an important feature of the atmosphere-ocean system, which has pertinence to a wide variety of oceanic problems, from biological productivity to numerical modelling. The thickness of the mixed layer is determined by the processes of both oceanic (e.g. buoyancy changes in the sea water, convective mixing) and atmospheric origin (e.g. transfer of momentum from the atmosphere to the ocean by winds and solar heating). The determination of the MLD from a density (or temperature) profile has been the subject of many studies, since, like many other oceanic problems, the determination of the MLD depends on a number

of factors, which vary on multiple temporal and spatial scales. Seasonal variability is the fundamental mode of variability in MLD. The aim of compiling seasonal MLDs is to study the range of seasonal MLD variability, as well as to provide a basic set of climatological MLD values, which can be used to initialize coupled ocean-atmosphere models or to compare their results.

There is no straightforward method to determine the MLD under all circumstances. However, a method proposed by Kara et al. (2000) provides promising results for its applicability to a large number of cases (Kara et al., 2003). According to this method, density profiles are scanned from top to bottom to find a density increase between two consecutive points which exceeds a pre-determined criterion. This density criterion can also be related to a preset temperature or salinity change. The original method sets the density criterion based on a preset temperature value. The Kara et al. (2000) method used in this study has been modified to capture some of the observed properties of the MLD in the Labrador Sea. First, a wider temperature change, $\Delta T = 2°C$, is chosen because the temperature does not have as strong an influence on density as the salinity at these latitudes. The density criterion is, then, defined as $\Delta \sigma_{t,s,0} = \sigma_{t,s,0} - \sigma_{t+2,s,0}$.

Since the climatologies are computed by taking the mean of individual observations over space and time, most of the fine-scale structure is eliminated. Therefore, the MLDs calculated from the seasonal climatologies are underestimated. The shallowest

MLDs are observed in fall (Figure 4.8c), with depths $\leq 65m$, when the stratification of near surface waters are strongest due to increased freshwater input to the Labrador Sea. This result agrees with the freshwater budget results discussed in Section 4.1. Unrealistically deep MLDs are found in the areas influenced by the IW, where the temperature criterion adjusted to work in the interior Labrador Sea seems to be inappropriate. However, resolving the MLD inside the Labrador Sea was given priority in this study. Since the intrusion of IW at mid-depths modifies the vertical profiles of the water column, setting a different criterion in the area affected by the IW might provide a solution. However, this causes MLD fields to be discontinuous in the study domain.

The deepest MLDs are found in winter (Figure 4.8d). Even though this is expected owing to increased wind mixing in winter, here, the location of the maximum MLD also coincides with a well-known deep convection site, just to the offshore of the $3000m$ isobath. The largest MLDs are in excess of 600 meters, and are concentrated over a small area, which is consistent with the fact that deep convection takes place in relatively small patches. The deepest MLD, albeit shallower, exhibits a structure similar to the found in a recent modelling study (Deshayes et al., 2007). In fact, $1/3°$ horizontal resolution is too large for resolving the MLD change due to convection; therefore, an MLD of ≥ 600 m, even though much smaller than the value obtained by direct observations of the deep convection, is reasonable for a climatological study.
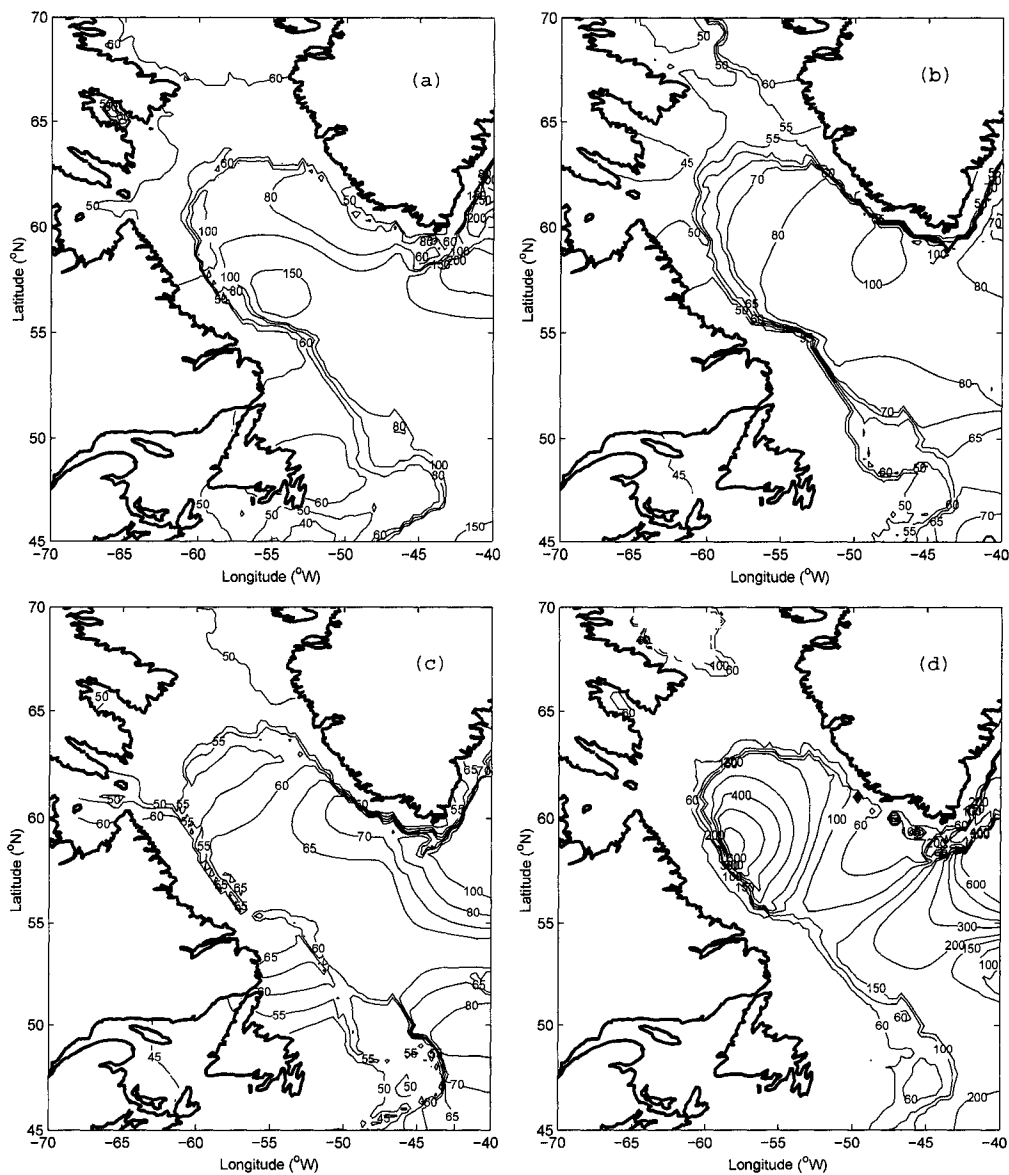
Figure 4.8: Mixed layer depths (MLDs) calculated from the seasonal climatologies by Kara et al. (2000) method. (a) spring, (b) summer, (c) fall, (d) winter.

Moreover, the climatology includes the winters when the convection was not strong enough to effectively mix the water column.

The centre of the MLD maximum shifts to the south in spring, after winter convection, and has a much lower value ($\leq$150 metres). Restratification of the water column occurs rapidly, following the convective overturning (Straneo, 2006). The lower MLD values found near the convection site are a result of restratification of the water column immediately after winter convection, in addition to the reasons stated above. Shoaling of the MLD continues in summer and fall.

Chapter 5

Inter-annual Variability

Encouraged by the results of the yearly and seasonal climatologies discussed in *Chapters* 3 and 4, the OA method (*Chapter* 2) is applied to data collected over shorter time periods, in an attempt to produce pseudo-time-series of the Labrador Sea hydrography.

The motivation for constructing the time-series comes from the knowledge that the Labrador Sea experiences variability on multiple timescales. For example, in addition to the reports of freshwater pulses circulating around the sub-polar gyre and entering into the Labrador Sea (e.g. Dickson et al., 1988; Belkin, 2004), there have been reports of long-term changes in intermediate-to-deep water masses in most of the North Atlantic water masses, including the Labrador Sea water masses (e.g. Dickson et al., 2002). These reports are, generally, based on repeated observations

along a ship-track, such as AR7W of the WOCE program, or point-wise observations, such as deployments near the OWS-Bravo. However, time-series based on such observations face limitations due to their incoherency in time, space or both, and other experimental factors such as inevitable changes in ship tracks and instrument failures.

In this study, grouping all the available data in overlapping three year periods and then objectively mapping them onto isopycnal surfaces is preferred. The advantage of gradually filling data laden grid points without superfluous smoothing of fronts, as discussed in detail in the methods chapter, is found to be critical in achieving a continuous time-series of the water properties everywhere in the study domain. Furthermore, diagnostic calculations are performed in the same manner as with the yearly (and seasonal) climatologies to calculate current velocities and volume fluxes.

In summary, such time-series allow us to re-construct the spreading of freshwater pulses as well as longer-term, steadier changes in the Labrador Sea; to examine the variability in the amount of heat and freshwater stored in the basin; to link those changes to atmospheric indices (e.g. the NAO index); and finally, to investigate variability in volume fluxes of various components of the MOC in and out of the Labrador Sea. The goal is to achieve a better understanding of the causes and effects of Labrador Sea variability.

5.1 Method

Before going into the discussion of the results from the time-series study, the modifications and new procedures introduced to adjust for the reduced data volumes are outlined. The first task was to decide on the period of the time-series. The number of observations available up until the mid-20th century was significantly low for performing short time period climatologies; therefore, 1948 and 2000 are set as the lower and upper bounds of the time-series. The last update of the data downloaded from the BIO database was performed in early 2002 and all the data collected up to 2001 were included in this study. Generally, it takes at least a couple of years for the raw data to be quality checked and added to such large databases.

The second important task was to choose an appropriate time period over which the individual climatologies would be produced. The major concern was to make sure that there are sufficient number of observations during each of these periods without compromising the inter-annual signal variability by keeping the period too long. It was decided that grouping all available data in overlapping three-year periods would provide the best solution for this purpose. For example, to objectively map property fields in the year 1949, the data collected in the year immediately before, the year 1948, and the year after, 1950, are binned together with the same weight. The climatological property fields of the year 1999 include all the data from 1998 to 2000, and so on. Since calling the individual three-year averages a climatology is

inappropriate given the short time period over which the mean state is calculated, from now on they are called triad (three-year) results.

During the objective analysis, special care was given to the imbalance of data volumes in different seasons. Typically, cold and stormy months have fewer observations available, and this was dealt with by assigning variable weights to each month in the yearly climatology. In the triad analysis, a seasonal weighting is introduced during the objective analysis to counteract temporal bias. Since the seasonal cycle is the most pronounced variability in the ocean, seasonally-skewed data volumes can mask or exaggerate inter-annual to decadal variability (Hátún et al., 2005). Figure 5.1 shows the seasonal distribution of data in each triad. Even though the winter properties are strongly under-represented compared to summer values, the relative contribution of seasons does not seem to vary inter-annually, which indicates that inter-annual to decadal oscillations are not a consequence of seasonal imbalances in the data volumes.

Another modification introduced during the objective analysis was to enlarge the three search radii from $R_1{=}500$ km, $R_2{=}300$ km, $R_3{=}150$ km of the yearly and seasonal climatologies to $R_1{=}600$ km, $R_2{=}400$ km, $R_3{=}200$ km, in the triad analysis. This is not a significant increase in the search radii, and considering that the depth dependence criterion was kept the same, it would not have made sense to increase them any further. However, to account for reduced data volumes in search radii,
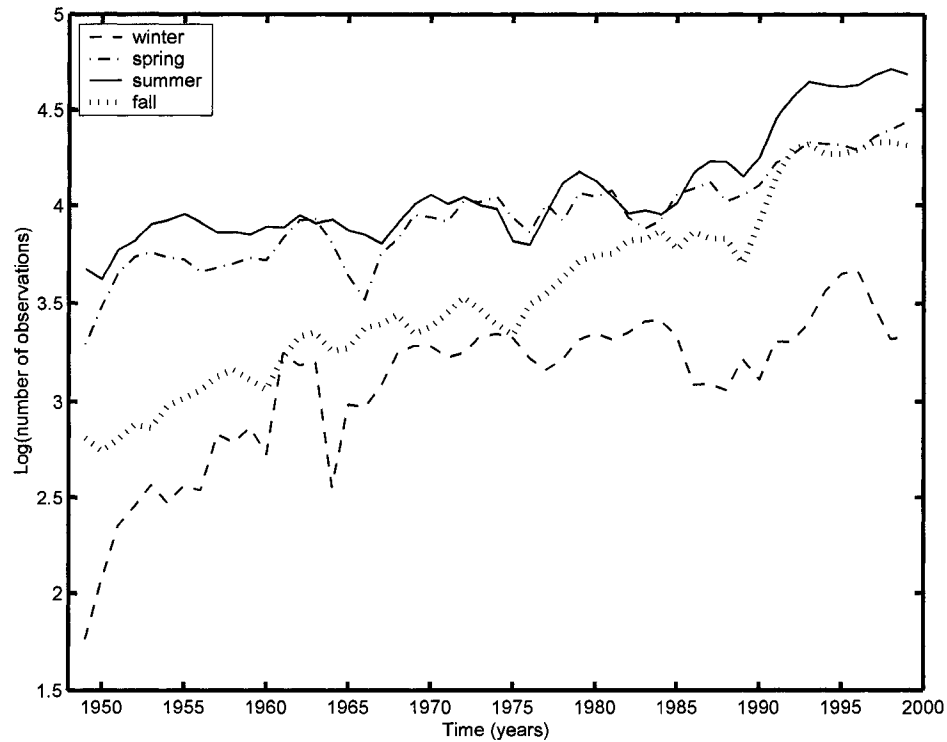
Figure 5.1: Seasonal distribution of data used in the triad (three-year running mean) analysis

a smoothing function, which has the same functional form of depth-dependency as the objective analysis scheme (*Chapter* 2) was applied after every iteration. Also the empty grid points were filled with the value calculated by this smoothing function during the first and second iterations.

The diagnostic calculations were performed in the same manner as described in *Chapter* 2 to produce a series of velocity fields for the period 1949-1999. Hydrographic fields (and hence the current velocities calculated from the diagnostic model) are

unchanged outside the study domain (40-70°W and 45-70°N) where the density field is fixed to the Lozier et al. (1995) climatology. However, inside the Labrador Sea the density field is replaced by the representative density field calculated from the triad analysis. As a result, a three-dimensional velocity field is calculated diagnostically, for each year between 1949 and 1999, for the Labrador Sea. The triad analysis provides us with continuous records of property fields and current velocities.

5.2 Results From the Triad Analysis

The results are discussed under four headings: temperature and salinity time-series, LSW types and their relation to the NAO index, heat and freshwater budgets, and the freshwater flux between the boundary region and the interior Labrador Sea. The oceanic variables are compared with each other and against the NAO index, the dominant mode of atmospheric variability in the area, when relevant. The fifty-one year long time-series provides a strong foundation for studying inter-annual and decadal variability.

5.2.1 Temperature and Salinity Time-series

The temperature and salinity data are objectively mapped throughout the Labrador Sea for the years between 1949 and 1999. Time-series of mean temper-

ature and salinity in the three key regions (Figure 1.2) are shown in Figures 5.2, 5.3, 5.4.

Near surface waters ($\approx$ 0 to 300 m of the water column) exhibit higher frequency oscillations in temperature and salinity, as they are in closer contact with the atmosphere and influenced by the changes in freshwater influx more directly. Also, since the volume of this depth range is smaller, relatively smaller changes in temperature and freshwater input can cause significant changes.

A significant cooling of the near surface waters, accompanied by a significant drop in salinity, is observed in all three regions around the years: 1970, 1984, and 1990. These times correspond to the previously reported GSA events advected around the subpolar gyre (e.g. Belkin, 2004). Although the cooling of surface layers is evident in all regions, the temperature and salinity signature of 1984 is the most noticeable in the LC region. This is consistent with the idea that the 1980s GSA was triggered by the cold winters experienced in the Baffin Bay/Labrador Coast area during the early 1980s (Belkin et al., 1998).

The temperature and salinity anomalies in the Labrador Sea are by no means limited to the surface waters. The time period between the mid-1950s and early-1970s are marked by the warming of near-surface to intermediate waters, in the interior Labrador Sea (Figure 1.2). Between 1952 and 1972, the increase in temperature at 1300m, a typical core depth for the LSW, was 0.5°C. During the same period, salinity
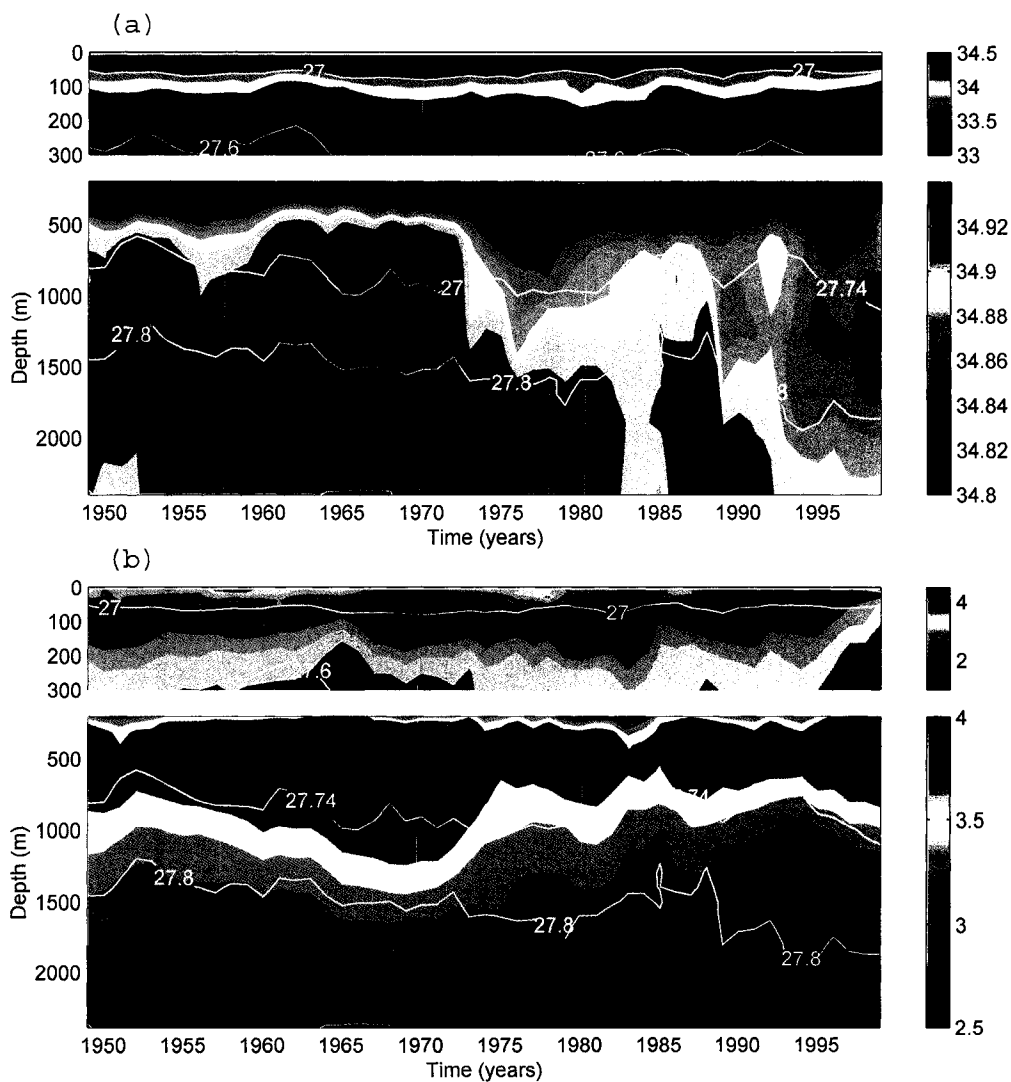
Figure 5.2: Time-series of (a) salinity, and (b) temperature of the WGC region.

increased by 0.03. As a result, the interior Labrador Sea became strongly stratified

and the deep convection was brought to a halt until the cooling of the surface waters

in the winter of 1971-72 was strong enough to break through the stratification (Lazier,

(a)

(b)
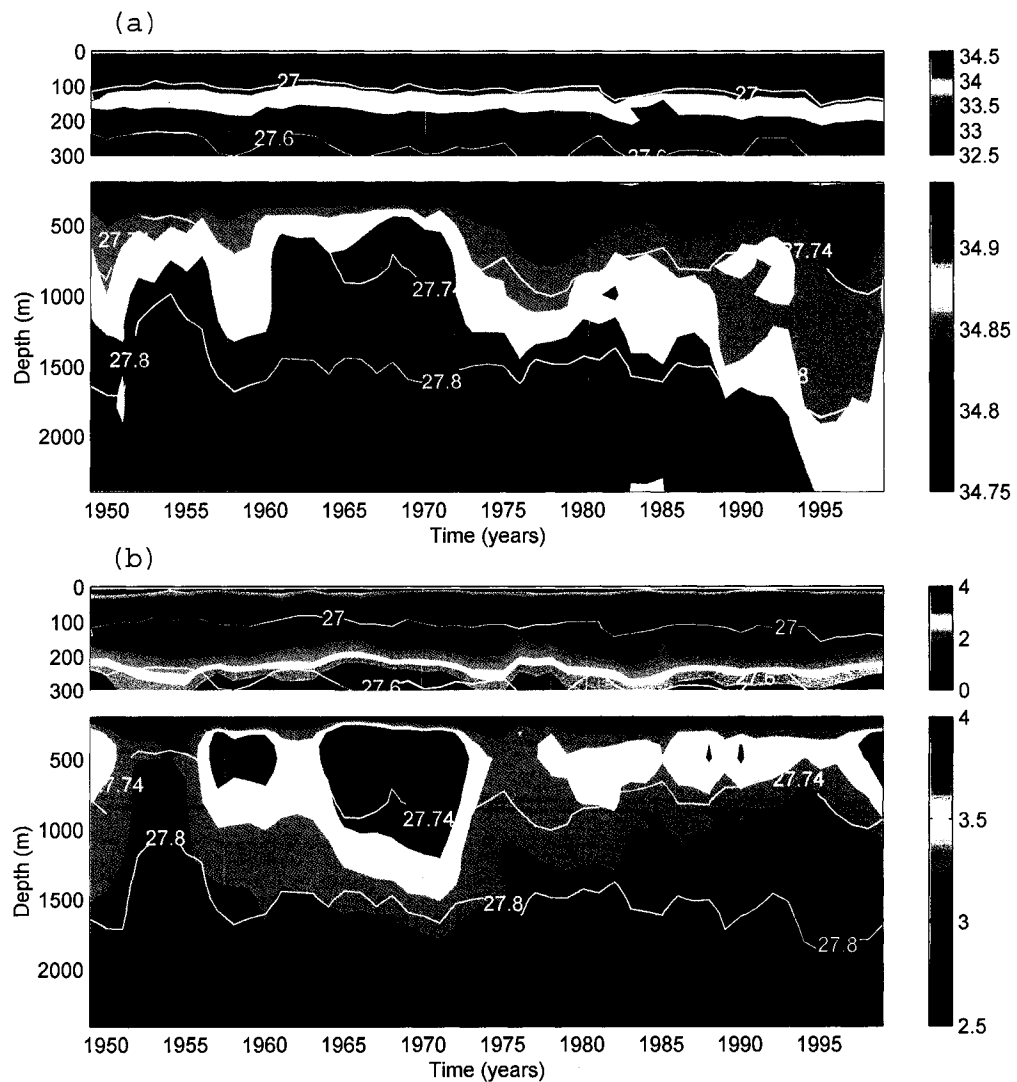
Figure 5.3: Time-series of (a) salinity, and (b) temperature of the LC region.

1980). The intense surface cooling can be seen in the temperature time-series plotted from the triad analysis (Figure 5.4b).

Lazier (1980) reported convective overturning at OWS-Bravo up to 1500 m in
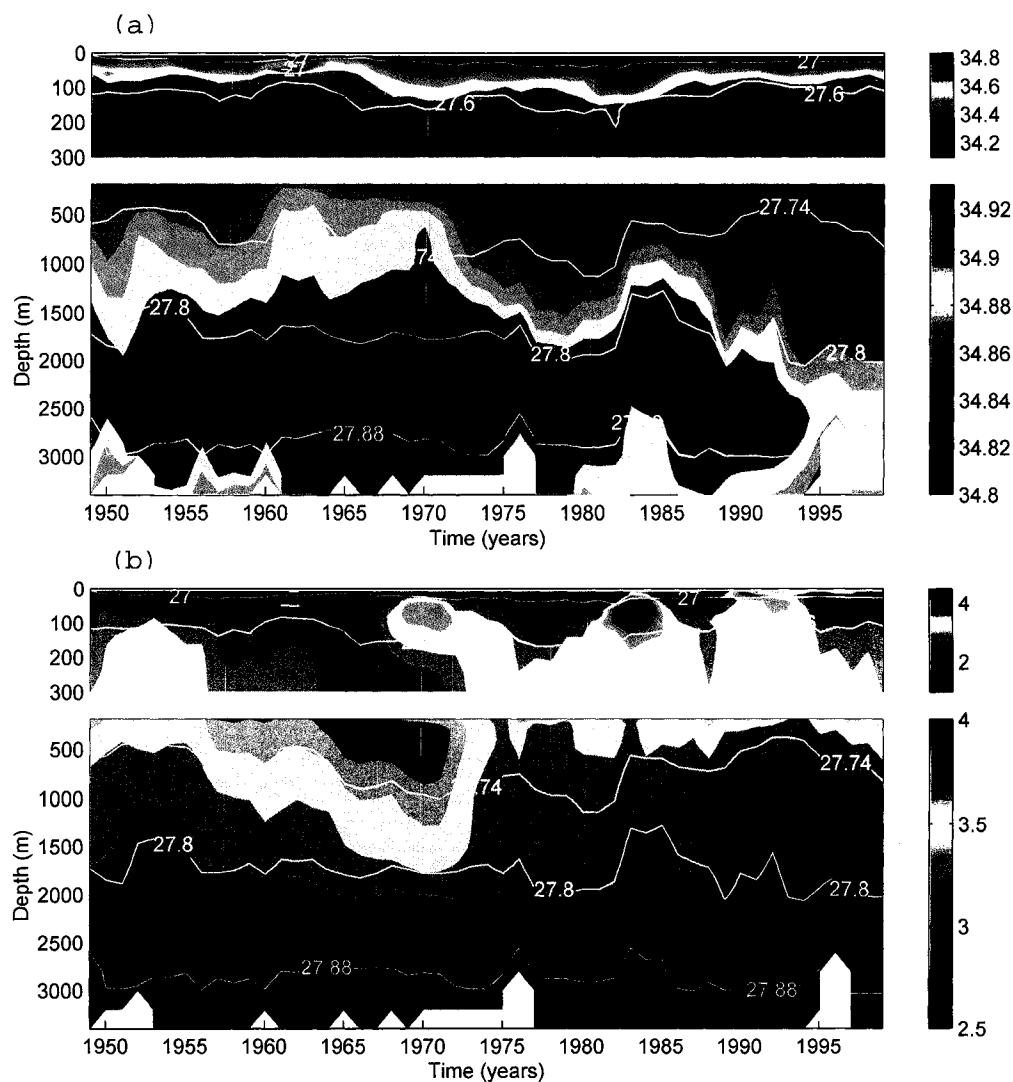
Figure 5.4: Time-series of (a) salinity, and (b) temperature of the interior Labrador Sea region.

1972; that was the deepest observed since this station became operational in 1964.

He also reported two other deep-reaching convective events ($> 1000m$) taking place in the winters of 1964-65 and 1966-67, which cannot be identified from the time-series

produced in this study. These time-series are based on triad analysis, so the results have a temporal accuracy of ± 1 year, which limits the discussion to inter-triad variability rather than inter-annual variability. Variability observed over smaller spatial and temporal scales are filtered out by objective mapping and regional averaging. Yet, considering the lack of long-term systematic observations with fine temporal and spatial resolution in the area (other than the OWS-Bravo and some repeated surveys during oceanographic programs such as WOCE) these results provide the best compromise between spatial coverage, temporal continuity, and precision.

When the deep convection is limited to the surface or shut down, as it was the case in the early 1970s, the cLSW starts to erode. This is reflected in the local minima found in cLSW volume (Figure 5.5). The lack of deep convection causes an increase in temperature (and in salinity) of the LSW density surface, since the mechanism which brings cold and fresh water from the surface to greater depths is interrupted. As a result, the water column becomes stratified even further, and it becomes progressively more difficult for the deep convection to commence. Heat and salt are also added to the LSW through advective and diffusive processes. A sudden change in the interior Labrador Sea temperature and salinity time-series (Figure 5.4) and an increase in the volume of cLSW in the interior Labrador Sea (Figure 5.5) is observed after 1972. With the re-initiation of the deep convection around 1972, warmer and fresher surface waters are brought down to depths greater than $1000m$ and mixed with intermediate

water masses, weakening the stratification.

Starting with the re-initiation of the deep water formation in the Labrador Sea in the early 1970s, the convectively formed LSW became progressively colder and fresher (Figure 5.4). The long-term freshening of the mid-depth waters of the Labrador Sea and the rest of the northern North Atlantic has received considerable attention (e.g. Dickson et al., 2002), as these waters are the key component of the northern branch of the MOC in the North Atlantic, thus providing a link between the atmosphere and mid-depth ocean (e.g. Curry et al., 1998).

The triad analysis shows that the LSW reached its maximum salinity of 34.92 in 1970 (taking the long-term mean core depth of the σ_θ= 27.74 - 27.80 level as $1300m$). The minimum salinity at the same depth is found to be 34.85, in 1995. The maximum temperature at this depth is in 1971 with 3.60°C, and the minimum temperature of the record is 2.85°C, in 1994. These values support the findings of Dickson et al. (1996) that when the deep convection is limited or shut down, the LSW becomes warmer and saltier. It should be noted here again that these values are averaged over time and space; therefore, they are not as extreme as the minima and maxima obtained from individual observations.

5.2.2 LSW types: cLSW and uLSW

The deep convection in the interior Labrador Sea showed signs of becoming weaker in the second half of the 1990s. Based on wintertime observations performed during this period, Pickart et al. (1997) reported that when atmospheric forcing is low, a lighter water mass is formed convectively within the boundary current. He called this lighter water mass the upper LSW (uLSW, σ_θ= 27.68-27.74), as opposed to the classical LSW (cLSW, σ_θ= 27.74-27.80). The uLSW sits above its denser and well-known counterpart. Formation of a variant of the LSW within the boundary current would provide a direct link between the northwestern Atlantic and the subtropics, causing a rapid transport of North Atlantic climate signal to the subtropics (Stramma and Rhein, 2001; Freudentral and Andrié, 2002). The export of LSW out of the basin has great importance in the maintenance of the MOC. Therefore, this section focuses on identifying the lighter convective product and its formation region.

The slope region[1] defined in Figure 1.2 lies onshore of the $3000m$ isobath. This area is kept ice-free by the heat supplied from the IW, exposing the surface waters to extensive heat loss to the atmosphere in winter months. Also the recirculation cells found in the area (Lavender et al., 2000) trap the surface waters enhancing their exposure, and hence increase the likelihood of deep convection.

---

[1]So as not to confuse this smaller region with the "boundary" region, which is used to indicate WGC and LC regions collectively throughout the text, this smaller region where "boundary convection" is proposed to happen is referred as the "slope" area.
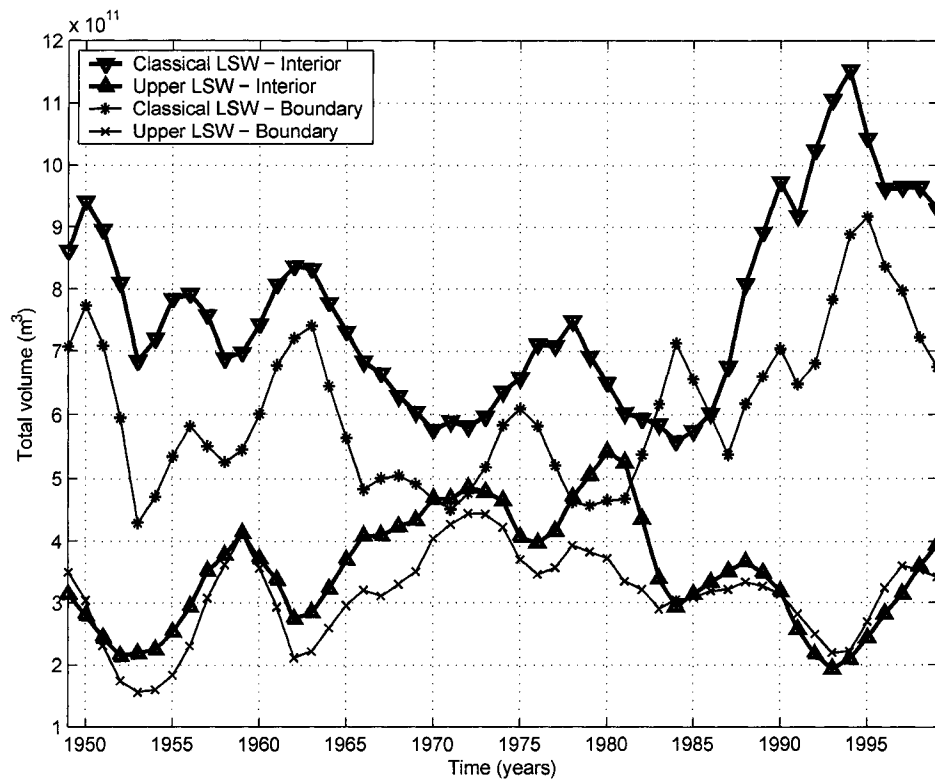
Figure 5.5: Volume of uLSW and cLSW masses in two different regions: the interior Labrador Sea and the "slope" region where "boundary convection" takes place.

The time-series of the upper and classical LSW volumes averaged over the interior and slope regions are presented in Figure 5.5. In both regions the upper and classical LSW volumes vary out-of-phase, i.e. when the uLSW volume increases, the cLSW volume decreases; this can be explained by variations in the strength of deep convection. Winters with strong deep convective overturning would produce the heavier cLSW, causing an increase in its volume. On the other hand, weak convective events will produce the lighter component, the uLSW, without adding new volume

to the classical LSW. Without the addition of newly formed water masses via deep convection, both water masses would shrink in volume as they both are transported out of the basin as part of the cyclonic sub-polar gyre circulation at depth.

A reduction in the classical LSW volume during the period 1962-1970 was followed by an increase during 1972-1977 (Figure 5.5). This is in agreement with deep convection becoming weak in most of the 1960s followed by the re-initiation of it in the early 1970s, as discussed in the temperature and salinity time-series section above. A shift in the NAO index (Figure 5.6) from a negative phase to a positive one is given as the reason for the re-initiation of convection in the central Labrador Sea (e.g. Curry et al., 1998). A positive NAO index is associated with stronger westerly winds blowing over the Labrador Sea. These winds bring cold and dry Arctic air into the area, enhancing the heat loss to the atmosphere by the ocean, which promotes deep convection since surface waters lose their buoyancy as they become colder.

As pointed out by Curry et al. (1998), the NAO index is not the only factor controlling deep convection in the Labrador Sea. Large freshwater anomalies (e.g. Dickson et al., 1988) which spread through the sub-polar gyre, influence the LSW water formation. During the 1970s GSA event, the cLSW volumes were decreasing in the both the slope and interior area while the volume of the uLSW showed a steady increase (Figure 5.5). This result suggests that the uLSW may be the only water mass formed when deep convection is weak.
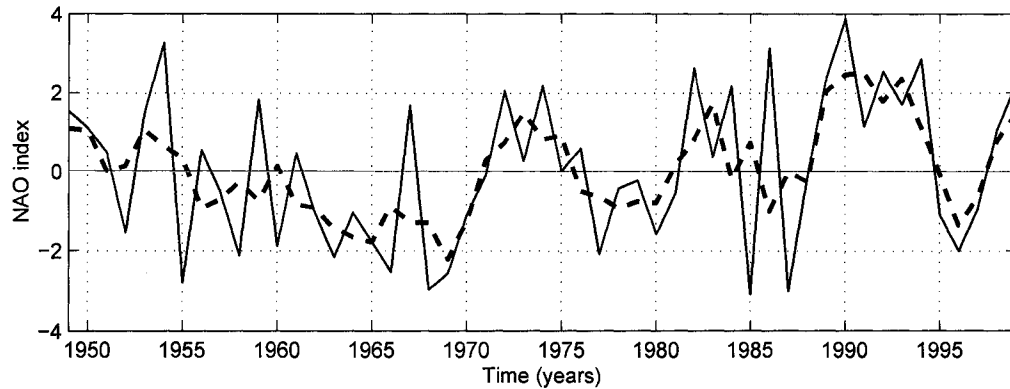
Figure 5.6: NAO index reproduced for the years between 1949 and 1999. Solid line is the annual NAO index, the dashed line is the 3-year running mean calculated from the annual NAO index

Important differences were noted between the 1970s GSA and the 1980s GSA, in terms of their origin (Belkin et al., 1998). The 1980s GSA is thought to have originated in the Labrador Sea, triggered by extremely cold winters experienced in the area immediately preceding it. The source of the 1980s GSA cannot be identified from the results shown here; however, the signature of the 1980s GSA is most prominent in the LC area. When the freshwater anomaly reached its peak in the LC area in 1984 (Figure 5.4), the volume of cLSW in the slope area also reached a local maximum while cLSW volume in all other regions decreased (Figure 5.5). This result suggests that, when conditions are right, boundary deep convection can produce cLSW.

After the spread of the 1980s GSA in the interior Labrador Sea, the volume of the classical LSW increases rapidly at first, then stays approximately constant be-

tween 1988 and 1991, before reaching its absolute maximum in 1994, with a value of $1,15 km^3$. The classical LSW volume in the slope region shows similar oscillations to that of the interior, although differences are also noticeable, suggesting that atmospheric and oceanic processes are different between the slope region and the interior Labrador Sea. The decrease observed in the classical LSW volume in the later part of the time-series is consistent with the slowdown of the deep convection in the interior Labrador Sea and drainage of this water mass out of the basin.

On the other hand, the upper LSW has increased in volume since the NAO index became weaker in 1998. Moreover, during the 1990s, the average volume of the upper LSW was slightly larger in the slope region than in the interior, which suggests higher formation rates for the upper LSW in the slope region. These results also imply that deep convection is occurring in the slope region, inshore of the $3000m$ isobath, and that this process might be happening at recognizable rates only recently.

5.2.3 Interior-boundary freshwater exchange

The boundary currents, WGC and LC, are the sources of freshwater for the interior Labrador Sea. The question of how much of the freshwater contained in the boundary currents leaks into the interior Labrador Sea and their inter-annual variability is examined.

The results of the boundary-interior freshwater flux calculations are summarized

in Figure 5.7. The largest positive input of freshwater into the interior Labrador Sea is from the WGC. The largest freshwater input from the WGC coincides with the 1970s GSA, whose signature embedded in the WGC was the largest, as shown in previous sections. Most of other peaks in the WGC freshwater supply to the interior roughly match the GSAs of other decades but not always.
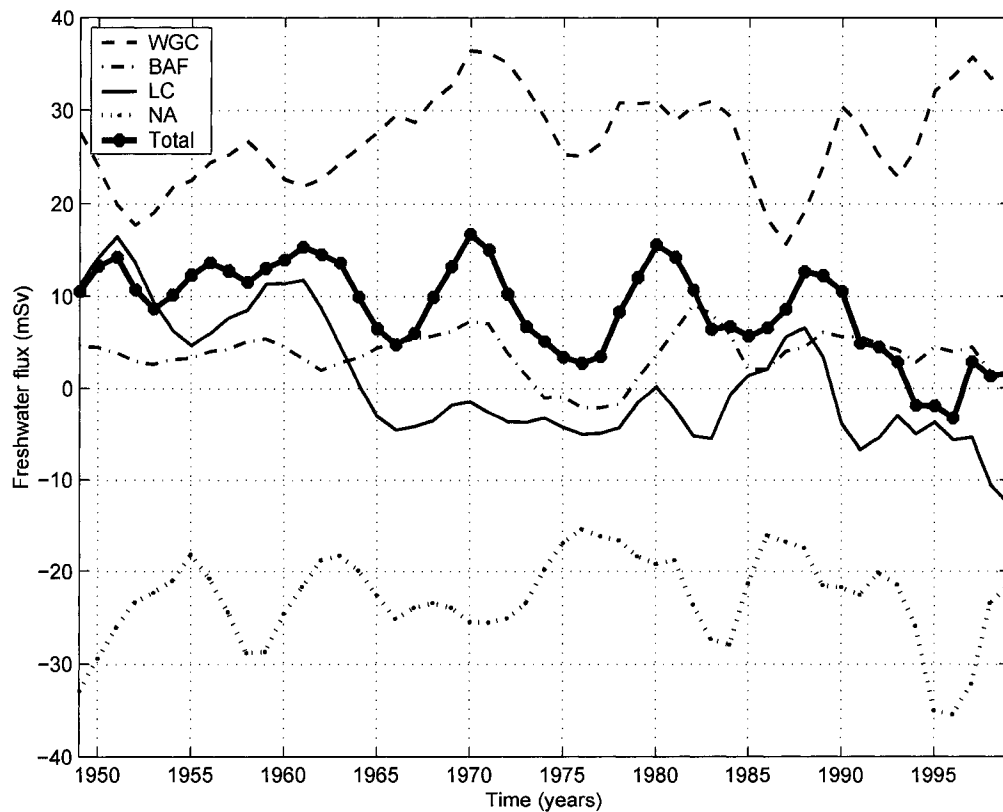
Figure 5.7: Time-series of the freshwater flux between surface and $2000m$. Different lines correspond to regions where these fluxes have originated or be directed to. See Figure 1.2 for the location of the closed contour along the $3000m$ isobath across which the freshwater fluxes are calculated.

The freshwater flux between the interior Labrador Sea and LC takes a negative value occasionally, indicating that LC can act as a freshwater sink for the interior Labrador Sea as well as a source (Figure 5.7). The negative freshwater flux is probably an artifact of the choice of the dividing line between the interior Labrador Sea and LC. The 3000 m isobath falls farther from the Labrador Coast than is the case for the WGC. Moreover, inter-annual variation in the sub-polar gyre strength and location can account for the negative supply of freshwater by the LC. The link between the reported weakening of the sub-polar gyre (Häkkinen and Rhines, 2004) and reduced freshwater supply by the LC during the 1990s is noted. Another important conclusion that can be drawn from the LC as a sink of freshwater is that, even though the surface LC carries fresher waters than the surface WGC (Table 3.4), since the former flows along isobaths rather than across isobaths, most of the freshwater contained in the LC leaves the Labrador Sea without meeting the interior waters.

The correlation coefficient between the freshwater flux by the WGC and LC is found to be -0.66. This result suggest that there is a significant, inverse relationship between the freshwater flux provided by the WGC and the LC to the interior. The mean and standard deviations of the freshwater fluxes by the four transects can be found in Table 5.1. Even though the freshwater flux by the LC is negative over some periods (1964-1984 and 1989-1999), the long-term average freshwater contribution of the LC to the interior is positive.

	Mean FW flux$(m^3 s^{-1})$	STD (σ)
WGC	2.62e4	5.04e3
BAF	3.74e3	2.36e3
LC	1.14e3	6.52e3
NA	-2.25e4	4.72e3

Table 5.1: 51-year mean and standard deviation of freshwater influx to the interior Labrador Sea.

The freshwater flux across the transitional zone between the WGC and LC reflects the importance of local factors and the Canadian Arctic Archipelago (CAA) as a freshwater supply to the interior Labrador Sea. The freshwater flux from this region is consistently small and positive, except during a brief period between 1974 and 1978. The maximum in the freshwater flux in 1982-1983 agrees with the observation of cold and fresh surface waters in this region (Belkin et al., 1998).

Among the four sections, the one that gives persistently negative freshwater volume fluxes, and hence balances the freshwater budget of the interior, is the long diagonal line which separates the interior Labrador Sea from the rest of the North Atlantic. This occurs because this cross-section is on the exit route of the major water masses such as the LSW and DWBC on the Labrador side, and on the route of warm and salty IW into the interior.

Chapter 6

Interdecadal Variability in Labrador Sea Precipitation Minus Evaporation and Salinity*

6.1 Introduction

A number of recent studies (Dickson et al., 2002; Curry et al., 2003; Curry and

Mauritzen, 2005) have suggested that the North Atlantic Ocean at high latitudes has

been freshening over the last several decades. As the North Atlantic is one of the

few regions of the world ocean where deep waters are formed, this freshwater signal is being transferred into the deep oceans (Dickson et al., 2002). The North Atlantic is a major source of deep waters for the world ocean and thus, a key player in the global meridional overturning circulation. This source is potentially very sensitive to additions of freshwater, through freshwater's role as a stabilizing element in the buoyancy budget. Sources for the enhanced supply of freshwater to the northern North Atlantic over recent decades include changes in excess precipitation (Josey and Marsh, 2005), river runoff (Peterson et al., 2002), melt from the Greenland ice cap (Steffen et al., 2004) and the export of sea-ice from the Arctic Ocean (Dickson et al., 2000; Vinje, 2001).

As well as the long term freshening, observations have been made of strong low salinity anomalies propagating around the sub-polar gyre (Dickson et al., 1988; Belkin et al., 1998) during the 1970's, 1980's and possibly 1990's. These events, termed Great Salinity Anomalies (GSAs), were tracked passing from the Nordic Seas, through the Irminger Sea into the Labrador Sea and then back into the eastern part of the gyre. The origin of these anomalies has been suggested to be enhanced export of freshwater/sea ice through Fram Strait (Dickson et al., 1988; Belkin et al., 1998), extreme winters in the Labrador Sea (Belkin et al., 1998), enhanced freshwater outflow from the Canadian Arctic Archipelago (Belkin et al., 1998) or some combination of the above.

Josey and Marsh (2005) examined the variability in the air-sea flux of freshwater in the eastern half of the sub-polar gyre. Using atmospheric reanalysis data (NCEP, ERA40) they showed a major increase in P-E within the region during the 1970s. They also found that this change in P-E was mainly driven by changes in precipitation and was linked to the East Atlantic Pattern, rather than the North Atlantic Oscillation (NAO). Integrating the effect of the enhanced atmospheric provision of freshwater to the sea surface, they found that this flux was large enough to explain observations by Reverdin et al. (2002) of sea surface freshening along a section at 60 N in this region. Gonzalez-Pola et al. (2005) also found that the P-E regime is the main driver for changes in the salinity of Eastern North Atlantic Central Water in the Bay of Biscay.

The Labrador Sea (Figure 7.1) is a northern arm of the North Atlantic Ocean, shaped as a large bowl open to the south, flanked by continental shelves, narrow along Greenland and wider along the Labrador Coast. Along these shelves and over the shelf breaks flow the West Greenland Current, the Baffin Island Current and the Labrador Current, linking the large scale cyclonic circulation of the region. Near the surface these boundary currents carry mainly cold and fresh water, isolated from the weakly stratified basin interior by strong fronts (Lazier and Wright, 1993).

Walsh and Portis (1999) also used reanalysis data to examine variations of precipitation and evaporation over the North Atlantic Ocean, during the last 4 decades.

They divided the basin into a number of sub-regions, one of which contained large parts of the Labrador Sea, as well as parts of Hudson Strait and lower Baffin Bay (their region R3). They found an inverse relationship between precipitation and the NAO in this region and some evidence for reduced precipitation in the mid 1960s to early 1970s. The variation in P and E for the Labrador Sea alone was not quantified and thus the magnitude of changes in the freshwater flux to the sea remains to be fully determined.

Houghton and Visbeck (2002) examined quasi-decadal fluctuations in salinity in the Labrador Sea and found that they were due to both local and remote forcing. More recently observational (Loder et al., 1998; Schmidt and Send, 2004) and modelling (Katsman et al., 2004) work has started to examine how freshwater is exchanged between the boundary currents and the interior, to influence restratification within the gyre interior. For example, Schmidt and Send (2004) suggest that the majority of the annual freshwater supply to the interior derives from the West Greenland Current. In contrast Myers (2005) suggested that increased export of freshwater from the Arctic into the Labrador Current on annual to decadal time scales does not necessarily lead to an enhanced freshwater content in the interior of the Labrador Sea. Thus, the question arises as to whether changes in P-E over the interior of the Labrador Sea play a role in the observed freshening within this basin. We address this question by examining interdecadal changes in the freshwater flux to the Labrador Sea using

both NCEP/NCAR and ERA40 reanalyses with the focus being on the interior of the basin. We use two definitions of the interior of the basin, both shown in Figure 7.1. One includes all of the basin beyond the continental shelves and upper slopes, defined where the water depth is greater than 1000 m. The area of this region is 10^6 km^2. We also focus on a smaller region more consistent with the zones of deep water formation (Lilly et al., 1999), defined where the water is deeper than 3000 m, with an area of 4 x 10^5 km^2. This central region covers our ocean data analysis, with a resolution of 1/3 degree. Our aims are to determine whether any long term changes in the atmospheric provision of freshwater to the basin have occurred, what is driving these changes and what their impact is on salinity.

6.2   Data

We use output from the two major atmospheric model reanalyses (NCEP/NCAR and ECMWF) as well as oceanic salinity data in this study. To be able to examine the links between atmospheric forcing and oceanic freshwater changes, we have considered the data over the longest possible period, even if some of the earlier data is less reliable. In all such cases we show that choosing a different starting year for the analysis does not change our main results.

The NCEP/NCAR and ERA40 atmospheric model reanalyses are described in Kistler et al. (2001) and Simmons and Gibson (2000), respectively. The NCEP/NCAR

reanalysis is based on the 1995 version of the NCEP model and has a horizontal resolution of about 210 km. We have analysed NCEP/NCAR output for the period 1949-2002 but focus on the interval from 1958 onwards. The earlier fields are less reliable due to reductions in the amount and type of data available for assimilation (Kistler et al., 2001). The ERA40 reanalysis covers the interval Sep 1957 - Aug 2002 and we have used 2.5 x 2.5 degree grid version of the output fields. As the NCEP/NCAR fields have a higher resolution than ERA40 we used them as the primary dataset for our study.

As proxy for the leading modes of atmospheric variability in the mid to high latitude North Atlantic, we employ several widely used indices. These are produced by the National Oceanic and Atmospheric Administration/National Weather Service Climate Prediction Center (CPC). The indices are obtained from a method described by Barnston and Livezey (1987) consisting of a rotated principal component analysis of observed 700 mb height anomalies. The indices we use are those for the NAO and Arctic Oscillation (AO) as well as those for the associated East Atlantic Pattern (EAP) and East Atlantic Jet (EAJ).

The ocean salinity data were extracted from the extensive hydrographic database maintained by the Bedford Institute of Oceanography (BIO). To allow us to examine the time variability in salinity and freshwater within the Labrador Sea, the data were mapped into overlapping 3-year running mean triads, covering the period 1949-1999.

Each triad was defined to include all the data collected in a given year, as well as all available data in the preceding and following year. The data were objectively mapped onto a 1/3 by 1/3 degree grid over the entire Labrador Sea using a modified version of the iterative difference-correction scheme with depth dependence of Reynaud et al. (1995). Vertical binning and averaging was carried out using isopycnal coordinates. The isopycnal averaging avoids unrealistic diapycnal mixing of the properties by averaging them over a smaller range of isopycnals. To concentrate on changes within the interior of the Labrador Sea, the triad data were then averaged over the region within the 3000 m isobath (Fig. 7.1) to give an average central Labrador Sea salinity for the central year of each triad, at each level. Details of the data processing (including quality control), as well as further analysis of the resulting fields can be found in Kulan and Myers (2007).

6.3 P-E Variability

Climatological mean (1960-2000) fields of surface freshwater fluxes are shown in figure 6.2. The P-E field has excess precipitation through most of the sub-polar gyre, with maxima along the Greenland and Labrador Sea coasts, and a transition to net evaporation south of 45N (not shown). The component fields show that E tends to decrease towards the coastal margins, possibly reflecting the effects of ice cover, whereas P remains relatively constant. These fields are consistent with other

observationally derived products (Josey and Marsh, 2005; Schmitt et al., 1989) as well as with the ERA40 reanalysis (Josey and Marsh, 2005). We have calculated the mean P-E for our Labrador Sea interior regions (Fig. 7.1) by averaging over each grid cell in the atmospheric analyses that falls within these domains. The full period mean value is an excess precipitation of 27 cm yr^{-1} for the 1000 m region and 20 cm yr^{-1} for the 3000 m region, both of which are smaller than previous estimates (e.g. 40 cm yr^{-1} - Walsh and Portis (1999)) that included the more precipitative boundary current regime. It should be pointed out that, at least in other regions of the globe, NCEP suffers from a strong dry bias (Li and Chen, 2005). (Josey and Marsh, 2005) also found a dry bias with respect to rain gauge measurements in the eastern subpolar gyre. In contrast there was good agreeement between the temporal variability in NCEP/NCAR and the rain gauges. It is this variability we are interested in here.

Time series of annual surface freshwater flux anomalies for our interior Labrador Sea regions are shown in Fig. 6.3. Although in details the time series for the two regions vary, the general structures are very similar. With respect to their variance, the P-E time series are dominated by interannual variability but the 5-year running means show a clear shift from negative to positive anomalies in the mid-1970s. The time series thus have two main phases, relatively low net precipitation from the 1950s through to the 1970s and relatively high net precipitation past the mid-1970s. Whether this shift is part of a long term trend to an environment with an increased

atmosphere to ocean freshwater flux or just two phases in a long period oscillation cannot be determined from the given time series length. This mid-1970s shift in Labrador Sea P-E shows similar timing to that described by Josey and Marsh (2005) for the eastern part of the North Atlantic sub-polar gyre.

A spatial field of the difference in P-E calculated for two sub-periods 1960-74 and 1975-2000 is shown in Figure 6.4a. A strong increase in excess precipitation is seen through most of the sub-polar gyre, as noted by Josey and Marsh (2005), including changes approaching 0.2 m yr^{-1} in the central and southern Labrador Sea. Clarke and Gascard (1983) have noted a cyclonic cooling gyre in the western Labrador Sea where surface waters lose buoyancy each winter through surface forcing, leading to the production of Labrador Sea Water (LSW). Their gyre falls well within the region of enhanced net precipitation in figure 6.4a. Since excess precipitation increases surface buoyancy, we anticipate that the P-E changes noted above will impact LSW formation and investigate changes to LSW salinities in Section 4.

The change in excess precipitation over the Labrador Sea is driven primarily by changes in the precipitation component rather than evaporation. This can be seen both in the time series of annual mean anomalies of P and E (Fig. 6.3) and the spatial fields of the changes in these components between the two sub-periods (Fig. 6.4 b-c). There is no clear long term change in E but the P time series exhibits a marked shift towards increased precipitation during the mid-1970s. The spatial fields show a major

increase in P over both the Labrador Sea, and a broader region of the subpolar gyre further east, with little change to E. Josey and Marsh (2005) have already noted that changes in P were the dominant cause of the interdecadal variability in the eastern subpolar gyre. Our analysis suggests that parallel changes in P over the Labrador Sea are the dominant factor influencing the changes in the freshwater flux to this basin.

The changes in E, P and P-E over the Labrador Sea interior are summarized in Table 6.1. Two alternative definitions of the first period (1950-1974 and 1960-1974) have been examined to determine whether our results are sensitive to the choice of initial date. If we take the first time period to be 1960-74, over which the NCEP data is considered to be more reliable, we find that the net precipitation has increased (as compared to considering 1950-74), and in this case, is entirely driven by the changes in precipitation. When we focus on the smaller (greater than 3000m depth) Labrador Sea region, the changes are even larger. We also note that the results are insensitive to the choice of the specific year in the 1970s that is used as the separator between the two periods. We recalculated the averages using every year from 1972 to 1978 as the bounding year and found no qualitative differences in the results.

We now investigate whether there is any seasonal dependence to the changes in P- E discussed above ((Fig. 6.5). In general, the period of strongest net precipitation occurs from May to November, with little net exchange in winter (January through March). Similar seasonal variations are found for the 3000m region (not shown). An

enhancement of the net precipitation from the earlier to the later period, up to 0.02 m/month, occurs throughout much of the year with the largest changes concentrated in spring and summer. In contrast there is a slight reduction in net precipitation, up to 0.005 m/month, from October to December and in February. In both regions, the net change in spring is driven primarily by an increase in precipitation, which is supplemented by reduced evaporation during this season. In late fall, increases in evaporation dominate over the slightly smaller increases in precipitation in the 1000m region but not in the 3000m region and this is the source of the differences in the P-E changes between the two regions at this time of year.

Considering all months, the spring and summer changes are the dominant factor in the increased annual P-E after the mid-1970s. In contrast to the eastern subpolar gyre, Josey and Marsh (2005) found significant contributions to the increase occurring in all months of the year and that changes in net precipitation were largest in winter. The Labrador Sea thus show a different seasonal dependence than the eastern gyre suggesting that they may be linked to a different mode of atmospheric variability. Josey and Marsh (2005) found that the variability in the eastern gyre was most strongly linked to the second main mode of atmospheric variability, the East Atlantic Pattern. This mode is primarily active in winter and does not have a strong expression over the Labrador Sea. Hence, the difference in seasonal behavior between the two regions is not surprising. Potential links between atmospheric variability and the

Labrador Sea changes are explored further below.

Timeseries of P-E, P and E anomalies in the dominant spring (April, May and June) season are shown in (Fig. 6.6). Although the time series show significant interannual variability, at lower frequency, changes in both components are observed, with an increase in P and decrease in E post-1975 compared to pre-1975. These reinforce to give a similar strong increase in net precipitation in the mid-1970s to that observed earlier for the annual means. We have found similar changes in summer but only higher frequency variations in autumn and winter (time series not shown). We have also examined the spatial variability of the differences between the spring fields of P-E, P and E in the two periods using NCEP and checked the results for consistency with ERA40, see (Fig. 6.7). Both reanalyses show similar patterns of change in all three fields with a larger increase in P-E centered on the Labrador Sea basin that is driven by a similar pattern in P with relatively little contribution from E. In contrast to the difference fields found with the annual means, the major change in P-E and P in spring is limited to the Labrador Sea basin and does not have a strong expression eastwards into the wider subpolar gyre.

Having quantified the major patterns of change over the last 40 years in the Labrador Sea we now examine whether they are linked to the dominant modes of atmospheric variability that affect this region. In particular we have determined correlation coefficients between various modes of variability and NCEP/NCAR annual

and seasonal P-E, P and E anomalies (Table 6.2). We have focused on the NAO and the AO, together with a more limited analysis for the East Atlantic Pattern. Whether the NAO and AO are distinct or simply reflect different aspects of the same phenomenon remains a matter of ongoing debate (Hurrell et al., 2003).

The calculations using annual anomalies (Table 6.2) reveal that evaporation over the Labrador Sea is strongly correlated with the NAO but also that this mode has an insignificant influence on precipitation. This result is consistent with the idea that when the NAO is in a positive state the frequency of cold air outbreaks which drive stronger evaporation over the Labrador Sea increases (Greatbatch, 2000). The overall influence of the NAO on P-E is relatively weak, the negative sign reflecting the increase in E as the NAO increases. For the AO, we find a similar correlation with E but a greater correlation with P. However, as it is positively correlated with each of the components, the overall correlation of the AO with P-E is very weak and insignificant. Thus, neither the NAO or AO has a strong impact on the net freshwater flux to the Labrador Sea.

In addition to the correlations between annual anomalies we have also calculated values using seasonal anomalies determined for each of the following two distinct seasons: April - June and September - March, for each year in the period 1950-2002. We are primarily interested in April-June as the seasonal analysis presented earlier found that the changes were strongest in these months. We find that the correlations

between the NAO and P-E and E in this season are similar to the annual mean, with a significant correlation between the NAO and E in both the 1000m and 3000m regions but no correlation between the NAO and P. Thus, the major increase in P that we find during April-June post-1975 is not related to the well known upward trend in the NAO. The same conclusion is reached for the AO.

We have also determined correlation values for the East Atlantic Jet (EAJ) which is the second mode of North Atlantic variability in summer but has its center of action in the eastern part of the basin (see Josey and Marsh (2005) for further details of this pattern). The correlation coefficients are again insignificant and we find no clear link between the April-June P increase and the leading modes of atmospheric variability. This is perhaps not surprising as the difference fields in figure 6.7c-d clearly show that the increase in P is largely confined to Labrador Sea, suggesting that it is due to a change in local atmospheric forcing as opposed to a trend in a large scale pattern of variability.

For completeness we have also investigated correlations in the winter centered season September - March. The results for the NAO show that the strongest correlation is again with E and the values for the 1000m and 3000m regions are similar to those found using annual anomalies. The correlation with P is significant only in the 3000m region and relatively weak while the P-E correlation remains insignificant in both regions. The AO correlation statistics are similar with slightly higher values

for P and E than those found for the NAO. The second mode in winter is the East Atlantic Pattern but we anticipate that as found for the EAJ it will be only weakly linked to the Labrador Sea variability because it is primarily confined to the eastern half of the basin. This suggestion is confirmed by the low values for the correlation coefficients for this mode (Table 6.2).

6.4 Salinity Changes

We now try to link the changes in the air-sea freshwater flux to the observed freshening in the Labrador Sea over the last several decades. As shown in Table 6.1, the atmospheric flux of freshwater to the surface of the interior of the Labrador Sea has increased for the 1975-2000 period as compared to the 1960-1974 period. Given the areas of our two Labrador Sea regions, the increase in P-E has led to the provision over the 25 year period 1975-2000 of an extra 2.25 x 10^{12} m^3 of freshwater to the interior region deeper than 1000 m, and an extra 1.8 x 10^{12} m^3 for the 3000 m region. This corresponds to an increased flux of 2.9 mSv (an increase from 7.0 to 9.9 mSv) for the 1000 m region. For the 3000 region, the increase is 3.2 mSv (from 5.7 mSv to 8.9 mSv).

Estimates of the provision of freshwater to the upper Labrador Sea between April and September, as the water column restratifies post convection, based on analysis of salinity changes, range from 11 mSv (Khatiwala et al., 2002) to 24 mSv

(Schmidt and Send, 2004) and 30 mSv (Lazier, 1980). The mean atmospheric signal during April to September is 6.0 mSv, suggesting that the atmosphere provides between 20% and 50% to the observed seasonal freshening. When taking into account the enhancement since 1975, 3/4 of which occurs in the April-September period, the atmospheric signal becomes even more important. thus, atmospheric forcing may play a greater role in explaining the seasonal freshening than suggested in previous work (Khatiwala et al., 2002; Schmidt and Send, 2004).

Curry and Mauritzen (2005) reported that the freshwater content of the subpolar gyre had increased by 15,000 km^3 between 1965 and 1995, of which 10,000 km^3 entered between the late 1960s and early 1970s, with a large contribution from the advective Great Salinity Anomaly. We suggest that part of the 5,000 km^3 increase reported to occur after 1975 is related to increases in the atmospheric P-E signal. In a pure budget sense, 2250 km^3 of additional freshwater was provided to the western sub-polar gyre (Labrador Sea) during the post 1975 period by the atmosphere. This last number is large in magnitude and indicates that the atmospheric freshwater flux could have played a significant role in the freshening. The Labrador Sea is only part of the sub-polar gyre region of Curry and Mauritzen (2005) and the analysis of Josey and Marsh (2005) reveals an additional gain of 4000 km^3 from the atmosphere within the eastern part of the sub-polar gyre. The increase in freshwater from the atmosphere will only contribute to the observed change in freshwater content if it is

stored within the sub-polar gyre and so the overall effect of the P-E increase remains to be fully determined.

Observations of the subpolar gyre circulation suggest that the additional freshwater supplied by the atmosphere to the Labrador Sea could remain in the gyre for long enough to contribute to the observed freshening. In a dataset of surface drifters examined by Cuny, Rhines, Niiler, and Bacon (2002), all drifters released in the Labrador Sea remained in the sub-polar gyre. Surface water is also taken up in the Labrador Sea Water (LSW) formed in winter. Three pathways for LSW have been documented (Lankhorst and Zenk, 2006), into the Irminger Sea, into the eastern basin under the NAC and south along the deep western boundary current. Only this last pathway involves the export of freshwater from the sub-polar gyre. We do not wish to overstate the importance of the increase in excess precipitation over the Labrador Sea (and the sub-polar gyre as a whole), as there are other processes that provide freshwater to the sub-polar North Atlantic. These includes outflow from the Arctic through Fram/Denmark Strait as well as Davis Strait, both of which have been estimated in the range of 100 mSv (e.g. Loder et al. (1998)). However, given the magnitude of the increase and the potential for it to be retained within the gyre, we think it is reasonable to suggest that the P-E increase has played an important role in the freshening of the sub-polar North Atlantic over the last 25 years.

Can the impact of the changes in the atmospheric provision of freshwater to the

Labrador Sea be observed locally? We have used the mapped 3-year triads of salinity to examine this question. We look at the changes in salinity through various layers in the Labrador Sea, between 1950-1975 and 1975-1999 - see Table 6.3. The freshening is largest at the surface, up to 0.19 psu, but remains significant through the water column, 0.04 - 0.05 psu at depths of 1000-2000 m. Thus, the long term freshening in the Labrador Sea, noted by others previously, is clearly seen with this data and the magnitude of the changes is consistent with those discussed in the Introduction. We have also computed the associated change in freshwater between the two periods, with respect to a reference salinity of 34.8. The results are given in table 6.3, with a change of 724 km^3 for the top 1500 m.

To examine this is more detail, we compare the 5-year running means of the E-P anomaly with the anomalies of the 3-year running means of salinity averaged through layers of different depth in the interior of the Labrador Sea, see Figure 6.8. Note that we plot E-P in the figure (unlike P-E as elsewhere in this paper) to show that the trends are in the same direction. The time series are in good agreement (over all depth levels) throughout most of the period considered. The correlation of the annual time series has a maximum r value of 0.76 for the salinities through 1500 m and 2000 m (decreasing to 0.70 for 1000 m and 0.55 for the 500 m layer). All correlation coefficients are significant at the 99% level.

Although the time series show a similar long term variation it is clear that not

all of the salinity changes can be linked to the changes in P-E. The biggest departure between the two time series occurs between the late 1960s and the mid 1970s, with a rapid drop of salinity leading the change in P-E. This rapid freshening is due to the first GSA. As discussed in Dickson et al. (1988) and Belkin et al. (1998), the first GSA is thought to have been caused by a pulse of freshwater exported from the Arctic Ocean through Fram Strait which circulated around the Labrador Sea. Although the potential contribution from P-E anomalies has not previously been considered in detail, the time series analysis (Fig. 6.3) shows that at the time of the 1970s GSA, the atmospheric regime was less precipitative (negative P-E anomalies) and thus local atmospheric forcing could not have played a role in the generation of this GSA. This is in agreement with the assertion of Belkin et al. (1998) that the first GSA was generated remotely.

Houghton and Visbeck (2002) found the magnitude of the freshwater anomaly associated with the first GSA (over the top 300 m) to be 700 km^3 which is close to the total change in freshwater in the Labrador Sea that we find between the two periods. However, although the first GSA may explain the rapid drop in salinity in the 1970s, consideration of flushing timescales indicates that it cannot explain all of the freshening between the two periods. The reason for this is that the interior of the Labrador Sea is a small region where advection is important. The flushing timescale for Labrador Sea Water has been estimated to be approximately 4 years

(Lazier et al., 2002). Thus, although some of the freshwater from the first GSA may have been stored in the Labrador Sea, most of it has probably been flushed out into other parts of the sub-polar gyre (for which the flushing timescale is much longer). In contrast to the short term nature of the first GSA, and subsequent advective events, the increase in P-E in the 1970s has been maintained to the present day (see Fig. 3) thus enabling the atmosphere to make an ongoing contribution to the freshening within the Labrador Sea.

6.5 Summary and Discussion

We have considered changes in the air-sea freshwater flux (P-E) to the interior of the Labrador Sea over the last 50 years using output from atmospheric model reanalyses and related it to freshening of this basin over the same period. Our analysis has been carried out in the context of a recent study (Josey and Marsh, 2005) which linked a significant increase in P-E over the eastern subpolar gyre to freshening of that region.

We find significant temporal variability in the Labrador Sea P-E which has a strong interannual component, but also reveals distinct lower frequency variability. The low frequency variation has two main phases: relatively low net precipitation prior to the mid-1970s, followed by a rapid transition to a higher net precipitation phase thereafter that persists through to the end, 2003, of the record considered.

The change in net precipitation amounts to 9 (or 18) cm yr^{-1} depending on the interior region considered, when examining the period 1975-2000 compared to 1960-74; similar results are obtained if the earlier period is extended to cover 1950-1974. It is driven largely by an increase in the precipitation component as the evaporation field shows no clear long term variation. This result is consistent with the study of (Josey and Marsh, 2005) who found a similar transition to stronger P-E in the eastern subpolar gyre which was also precipitation driven. However, there are major differences between the seasonal dependence of the two events. The eastern gyre change is distributed over all months of the year with a small increase in winter. In contrast, the Labrador Sea enhancement in net precipitation is concentrated in spring and summer, with a decrease occurring in fall.

We have also examined whether the P-E increase in the Labrador Sea is linked to trends in the dominant modes of atmospheric variability that are likely to affect this region. Annually averaged evaporation anomalies over the Labrador Sea are strongly correlated with the NAO. However, this mode has an insignificant influence on precipitation and its overall correlation with P-E is not really significant. For the AO, the correlation with annual P-E is insignificant, thus neither mode has a strong impact on the net freshwater flux to the Labrador Sea. Similar conclusions regarding the lack of influence of large scale modes on P-E are reached when seasonal anomalies are considered suggesting that the observed net precipitation increase must be a

response to local changes in the freshwater forcing of the basin by the atmosphere.

M G Bosilovich and Walker (2005) examined changes in the global water cycle intensity based upon a series of climate simulations. They found that over the last 50 years, precipitation over land has been decreasing while oceanic precipitation has been increasing. This is consistent with our study and that of Josey and Marsh (2005) that found significant increases in precipitation over the sub-polar gyre. Groisman et al. (2005) examined trends in intense precipitation events over the last 3 decades and found that in those regions where precipitation had increased, it was mainly associated with an enhancement of intense events, including along the north-eastern border of North America. In figure 6.9, we divide the precipitation events over the interior of the Labrador Sea (1000 m depth region) into four categories based upon the amount of precipitation involved on each day and examine how this changes between 1975-2000 as compared to 1960-74. As can be seen, the increase in precipitation discussed in this paper does seem to be linked to an increase in the frequency of stronger events.

What role do the changes in net precipitation play in the observed freshening of the Labrador Sea and sub-polar North Atlantic? This issue is easier to examine for the sub-polar gyre as a whole, as most of the water modified by the surface fluxes over the Labrador Sea will remain in the sub-polar gyre considering the 25 year timespan (1975-2000) we are looking at. We find a provision of an extra 2250 km^3 of freshwater

to the Labrador Sea by the atmosphere during this time period. Considering that Josey and Marsh (2005) found an additional provision of 4000 km^3 to a region centered on the eastern sub-polar gyre, these amounts compare favourably with the 5,000 km^3 of post GSA freshwater found in the gyre by Curry and Mauritzen (2005). The freshening of the Labrador Sea is harder to attribute, as its flushing timescale is such that additional freshwater provided to it can easily be removed within a few years and thus its contribution to the longer term (25 year) storage is difficult to determine. However, as the 1800 km^3 of extra freshwater provided by the atmosphere is much larger than the observed freshening over the same period (726 km^3 integrated over the upper 1500 m), and is provided as a continuous source (rather than as a pulse like the GSA events), we suggest it must play a role in the observed freshening.

To conclude, we have found a major enhancement of excess precipitation over the Labrador Sea in the mid-1970s which is maintained to the present day. This increase is likely to have played an important role in the freshening of both the Labrador Sea and the wider sub-polar North Atlantic region over the last 25 years. Furthermore, when compared with an earlier analysis for the eastern gyre (Josey and Marsh, 2005) it is clear that the seasonal dependence of the freshwater flux varies significantly with region and that variability in both large scale atmospheric modes and local forcing needs to be taken into account. Detailed understanding of the freshening of the mid-high latitude North Atlantic will thus require consideration of a range of atmospheric

processes combined with changes that are due to advective signals within the ocean itself.

Table 6.1: Long term mean P-E, P and E over both our Labrador Sea interior regions. All units are given in m yr^{-1}.

	1000 m region			3000 m region		
Period	P-E	E	P	P-E	E	P
1950-74	0.23	0.66	0.89	0.11	0.74	0.85
1960-74	0.22	0.65	0.87	0.10	0.73	0.83
1975-2000	0.31	0.65	0.97	0.28	0.73	1.01
1975-2000 minus 1950-74	0.08	-0.01	0.07	0.17	-0.01	0.16
1975-2000 minus 1960-74	0.09	0.00	0.09	0.18	0.00	0.18

Table 6.2: Correlation coefficient between Labrador Sea P-E, P and E and the major atmospheric modes of variability for various time periods (annual and seasonal). Values in bold font are significant at the 95% level.

	1000 m Region			3000 m region		
	P-E	P	E	P-E	P	E
NAO Annual	-0.19	0.14	**0.36**	-0.21	0.15	**0.49**
AO Annual	-0.07	**0.28**	**0.38**	-0.04	**0.33**	**0.49**
NAO Apr.-Jun.	**-0.33**	-0.16	**0.47**	**-0.29**	-0.04	**0.59**
AO Apr.-Jun.	-0.21	-0.12	0.23	-0.13	0.06	**0.41**
EAJ Apr.-Jun.	0.01	-0.18	-0.18	0.12	0.02	-0.24
NAO Sep.-Mar.	-0.14	0.24	**0.42**	-0.15	**0.39**	**0.62**
AO Sep.-Mar.	-0.16	0.26	**0.43**	-0.16	**0.44**	**0.67**
EAP Sep.-Mar.	-0.12	-0.14	0.12	0.09	0.12	0.02

Table 6.3: Salinity Anomalies (compared to 1950-1999 mean) for various layers, in the interior of the Labrador Sea, for 2 time periods, as well as the increase in freshwater between the two periods (with respect to a reference salinity of 34.8).

Layer	1950-1975 Anomaly	1976-1999 Anomaly	Difference	Freshwater Increase
0-100 m	0.089 psu	-0.100 psu	-0.189 psu	217 km^3
0-500 m	0.031 psu	-0.035 psu	-0.066 psu	391 km^3
0-1000 m	0.023 psu	-0.026 psu	-0.049 psu	563 km^3
0-1500 m	0.020 psu	-0.022 psu	-0.042 psu	724 km^3
0-2000 m	0.018 psu	-0.020 psu	-0.038 psu	874 km^3
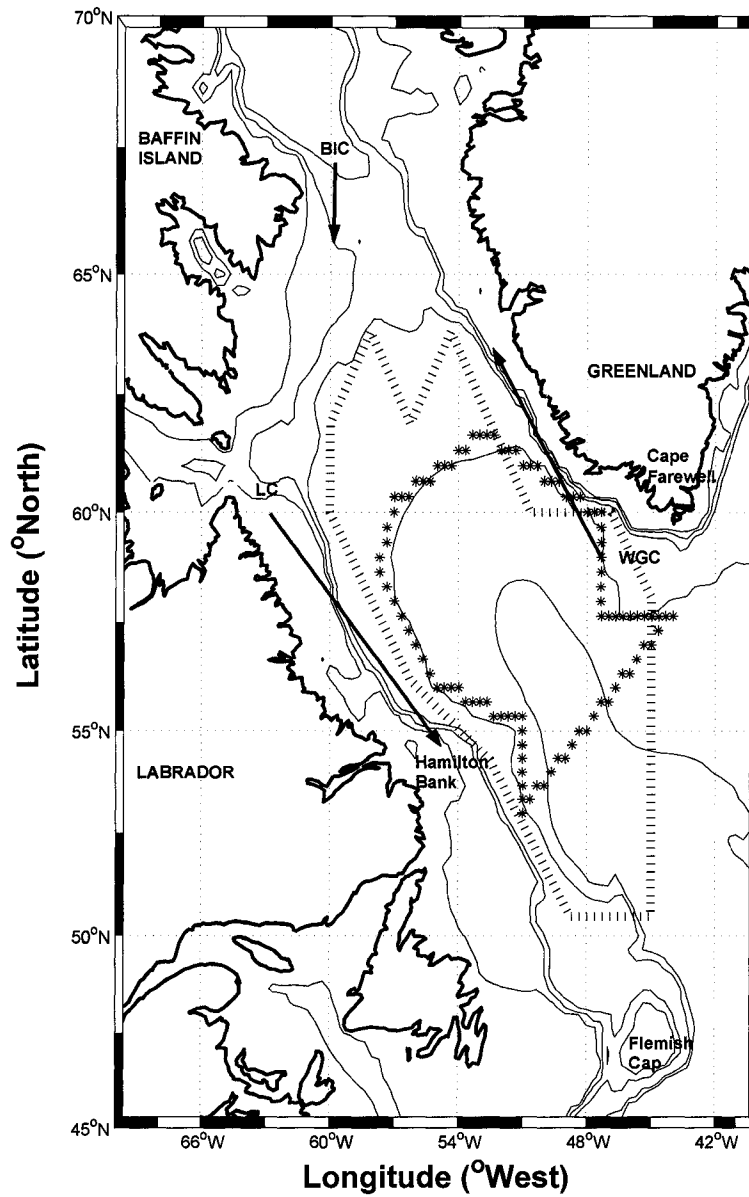
Figure 6.1: Map of the Labrador Sea study region. The dashed line bounds our study region within the 1000 m contour, while the starred line bounds our study region within the 3000 m contour. The abbreviations for the currents are: WGC - West Greenland Current; BIC - Baffin Island Current; LC - Labrador Current.

a.) NCEP P-E [1960-2000]

b.) NCEP P [1960-2000]

c.) NCEP E [1960-2000]
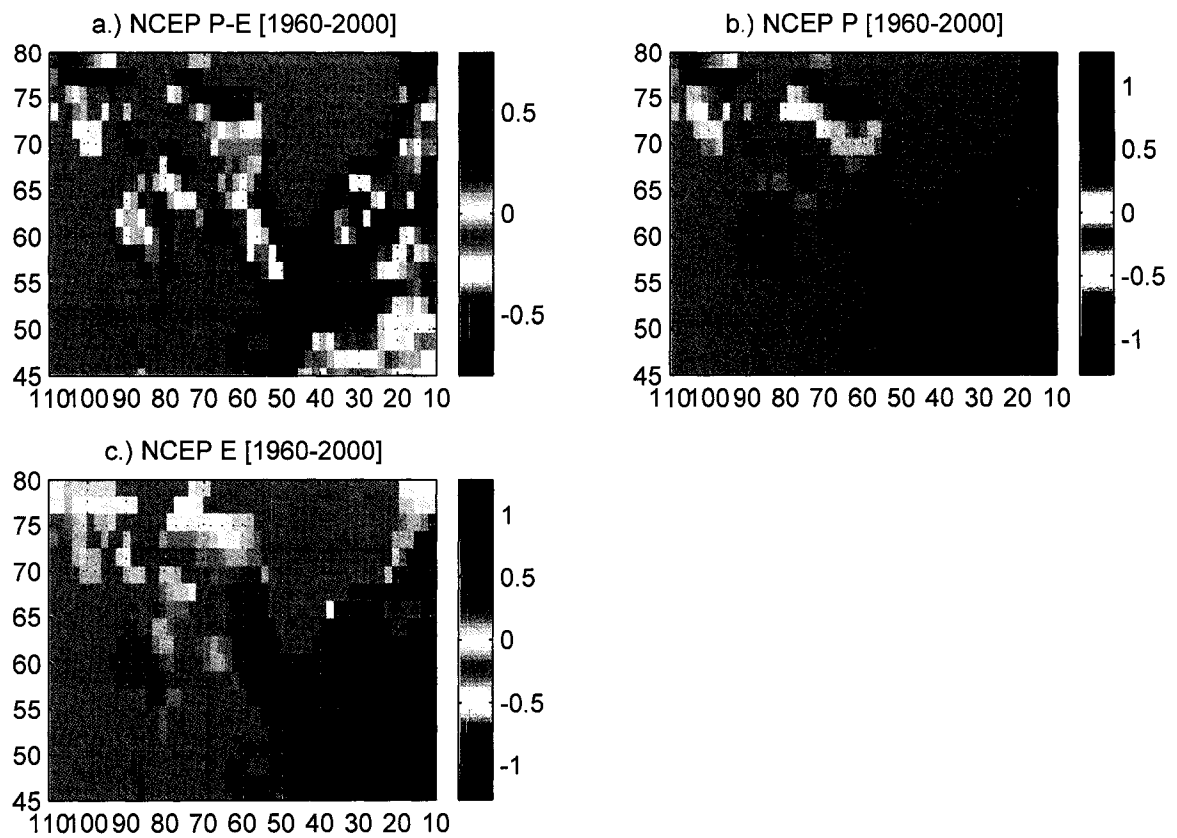
Figure 6.2: Climatological mean fields of a) P-E and its components (b) P and c) E for 1960-2000 from NCEP/NCAR. Units are m yr^{-1}.
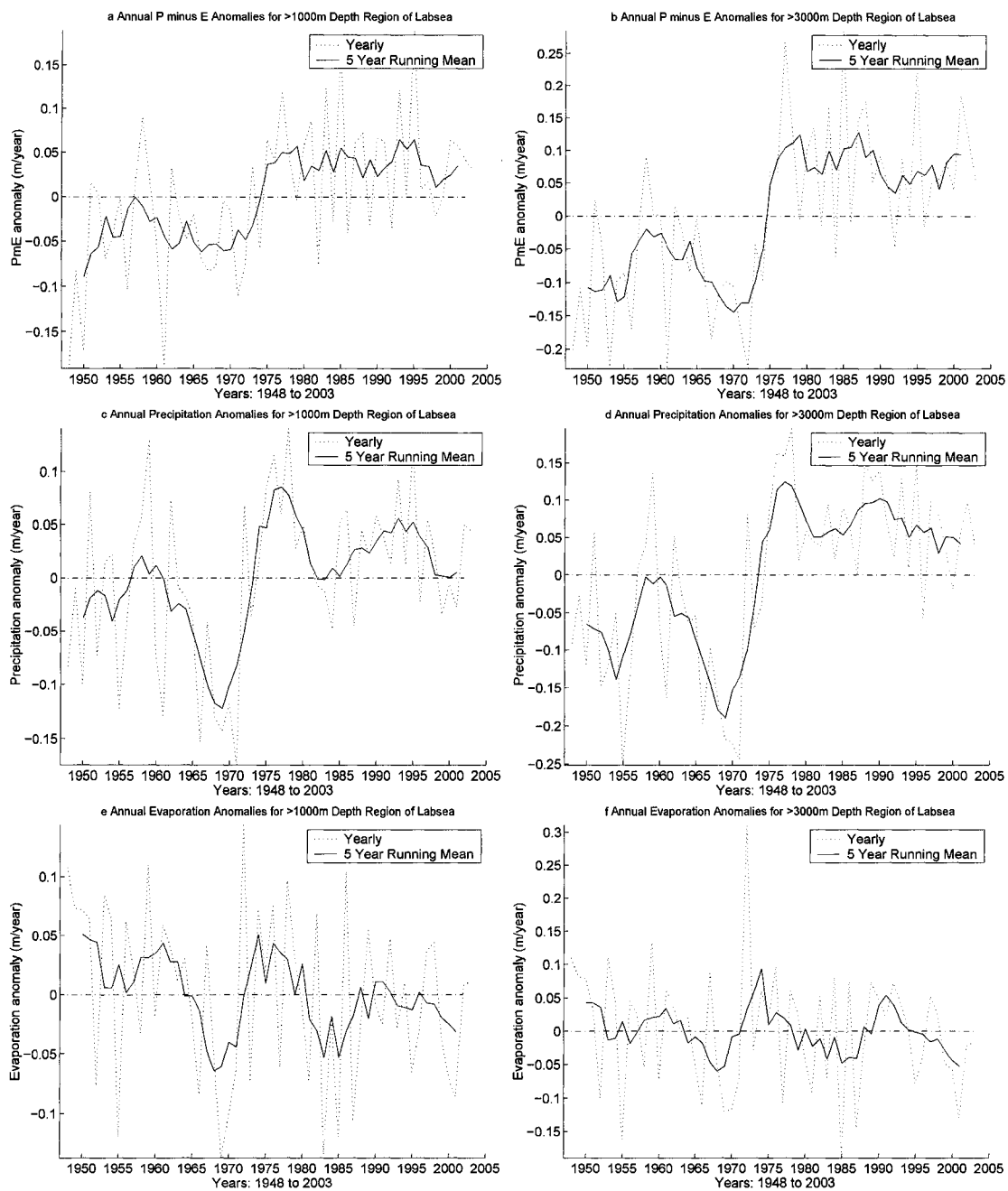
Figure 6.3: Timeseries of annual anomalies and corresponding 5-year running means for a) P-E and its components c) P and e) E from NCEP/NCAR for the 1000 m depth interior region. The 3000 m interior region results are shown in b) P-E; d) P and f) E. Anomalies have been formed by subtracting the full period annual mean from the individual annual means.
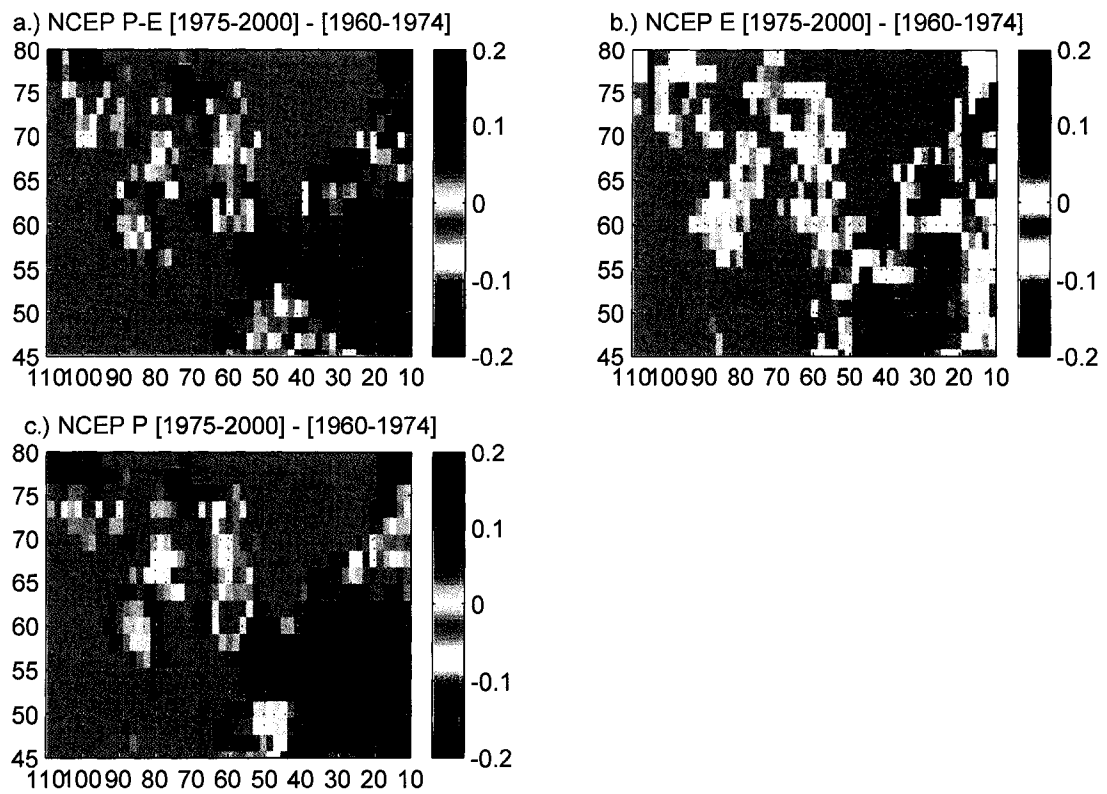
Figure 6.4: Annual mean fields of the difference in a) P-E and its components b) E and c) P for the period 1975-2000 relative to 1960-1974 for the 1000 m depth interior region.
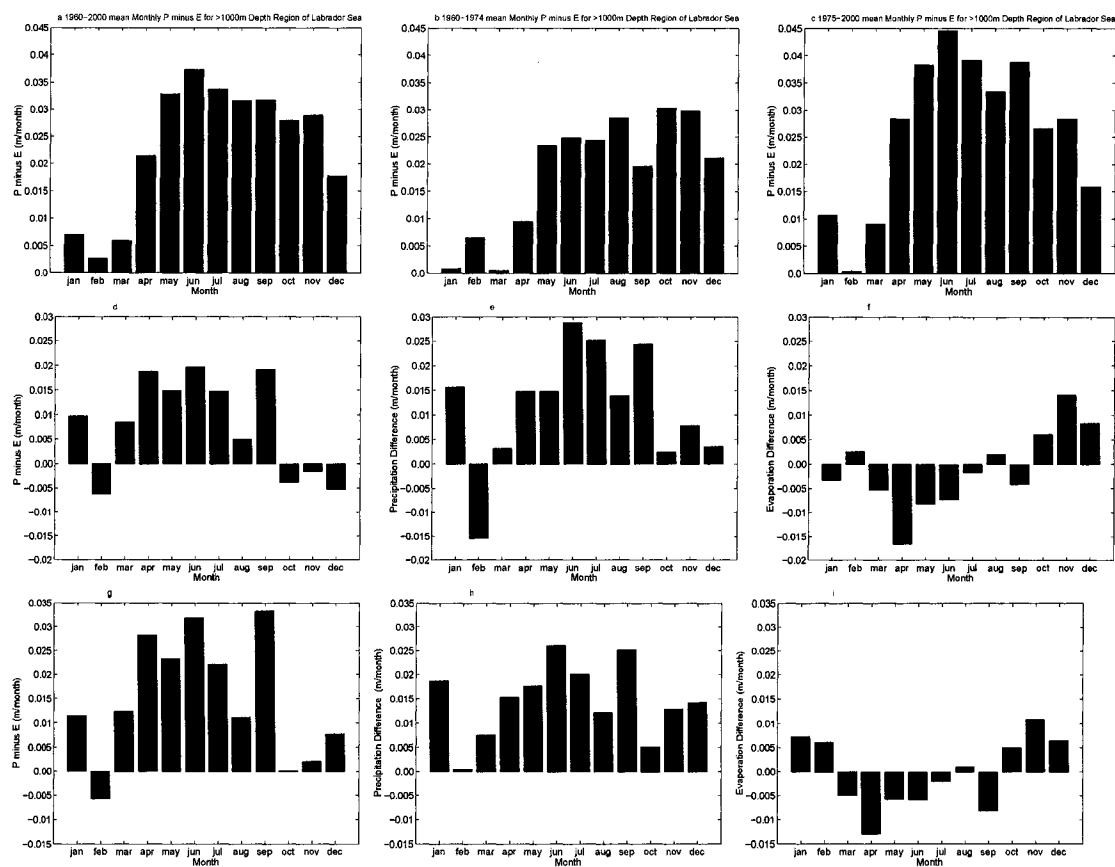
Figure 6.5: Monthly bar charts of P-E for a) 1960-2000; b) 1960-74 and c) 1975-2000. Additionally shown are monthly bar charts for the difference of d) P-E and its components (e) P and f) E for the period 1975-2000 relative to 1960-1974 for the 1000 m depth interior region as well as the g) P-E difference and its components h) P and i) E for the 3000 m region.
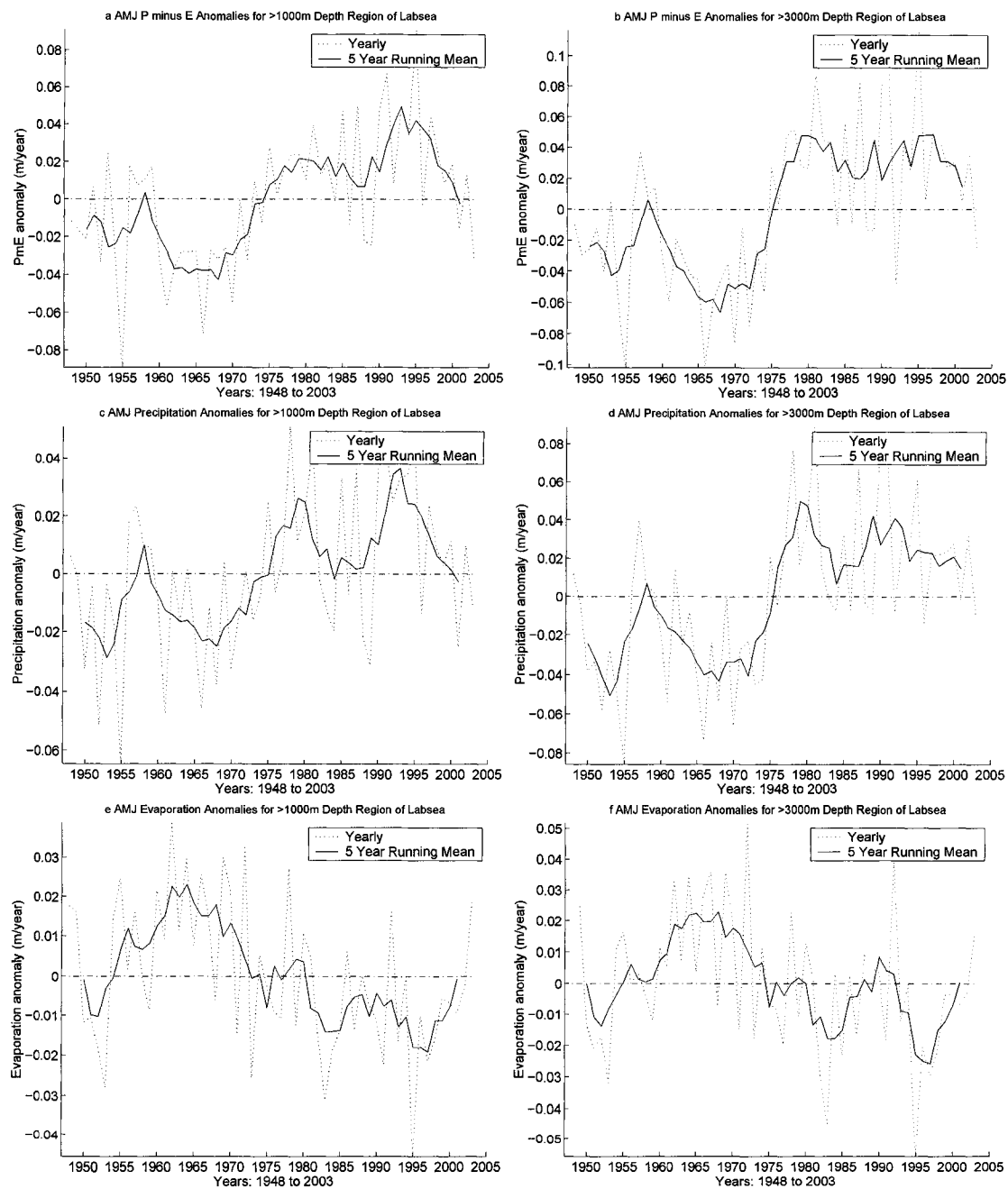
Figure 6.6: Timeseries of spring (AMJ) anomalies and corresponding 5-year running means for a) P-E and its components c) P and e) E from NCEP/NCAR. The 3000 m interior region results are shown in b) P-E; d) P and f) E.
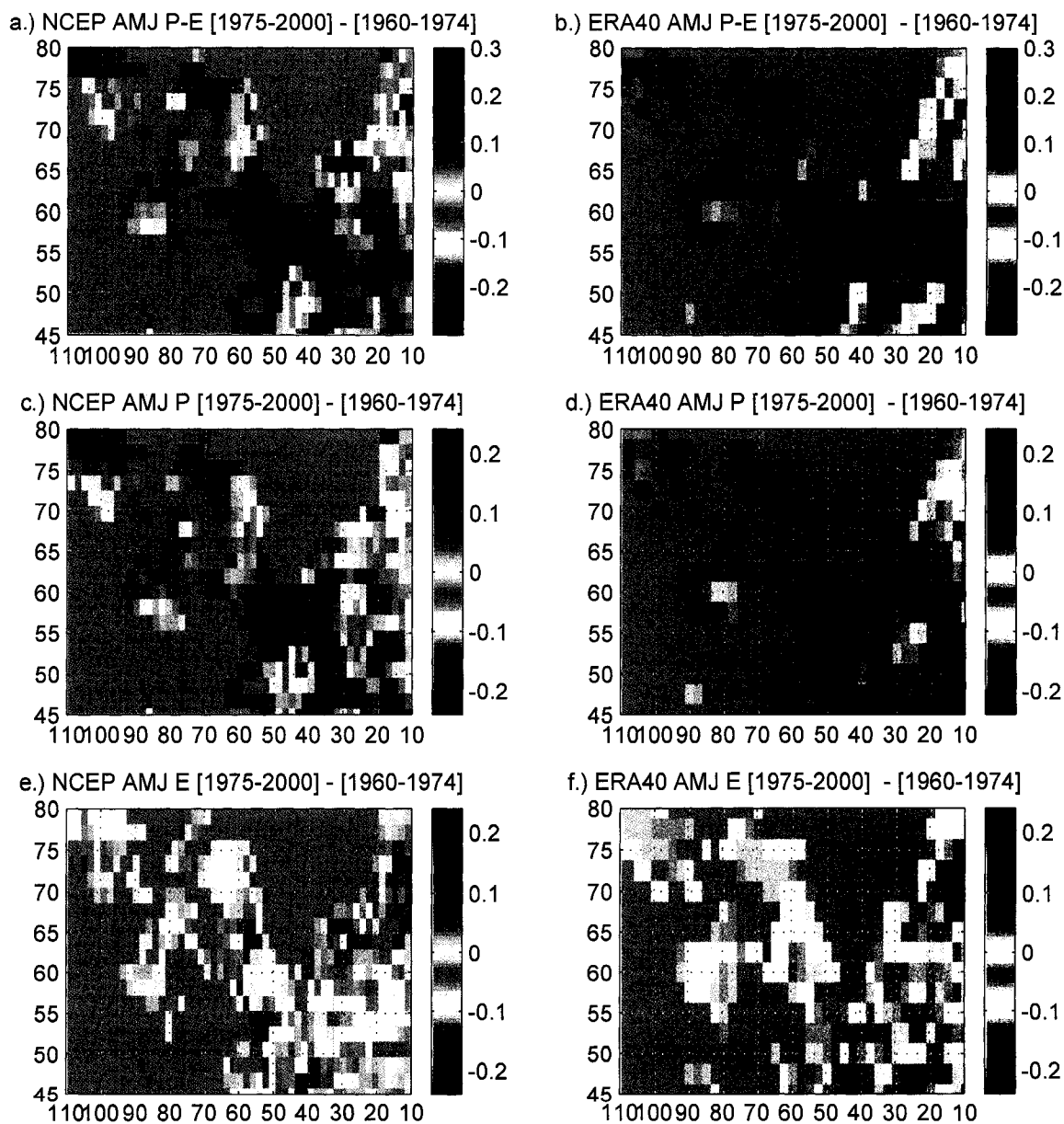
Figure 6.7: Change in spring (AMJ) a,b) P-E and its components c,d) P and e,f) E for the period 1975-2000 relative to 1960-1974 for NCEP/NCAR and ERA40.
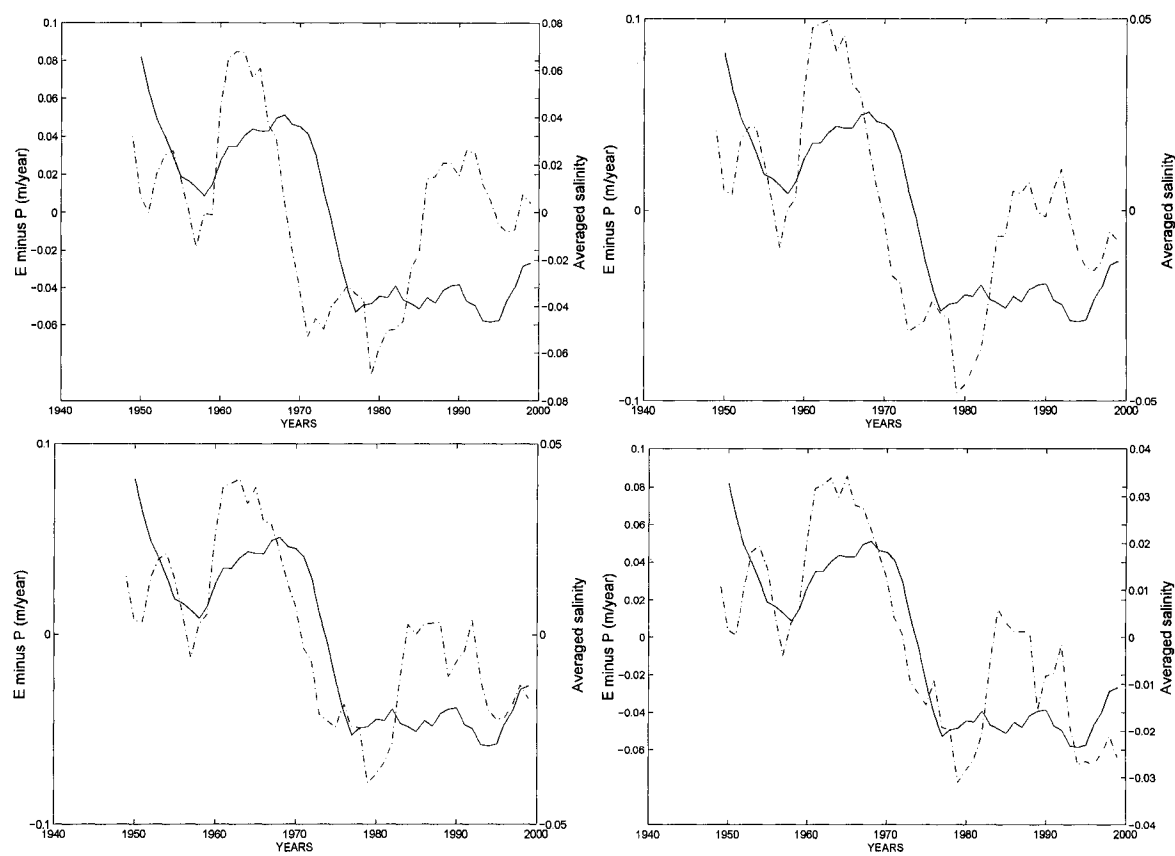
Figure 6.8: Timeseries of the 5-year running mean E-P anomaly (blue line) from NCEP/NCAR and the overlapping 3-year running mean salinity anomalies (green line) integrated from the surface to a) 500 m; b) 1000 m; c) 1500 m and d) 2000 m.
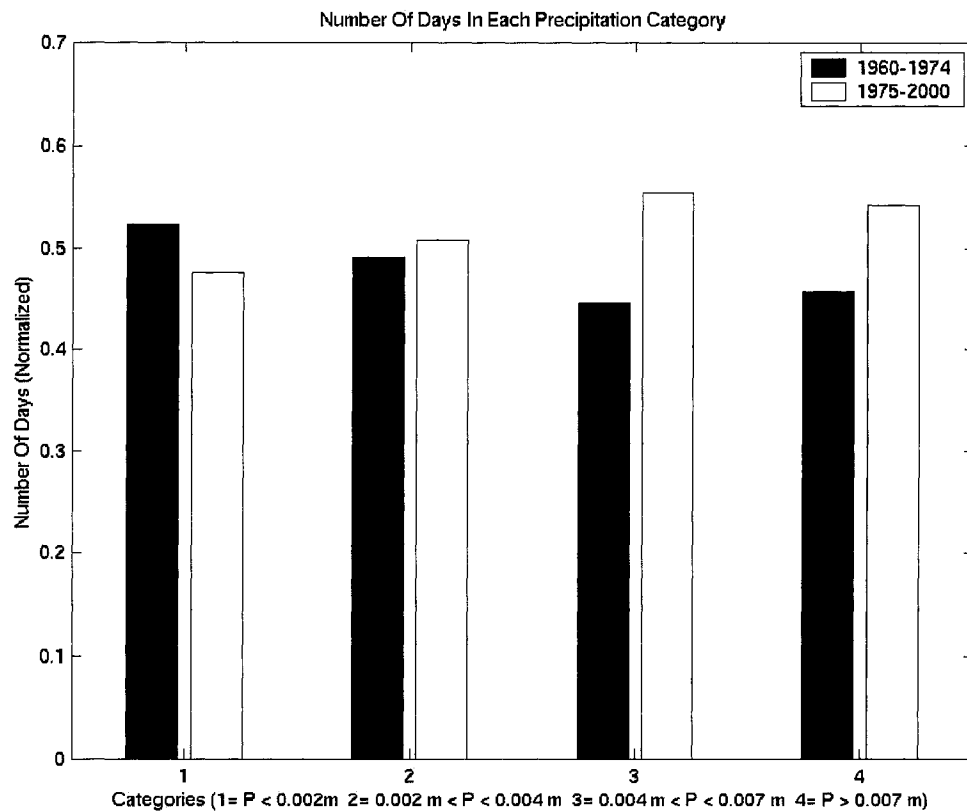
Figure 6.9: Histogram dividing the observed daily precipitation amounts, over two periods, 1960-1974 and 1975-2000, into 4 categories based on the intensity (amount) of water falling that day (P < 0.002 m, 0.002 m < P < 0.004 m, 0.004 m < P < 0.007 m, P > 0.007 m). The vertical axes has been normalized based on the percentage of events in each category falling in the two time periods).

Chapter 7

Irminger Water Variability in the West Greenland Current**

7.1 Introduction

The principle source of heat to restratify the interior of the Labrador Sea after convection events is thought to be the input of warm and salty Irminger Water (IW) (Cuny et al., 2002; Lazier et al., 2002). As a remnant of the sub-polar mode waters that have travelled cyclonically around the sub-polar gyre (Cuny et al., 2002) it enters the Irminger Current along the east coast of Greenland (Pickart et al., 2005) before rounding Cape Farewell and propagating north in the West Greenland Current (Fig.

7.1), along the slope at 200-700 m (Straneo, 2006). Buch et al. (2004) discuss how there are two components of this water mass, pure and modified, depending on how much mixing has occurred with surrounding water masses during its transit to West Greenland waters.

Bersch (2002) showed temporal variations in the upper 600 m mean salinity between 1992 and 1998 along a section in the Irminger Sea, possibly responding to the North Atlantic Oscillation with a lag of 2 years. Buch et al. (2004) showed significant variability in IW at a single station at Cape Farewell, with a shift from pure IW prior to 1970 to modified Irminger Water in 1970-95 (with a potential return of pure IW after 1995). Both Buch et al. (2004) and Stein (2004) reported similar variability in IW along a section at Fylla Bank. However, Cuny et al. (2002) examined the maximum temperature and salinity of the IW in the Labrador Sea during the 1990's and found no clear trends along the West Greenland Current. Straneo (2006) found a large difference in the lateral heat transport into the interior of the Labrador Sea between the years of Ocean Weather Station Bravo (1964-74) and a later float data set (1996-2000), which she suggested may have been related to a change in the vertical partitioning of IW. Yashayaev (2006) noted a large volume of warm and salty water appearing over the continental slopes of West Greenland during the 2000s, which he thought came from the Irminger Sea. Hatun et al. (2005) reported on record high salinities in the inflow to the Nordic Seas and showed that the salinity change was

linked to the dynamics of the sub-polar gyre circulation.

Here we examine the temporal variability of IW (both properties and trans-ports) along three sections across the West Greenland Current. Two datasets (not necessarily completely independent) are used to allow us to consider the entire period of 1949 to the present. We attempt to link the observed variability to variability elsewhere within the sub-polar gyre.

7.2 Data and methods

The first data set we use is a set of standard sections handled by the Danish Meteorological Institute every year in June-July on behalf of the Greenland Institute of Natural Resources. We focus on the Cape Farewell, Cape Desolation and Paamiut sections (Fig. 7.1). Observations were normally performed annually between 1984 and 2005 (albeit with years missing for each section) on the same 5 repeat stations on each section, but in some years only 3-4 stations were occupied due to multi-year-ice on the inner stations. In most years, the section was performed in late June or early July, but during the period 1984-87, the occupations occurred earlier in spring (March through May). For 1984-87, the analysis is based on bottle data while CTD data is used for the other years. Accuracy is to the second digit on temperature and $\pm(0.003 - 0.004)$ for salinity based on comparison with water samples (Ribergaard, 2006). We carry out our analysis on the top 700 m, the deepest depth common to all

years.

The second data set used is based upon a climatological analysis of the Labrador Sea (Kulan and Myers, 2007). All available stations with both temperature and salinity measurements that were in the Fisheries and Oceans Canada hydrographic climate database (Gregory, 2004) prior to 2000 were used. The data (with a precision of two decimal places) was divided into overlapping 3-year running mean triads covering the period 1949-1995. The data was binned into 2.5 degree (south of 55° N) or 5.0 degree boxes (north of 55° N) to provide a first guess for an objective analysis procedure that used three passes with decreasing correlation lengths of 600, 400 and 200 km, weighted by a topographic constraint to minimize mixing of waters across the shelf break. The mapping was carried out in an isopycnal framework using 44 density layers and 1/3 degree spatial resolution. The mapped time-varying triad fields were then interpolated to the location of the 5 stations along each section. Although the mapped triad data is not a unique dataset as it contains the section data, it allows us to extend the analysis much further into the past. Correlations between the triad and section data for Cape Farewell, Cape Desolation and Paamiut are respectively, 0.71, 0.43 and 0.72 for temperature and 0.87, 0.88 and 0.93 for salinity.

We took the data and examined it for each station and each section on a 2 m grid in the vertical (requiring significant interpolation only in the early years with bottle data). To determine average properties, we examined each data point and included

all of those where our definition for IW (see below) was satisfied. For transports, we determined the geostrophic velocity, relative to 700 db (or the bottom in shallower water) for each pair of stations at each depth, added an estimate of the barotropic velocity, calculated the resulting transports and then summed those whose T and S (which was interpolated onto the geostrophic velocity point) was consistent with IW. If data was missing, we did not include that point(s) in the calculation. That said, the inshore station is in shallow water with little or no IW present. Since IW is not found above 100 m, issues with the first measurement in a profile not being until 8-14 m should not effect the results. Missing measurements towards the base of a profile may be more significant.

To obtain estimates of the barotropic component of the velocity, a mean spring (April to June) climatology of the Labrador Sea produced in a similar manner to the triads (but using all data collected in the given months available in the Department of Fisheries and Oceans Canada climate database prior to 2000 irregardless of the year collected) was used as input to a regional ocean general circulation model of the sub-polar gyre (Myers, 2002) run in diagnostic mode. The component of the barotropic velocity perpendicular to the sections was then used, giving estimates of 5-7 cm/s, which based on Clarke (1984); Pickart et al. (2005) are probably a lower bound. The use of mean spring data for estimating the barotropic velocities was done so that all the variability would be contained within the baroclinic component based

on the hydrography (i.e. the barotropic variability is not included).

A number of definitions of pure and modified IW exist (Buch et al., 2004; Cuny et al., 2002; Clarke, 1984; Reynaud et al., 1995; Ribergaard, 2006), although all generally consider the water mass to have temperatures and salinities within the range 3.5-6° C and 34.85-35.10. For the purpose of this study, we choose a broad definition including both pure and modified IW, with temperatures $> 3.5°$ C and salinities > 34.88.

7.3 Results

Time versus depth plots of temperature and salinity averaged across the stations in each section where IW was present, as well as Hovmoller diagrams of the vertical average of salinity around the salinity maximum at each station are shown in figure 7.2. At Cape Farewell, salty and warm IW can be seen at 150-300 m in the early 1990s and post 1995 with two periods of maximum salinity occurring 1997-99 and post 2003. Reduced quantities of IW can be seen during the mid-1980s. Based on the single section per year, we can't differentiate whether this lack of IW is a seasonal feature with the IW not showing up at Cape Farewell until later in the spring or is truly interannual variability, although Buch et al. (2004) suggest that IW transport was lower during the 1980s. Similar variability is seen at the other sections although the salinities are generally lower.

Timeseries of mean temperature and salinity for IW (Fig. 7.3) show a trend to saltier (+0.004 per year) and warmer (+0.03° C per year) IW entering the Labrador Sea over 1984-2005. Transports are given in table 7.1, increasing post 1995 (albeit with decreased standard deviation). The mean transport of IW at Cape Farewell was estimated as 8.5-11 Sv (Clarke, 1984) from a cruise in 1978 while Pickart et al. (2005) estimated a transport of 13.6 Sv for the Irminger Current just east of Cape Farewell in 2001. Our transports of IW (2.8 ± 0.9 Sv over 1984-2005) are much smaller than that reported by Clarke (1984) but this is not surprising since his estimate is based on a much broader definition of the Greenland slope and is a snap shot from a single hydrographic section. During 1995-2005, the transport of IW at Cape Desolation is actually larger than at Cape Farewell. We suspect this is because the Cape Desolation section extends farther offshore and thus more of the IW transport is measured.

We present the triad data interpolated to the 5 stations on each section in the same way as the station data (Fig. 7.4). Due to interpolation issues, the front separating the fresh coastal component of the West Greenland Current and the IW is farther offshore in the triad data set. Despite this obvious issue, the basic characteristics of the two timeseries agree for the most part during the periods that they overlap, with very low salinities in the middle 1980s and salinities increasing in the 1990s.

The main core of the IW is in the same 100-200 m range in the triad data,

although there are some years with very low salinities and little if any IW present. Local maximums are seen in the early 1950s, the 1960s, early 1980s and the early 1990s, consistent with the results presented by Stein (2004). The depth of the IW core is deepening through the analysis period. It is also supportive of two different core depths for the IW, a shallow regime around 200-400 m (early 1950s, early 1960s and early 1980s) and a deep regime with a core at depths > 500 m (middle 1960s and early 1990s). Mean salinity and temperature similarly vary on a quasi-decadal scale, decreasing from a maximum in the 1960s (Fig. 7.3) although increasing again from the mid-1990s. Transports are comparable to those from the section data (Table 7.1) except maybe at Paamiut, where too small transports are probably the result of slightly too cold and/or fresh waters just missing the criterion we use for IW.

7.4   Summary and Discussion

Our results, consistent with previous work (Buch et al., 2004) show that there is significant variability in time with respect to the amounts and the properties of IW that enter the Labrador Sea. Strong transport coinciding with increases in the volume, salinity and temperature are generally seen through the 1960s as well as the 2000s. Fresher and colder IW is seen during the intervening period. Transport of this lower salinity mode of IW is variable, being significant in some years while in others very little if any IW is transported into the Labrador Sea. The depth of the core of

the IW also seems to vary with time, from high up in the water column (200-400 m) to deeper (400-700 m).

The increase in IW salinities seen through the late 1990s agrees with the findings of Bersch (2002). During the most recent years, we find near record high salinities (comparing with a previous maximum in the 1960s) and record high transports (both volume and salt) into the Labrador Sea. This is consistent with the record high salinities that Hatun et al. (2005) found at the entrance to the Nordic Seas as well as Yashayaev (2006) who found an increase in high salinity IW in the Labrador Sea over the last few years. Such changes were also seen at Fylla Bank (Ribergaard, 2006).

IW is a dense form of sub-polar mode water (SPMW) on its progression around the sub-polar gyre before entering the Labrador Sea (Talley and McCartney, 1982). Thierry et al. (2007) show that mode waters have become warmer, saltier and lighter since the late 1980s in the Iceland Basin and along Reykjanes Ridge, as we find farther downstream. Observations suggest that the sub-polar gyre circulation has weakened over this same period (Häkkinen and Rhines, 2004; Hatun et al., 2005), leading to changes in the North Atlantic Current transport and thus the salinity in the north-east Atlantic, which Thierry et al. (2007) then suggested fed back upon the mode water properties.

Besides impacting the circulation of the sub-polar gyre (Curry and McCartney, 2001), the low (high) phase of the North Atlantic Oscillation (NAO) can be associated

with strong (weak) heat losses in the eastern basin (Hurrell et al., 2003) leading to an increased (decreased) production of SPMW (Joyce et al., 2000). Such forcing also plays a role in driving IW variability. We use the indices produced by the National Oceanic and Atmospheric Administration/National Weather Service Climate Prediction Center (CPC). Considering only the years with non-zero IW transport in our data, the correlation coefficient between the volume transport and the winter (JFM) NAO index is maximum at a lag of one year, at -0.41 (-0.51 for the triad data prior to 1995), significant at the 99% level.

The small decreases in transports between the Cape Farewell and Cape Desolation sections show that little of the IW is transported offshore into the Labrador Sea in this region, with much of this exchange occurring between the Cape Desolation and Paamiut sections, consistent with estimates of high eddy kinetic energy and eddy fluxes in this region (Jacobsen et al., 2003). Taking the export into the interior of the Labrador Sea (taken to have an area of 10^6 km^2) as simply the difference in transports between the Cape Farewell and Paamiut sections and assuming, for lack of better estimates, that our snapshot estimates are representative for the whole year, we find mean lateral exchanges of heat and salt into the Labrador Sea due to IW for 1984-05 of $3.4 \times 10^{13} Js^{-1}$ and 3.6 mSv. Larger values (4.6 and $3.8 \times 10^{13} Js^{-1}$; 4.9 and 4.5 mSv) are found for 1995-05 and 1949-95.

These estimates agree with the contention of Straneo (2006) that the mean

annual heat loss to the atmosphere over the central Labrador Sea of 1 GJm^{-2} is balanced (and exceeded) by the subsurface transport of heat by IW. The larger IW heat transport to the interior of the Labrador Sea during the 1990s/2000s is also consistent with the increase in heat content seen during this period (Lazier et al., 2002; Straneo, 2006). Myers and Donnelly (2007) estimated LSW formation using a water mass formation approach and interannually varying fluxes and surface water properties. We find the maximum correlation between their estimates of dense LSW formation and the transport of IW at Cape Farewell to be 0.51 over the years 1960-1995, with a lag of one year, which may suggest that IW plays a role in providing salt to the Labrador Sea to drive convection (e.g. (Lazier et al., 2002; Straneo, 2006)).

Table 7.1: Volume, heat and freshwater transports of IW - means with uncertainty. References used are $0°$ C for temperature and 35.0 for salinity. Triad estimates (1949-1995) are averaged only over those years with non-zero IW transport.

Section	Volume - Sv			Heat - $10^{13} Js^{-1}$			Salt - mSv		
	1984-2005	1949-1995	1995-2005	1984-2005	1949-1995	1995-2005	1984-2005	1949-1995	1995-2005
Cape Farewell	2.8 ± 0.9	3.2 ± 0.6	3.6 ± 1.1	5.5 ± 1.7	5.8 ± 1.2	7.2 ± 2.2	6.4 ± 1.8	8.4 ± 0.4	8.1 ± 2.2
Cape Desolation	2.5 ± 0.9	2.9 ± 1.2	3.9 ± 1.2	4.7 ± 1.6	5.0 ± 2.0	7.4 ± 2.2	6.7 ± 2.5	8.0 ± 3.0	10.3 ± 3.1
Paamiut	1.1 ± 0.6	0.9 ± 0.6	1.3 ± 0.7	2.1 ± 1.1	1.6 ± 1.3	2.6 ± 1.5	2.8 ± 1.5	2.6 ± 2.0	3.2 ± 1.8
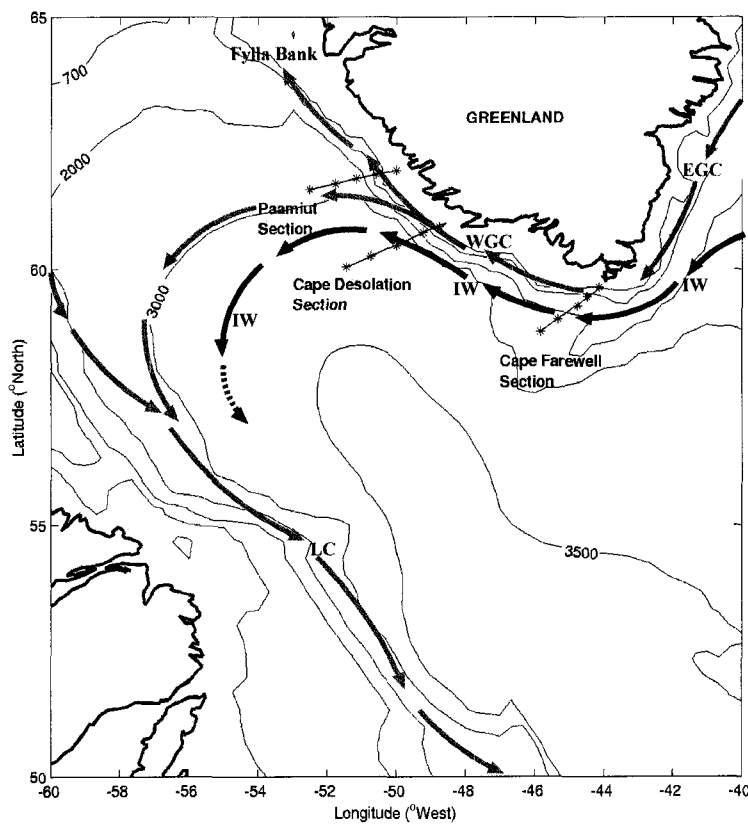
Figure 7.1: A map of our study region showing the locations of the sections used. Some of the major currents in the region are also indicated. The abbreviations used are: EGC - East Greenland Current, WGC - West Greenland Current, LC - Labrador Current and IW - Irminger Water.
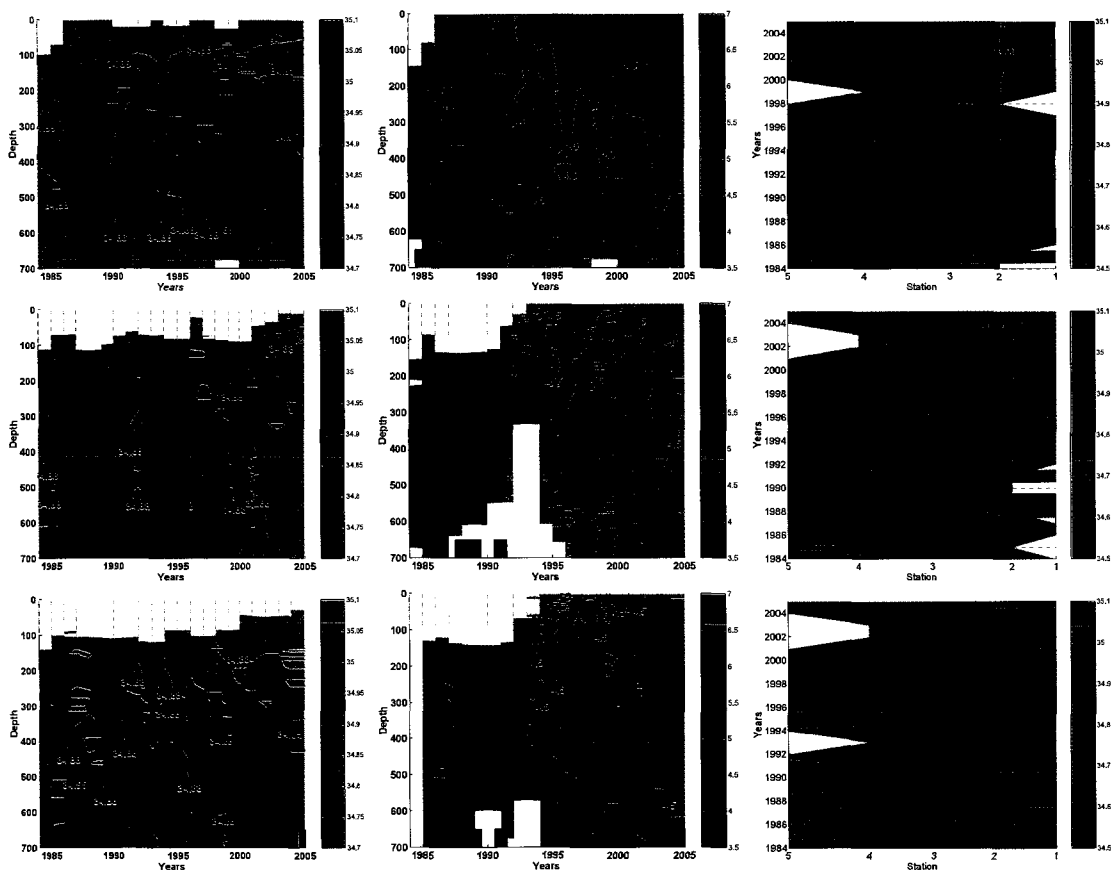
Figure 7.2: Time versus depth plots of salinity (left column) and temperature (middle column) averaged over the stations on each section (top - Cape Farewell, middle - Cape Desolation and bottom - Paamiut). Grid points with salinities less than 34.7 and temperatures less than 3.5 °C where not included in the averages. The right column shows Hovmoller plots of salinity formed by averaging in the vertical all data points with a salinity within 0.1 of the maximum salinity at that station. The red dashed lines indicate the years when the data was collected while the the black boxes indicate the years for which no data was available, with these periods filled in by linear interpolation. The white regions indicate where the temperature or salinity at no station along the given section was in the ranges plotted (34.7-35.1 and 3.5-7 °C).
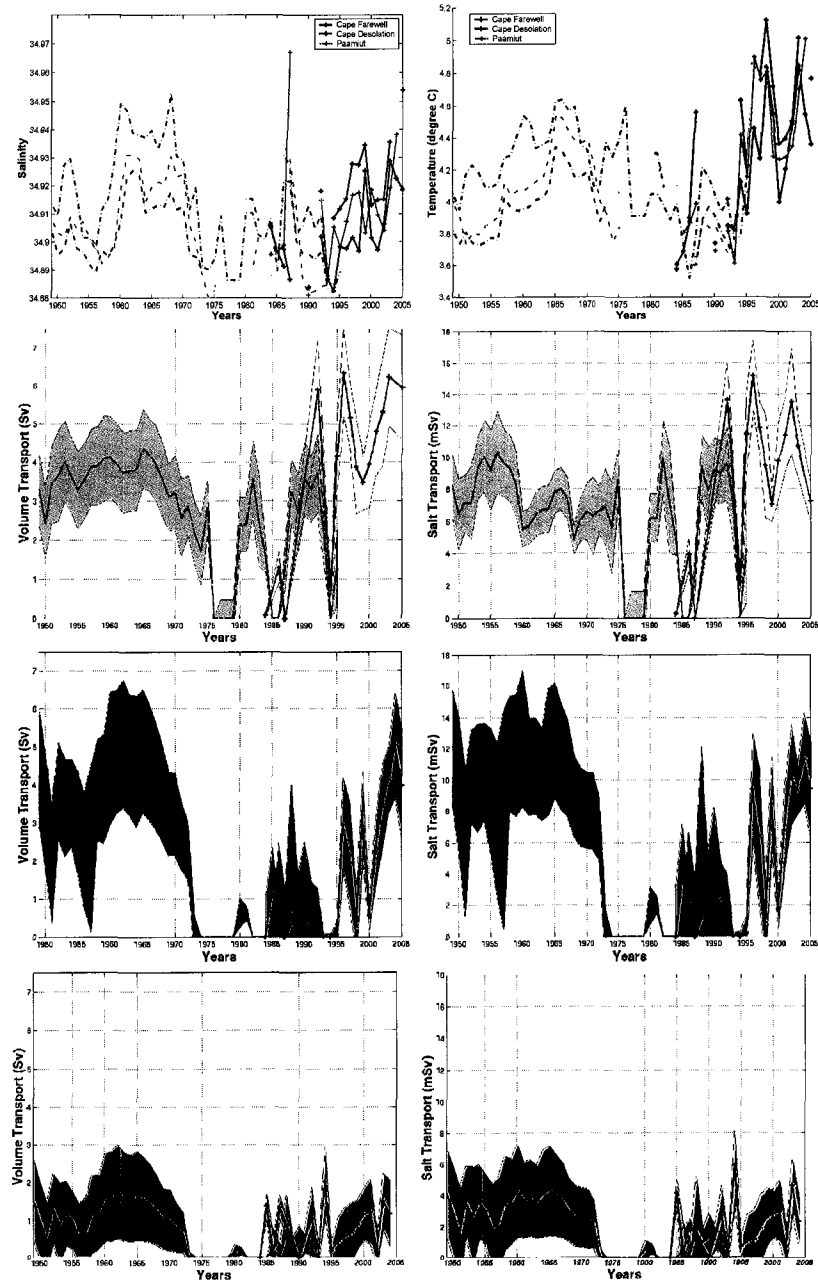
Figure 7.3: IW Timeseries of mean salinity (top left), temperature (top right), volume transport (left) and salt transport (relative to 35.0) (right) for the 3 sections (Cape Farewell - Row 2, Cape Desolation - Row 3 and Paamiut - Row 4). A dash pattern is used for the triad data (with uncertainties given in dark gray, blue and red respectively) while the section data is shown using a solid line (and lighter shades). The uncertainty estimates for transports are based on the given precisions for property measurements and an estimate of 2.0 cm/s for the barotropic velocity.
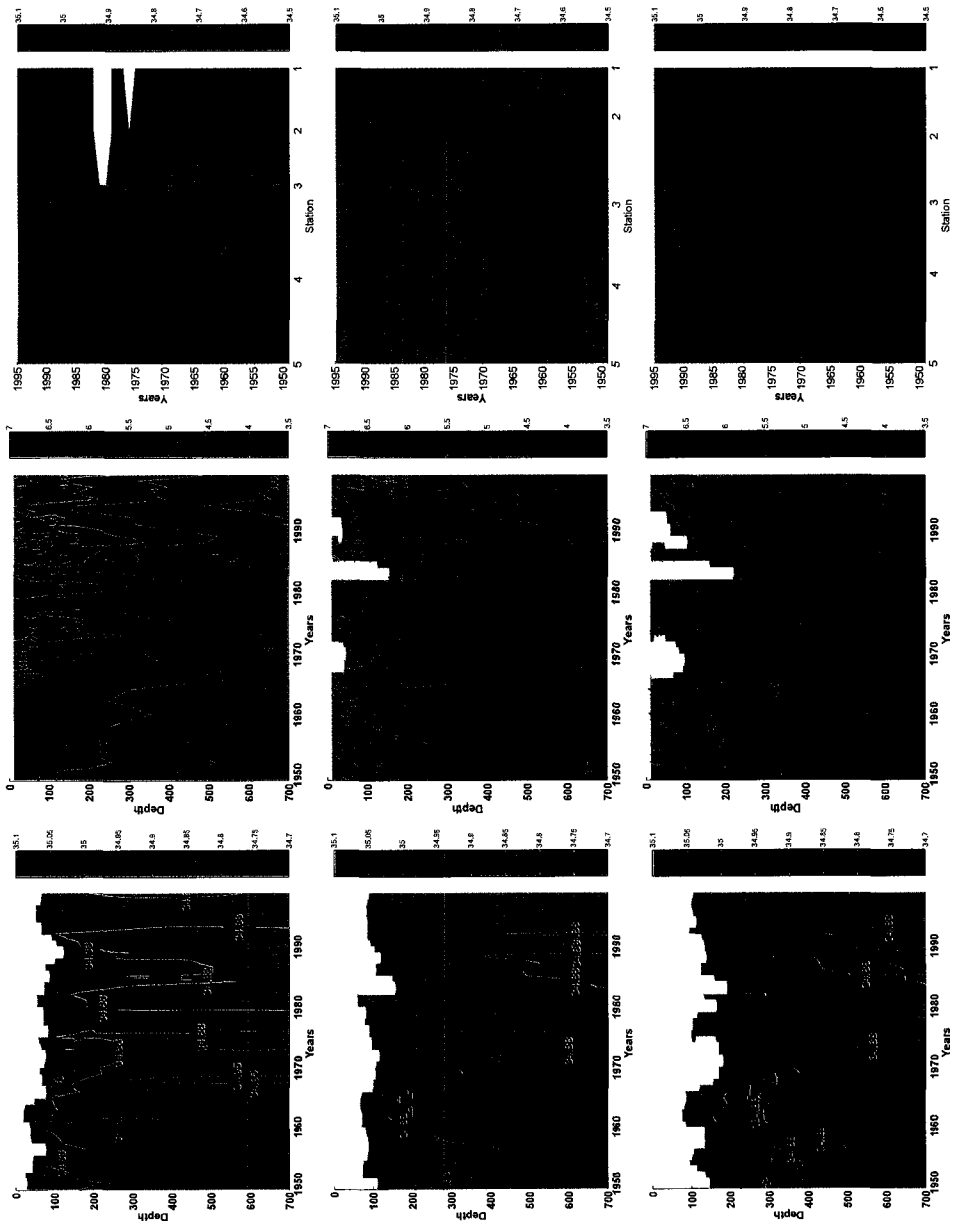
Figure 7.4: As per figure 2, except using the interpolated triad data.

202

Chapter 8

Conclusions

This final chapter of the dissertation provides a summary of the purpose, methods and results discussed in the earlier chapters.

The starting point of the project was to take advantage of increased data volumes to build a current and high-resolution climatology for the Labrador Sea. The method preferred for the development of the climatology was the one that employs isopycnal coordinates in the vertical. However, a more traditional geopotential climatology was also produced to study the differences between the two.

The results discussed in detail in *Chapter* 3 show that using isopycnal coordinates in the vertical improves the results. Evidence of this improvement is seen in the DWBC salinity signal (Figures 3.3 and 3.6) since the baroclinicity of the flow field is better preserved in the isopycnal climatology. This occurs, because in the

isopycnal method, the data are binned according to their density classes, and this avoids artificial mixing of water properties between different water mass types.

Apart from the vertical coordinates, the two climatologies use almost identical data, and the same objective analysis scheme. An advantage of the objective analysis scheme used in this study is the additional depth-dependence criterion. It is known that the currents tend to follow f/h lines (where f is the coriolis parameter and h is the water column depth). Fronts are preserved by restricting the depth range over which data can be included in the calculation of the correction term for the temperature and salinity at a grid point (Figure 3.5).

Looking at the results on isopycnal surfaces directly gives information about the temperature and salinity properties, and advection of particular water masses, such as the LSW (e.g. Figure 3.8). The climatological core temperature and salinity of the LSW is found to be 3.3 °C and 34.88 in the interior Labrador Sea. The advection pathways of the LSW can also be seen from its property distribution at this density surface.

Results from the climatologies were used in diagnostic calculations to get current velocities and fluxes. The isopycnal climatology does a better job of separating water masses in general. Sharper fronts, which are found between the shelf-break and the interior in the ISO, yield larger velocities for the boundary currents in the diagnostic calculations ($\approx 25cm/s$, Figure 3.4). The boundary circulation is cyclonic and

strongly barotropic as seen in Figure 3.4. The DWBC reaches speeds up to $20cm/s$ at $2400m$ as calculated from the ISO.

The surface waters off Baffin Island have a temperature and salinity of ≈ -1.45 °C and ≈ 32.5, respectively. Surface current velocities on the Baffin Island side reach up to $8cm/s$ southwards (Figure 3.10). The volume, freshwater, and heat fluxes across the 66.3 °N are $21.2mSv$, $-31.7mSv$ (referenced to a salinity of 35), and $7,720GW$, respectively (Table 3.2).

Based on the regional definitions used in this study (Figure 2.2), the amount of freshwater stored in the top $300m$ of the LC is found to be approximately three times as large as that of the WGC (Table 3.4). Differences between the ISO and GEO become less pronounced away from the surface. The differences between the ISO and GEO heat contents are less significant than the differences between the freshwater budgets. The largest differences between the ISO and GEO are observed in the WGC freshwater budget.

The total volume transport across the 52.7 °N transect in the southern Labrador Sea is found to be $46.6Sv$ in the ISO and $26.1Sv$ in the GEO. The ISO-based transport value is consistent with previous diagnostic estimates of the the sub-polar gyre (Reynaud et al., 1995; Myers et al., 1996, e.g.). This difference in the southward volume flux of the boundary currents arises mainly from rapidly dying baroclinic velocities found in the GEO (see *Section* 3.3 for further detail).

The most significant improvement these new climatologies provide is in the representation of fronts. The additional depth-dependency of the objective analysis scheme preserves the strength of temperature and salinity gradients (Figure 3.13) and this, in turn, gives more realistic current velocities and fluxes (calculated by the diagnostic methods).

Seasonal variability, the most fundamental mode of variability in the atmosphere-ocean system, is discussed in *Chapter* 4. The largest variability in water mass properties is observed over winter. Moreover, near surface ($< 300m$) waters and boundary currents exhibit greater variability than the deeper waters and interior Labrador Sea (Tables 4.1 - 4.4).

Noticeable differences are seen in the seasonality of the freshwater budgets of the WGC and LC. The LC freshwater content increases from spring to fall, stays relatively constant between fall and winter, and drops considerably between winter and spring. The WGC freshwater content, on the other, increases between spring and fall, and decreases from summer towards winter (Tables 4.1 - 4.4). These differences can be attributed to differences in the freshwater sources between the two boundary currents. Unlike the freshwater budgets, the seasonal cycles of the WGC and LC heat budgets are similar.

The seasonal temperature and salinity profiles for the LC area (Figure 4.2) indicate that the stratification is weakest in winter. This could be a result of deep

convection taking place within the boundary current (Pickart et al., 1997, e.g.). However, the resolution and the time-scale of the seasonal climatologies are insufficient to reach such a conclusion.

The possibility of a temporal bias in a climatological study is considered when interpreting the results, since that might cause artificial extremes in properties. A detailed analysis of the source data helps to understand the true nature of these extremes as discussed in *Section* 4.1.2.1.

An average ocean to atmosphere heat flux of $\approx 136 Wm^{-2}$ is estimated between fall and winter. This value is consistent with other seasonal estimates (Straneo, 2006, e.g.). Also from the seasonal climatologies, it is estimated that an additional $28,000 km^3$ of the LSW is formed each year. This value corresponds to a formation rate of $\approx 3.6 Sv$ for the LSW.

The largest contributor to the interior Labrador Sea freshwater budget is found to be the WGC. The seasonal freshwater flux through the WGC varies between $20.8 mSv$ in winter and $38.7 mSv$ in fall. Even though the LC has a larger freshwater budget than the WGC, its contribution to the interior Labrador Sea is less significant. The amount of freshwater supplied to the interior by the LC varies between nil in winter and $6.7 mSv$ in spring.

Seasonal MLD variability was investigated as part of the seasonal climatological analysis. The deepest MLDs in the Labrador Sea are found just offshore of the

$3000m$ isobath in winter (Figure 4.8). Winter MLDs are profoundly larger than other seasonal MLDs. Winter MLDs, albeit shallower, agree with the MLD pattern reported by Deshayes et al. (2007) in a recent numerical modelling study of the Labrador Sea. Due to extensive spatial and temporal averaging, deepening of the mixed layer during short-lived and localized deep convection events are not adequately represented. The shallowest MLDs are found in fall with depths of about $65m$.

The OA scheme used to compile yearly and seasonal climatologies was applied to data grouped over shorter periods. Increased search radii and additional smoothing and filling were introduced to counteract reduced data volumes. By applying the modified OA scheme to the data grouped in overlapping three-year periods, a pseudo-time-series was constructed.

Near surface temperature and salinity time-series (Figures 5.2 - 5.4) suggest that in addition to the GSAs of the 1970s and the 1980s, the central Labrador Sea might have experienced other transient freshwater anomalies in the mid-to-late 1950s and early 1990s. Also, these freshwater anomalies are usually accompanied by lower than normal surface temperatures.

The 1980s GSA is most pronounced in the LC and interior Labrador Sea, but has a weaker signal in the WGC. This supports the theory that the GSAs can be triggered by different mechanisms in various parts of the sub-polar gyre (Belkin et al., 1998).

The temperature and salinity time-series for the interior Labrador Sea provides

a continuous record of the variability between 1949 and 1999. This period includes the years when deep convection was hindered in the late 1960s. Higher freshwater influx ($\approx 12mSv$ as calculated from the triads over the 1950-1964 period) increased the effect of low NAO indices of 1955-1970 by increasing the stability of the surface waters.

The interior Labrador Sea is found to have a positive freshwater budget (integrated between surface and $2000m$) with an average of $\approx 10mSv$. Even though the LC supplies an average of $1.14mSv$ of freshwater to the interior, its contribution has not always been positive (Figure 5.7). The WGC brings a long-term average of $26.2mSv$ of freshwater into the interior Labrador Sea. There is a significant inverse correlation ($r = -0.66$) between the amount of freshwater contributed by the WGC and the LC to the interior, which is perhaps related to the sub-polar gyre dynamics.

The time-series constructed from the triad analysis have been used to address important questions, such as the source of freshening in the western sub-polar gyre (*Chapter* 6) and IW variability (*Chapter* 7). These are some examples of how these climatologies can be used to further our understanding of the climate variability in the Labrador Sea.

Historically, atmospheric variables have been observed more regularly and at higher rates than oceanic variables. Myers et al. (2007a) (*Chapter* 6) studies the link between the atmospheric precipitation/evaporation budgets and the freshwater

budget of the Labrador Sea. For the atmospheric part of this study, NCEP/NCAR and ERA40 reanalyses data were used. The oceanic freshwater budgets were derived from the triad analysis (*Chapter* 5). Examining the long-term (1950-1999) variability and relationship between atmospheric and oceanic parameters would not have been possible without the continuous, oceanic time-series built in this study.

Another application of the triad analysis is shown in *Chapter* 7 (Myers et al., 2007b). This study concerns the variability of the IW, an important source of heat and high salinity waters for the Labrador Sea. There have been some direct observations performed by the Danish Meteorological Institute, in June-July of most years between 1984 and 2005. However, in order to expand the analysis further back to 1949, triad results are used. Considering the longer response time of the oceans than that of the atmosphere and seawater's high heat capacity, such long-period time-series are necessary to address variability of the water masses adequately.

Some other possible applications of the climatologies developed in this study include: diagnostic and modelling studies, as a benchmark to asses variability since the year 2000, and for the quality control of recently collected data.

Since the Labrador Sea is a key part of the North Atlantic branch of the MOC, its variability deserves more detailed study. The time-series of temperature and salinity obtained from the triad analysis can be used to further examine the changes in all water masses of the Labrador Sea, especially the LSW.

Formation rates, locations, and types of the LSW and their links to atmospheric variability can also be examined. With the help of the 51-year long time-series of temperature, salinity, heat and freshwater budgets, oceanic indices can be established and linked to atmospheric indices, such as the NAO-index.

It is found that improving the OA scheme by adding extra constraints on the type of data that can be included in the calculation of the correction term at a grid point preserves the fronts that exist between onshore and offshore waters. As shown in *Section* 3.4 the most up-to-date world ocean climatology, the WOA05, greatly smooths out these features. The same restrictions on OA cannot be applied to a global climatology due to data limitations at the moment. However, the OA scheme used in this study can be applied to neighboring regions.

Expanding the climatologies in terms of both regional and temporal coverage is the next step. In recent years, there has been an increase in data volumes with the help of many autonomous floats launched in the world oceans (e.g. the Argo project). The climatologies can be expanded by including data from Argo floats. On the other hand, the current climatologies developed in this study can be used to validate the float data.

Numerical modelling studies can also make use of the climatologies. The climatologies can be used in two ways, to initialize the ocean properties, or to compare with the model results. High resolution of the climatologies, i.e. the strength of tempera-

ture and salinity gradients in key areas is important in producing a more realistic flow field. The current climatologies can enhance the numerical model results, especially for those which have a focus on the Labrador Sea.

As discussed throughout the dissertation, diagnostic calculations based on the climatologies provide information about current velocities and fluxes of volume, heat and freshwater. The triad analysis, combined with the diagnostic calculations, can be used to study the long-term variability of the export from the Labrador Sea. The link between the variability observed in the Labrador Sea and the variability in the North Atlantic and the rest of the world oceans can be examined. Moreover, these climatologies can be used in to calculate the baroclinic and and barotropic components of the flow field and their variability.

Freshwater transport variability by the WGC and LC is another subject which can be studied by combining the triad analysis with diagnostic calculations. A link between the salinity of the IW and the strength of the sub-polar gyre is indicated (Häkkinen and Rhines, 2004). A similar link between the amount of freshwater supplied by the WGC versus LC and sub-polar gyre dynamics is plausible and merits a more detailed investigation.

Bibliography

Adcroft, A., C. Hill, and J. Marshall, 1997: Representation of topography by shaved cells in a height coordinate ocean model. *Mon. Weather Rev.*, **125**, 2293–2315.

Barnes, S. L., 1964: A Technique for Maximizing Details in Numerical Weather Map Analysis. *J. of App. Meteo.*, **3**, 396–409.

Barnston, A. G. and R. E. Livezey, 1987: Classification, seasonality and persistence of low-frequency atmospheric circulation patterns. *Monthly Weather Review*, **115**, 1083–1126.

Belkin, I. M., 2004: Propagation of the "Great Salinty anomaly" of the 1990s around the northern North Atlantic. *Geophysical Research Letters*, **31**, L08306, doi:10.1029/203GL019334.

Belkin, I. M., S. Levitus, J. Antonov, and S.-A. Malmberg, 1998: "Great Salinity Anomalies" in the North Atlantic. *Prog. in Ocenaogr.*, **41**, 1–68.

Bersch, M., 2002: North Atlantic Oscillation-induced changes of the upper layer circulation in the northern North Atlantic Ocean. *Journal of Geophysical Research*, **107**.

Boyer, T., S. Levitus, H. Garcia, R. A. Locarnini, C. Stephens, and J. Antonov, 2005: Objective Analysis of Annual, Seasonal, and Monthly Temperature and Salinity for the World Ocean on a 0.25ô Grid. *Int. J. of Climatol.*, **25**, 931–945.

Boyer, T. P. and S. Levitus, 1994: Quality control and processing of historical temperature, salinity and oxygen data. NOAA Technical Report NESDIS 81.

Boyer, T. P., C. Stephens, J. I. Antonov, M. E. Conkright, R. A. Locarnini, T. D. O'Brien, and H. E. Garcia, 2002: World Ocean Atlas 2001 Volume 2: Salinity. NOAA Atlas NESDIS 50.

Brandt, P., F. A. Schott, A. Funk, and C. S. Martins, 2004: Seasonal to interannual variability of the eddy field in the Labrador Sea from satellite altimetry. *Journal of Geophysical Research*, **109**, C02028, doi:10.1029/2002JC001551.

213

Bretherton, F. P., R. E. Davis, and C. B. Fandry, 1976: A technique for objective analysis and design of oceanographic experiments applied to MODE-73. *Deep-Sea Res.*, **23**, 559–582.

Buch, E., S. A. Pedersen, and M. H. Ribergaard, 2004: Ecosystem variability in west greenland waters. *Journal of Northwest Atlantic Fishery Science*, **34**, 13–28.

Clarke, R. A., 1984: Transport through the Cape Farewell-Flemish Cap section. *Rapp. P.-v. Réun. Cons. int. Explor. Mer*, **185**, 120–130.

Clarke, R. A. and J.-C. Gascard, 1983: The Formation of Labrador Sea Water. Part I: Large-Scale Processes. *Journal of Physical Oceanography*, **13**, 1764–1778.

Colbourne, E. B. and G. Mertz, 1998: Spatial and Temporal Variability of Ocean Temperature over the Labrador Shelf. *Atmosphere-Ocean*, **36**, 299–317.

Cooper, C. and C. Gordon, 2002: North Atlantic Oceanic Decadal Variability in the Hadley Centre Coupled Model. *J. of Climate*, **15**, 45–72.

Cressman, G. P., 1959: An operational objective analysis scheme. *Mon. Weather Rev.*, **87**, 329–340.

Cuny, J., P. B. Rhines, P. P. Niiler, and S. Bacon, 2002: Labrador Sea Boundary Currents and the Fate of the Irminger Sea Water. *Journal of Physical Oceanography*, **32**, 627–647.

Curry, R., B. Dickson, and I. Yashayaev, 2003: A change in the freshwater balance of the Atlantic Ocean over the past four decades. *Nature*, **426**, 826–829.

Curry, R. and C. Mauritzen, 2005: Dilution of the northern North Atlantic Ocean in recent decades. *Science*, **308**, 1772–1774.

Curry, R. G. and M. S. McCartney, 2001: Ocean gyre circulation changes associated with the North Atlantic Oscillation. *Journal of Physical Oceanography*, **31**, 3374–3400.

Curry, R. G., M. S. McCartney, and T. M. Joyce, 1998: Oceanic transport of subpolar climate signals to mid-depth subtropical waters. *Nature*, **391**, 575–577.

Daley, R., 1991: *Atmospheric Data Analysis*. Number 457 pp., Cambridge University Press.

Deser, C. and M. L. Blackmon, 1993: Surface Climate Variations over the North Atlantic Ocean during Winter: 1900-1989. *J. of Climate*, **6**, 1743–1753.

Deshayes, J., C. Frankignoul, and H. Drange, 2007: Formation and export of deep water in the Labrador and Irminger Seas in a GCM. *Deep-Sea Research I*, **54**, 510–532.

deYoung, B., F. Perry, and R. Greatbatch, 1994: Objective Analysis of Hydrographic Data In The Northwest Atlantic. Canadian Technical Report of Hydrography and Ocean Sciences 130, Fisheries and Oceans.

Dickson, B., I. Yashayaev, J. Meincke, B. Turrell, S. Dye, and J. Holfort, 2002: Rapid freshening of the North Atlantic Ocean over the past four decades. *Nature*, **416**, 832–836.

Dickson, R., J. Lazier, J. Meincke, P. Rhines, and J. Swift, 1996: Long-term coordinated changes in the convective activity of the North Atlantic. *Prog. Oceanog.*, **38**, 241–295.

Dickson, R. R., J. Meincke, S. A. Malmberg, and A. J. Lee, 1988: The "Great Salinity Anomaly" in the North Atlantic. *Prog. in Oceanogr.*, **20**, 575–577.

Dickson, R. R., T. J. Osborn, J. W. Hurrell, J. Meincke, J. Blindheim, B. Adlandsvik, T. Vinje, G. Alekseev, and W. Maslowski, 2000: The Arctic Ocean response to the North Atlantic Oscillation. *Journal of Climate*, **13**, 2671–2696.

Eden, C. and C. Böning, 2002: Sources of Eddy Kinetic Energy in the Labrador Sea. *Journal of Physical Oceanography*, **32**, 3346–3363.

Fischer, J., F. A. Schott, and M. Dengler, 2004: Boundary Circulation at the Exit of the Labrador Sea. *Journal of Physical Oceanography*, **34**, 1548–1570.

Flatau, M. K., L. Talley, and P. P. Niiler, 2003: The North Atlantic Oscillation, Surface Current Velocities, and SST Changes in the Subpolar North Atlantic. *J. of Climate*, **16**, 2355–2369.

Fofonoff, N. P. and R. C. Millard, 1983: Algoritms for computation of fundamental properties of seawater. UNESCO technical papers in marine science. No. 44.

Fratantoni, D. M., 2001: North Atlantic surface circulation during the 1990's observed with satellite-tracked drifters. *Journal of Geophysical Research*, **106**, C10, 22,067–22,093.

Freudentral, S. and C. Andrié, 2002: The arrival of a "new" Labrador Sea Water signal in the tropical Atlantic in 1996. *Geophysical Research Letters*, **29**, 15, 1741, 10.1029/2002GL015062.

Frich, P., L. Alexander, P. Della-Marta, B. Gleason, M. Haylock, A. M. G. K. Tank, and T. Peterson, 2002: Observed coherent changes in climatic extremes during the second half of the twentieth century. *Clim. Res.*, **19**, 193–212.

Gascard, J.-C. and R. A. Clarke, 1983: The Formation of Labrador Sea Water. Part II: Mesoscale and Smaller-Scale Processes. *Journal of Physical Oceanography*, **13**, 1779–1797.

Gonzalez-Pola, C., A. Lavin, and M. Vargas-Yanez, 2005: Intense warming and salinity modification of intermediate water masses in the southeastern corner of the Bay of Biscay for the period 1992-2003. *Journal of Geophysical Research*, **110**.

Greatbatch, R. J., 2000: The North Atlantic oscillation. *Stochastic Environmental Research and Risk Assessment*, **14**, 213–242.

Greatbatch, R. J. and A. Goulding, 1989: Seasonal variations in a linear baratropic model of the North Atlantic driven by the Hellerman and Rosentein wind stress field. *Journal of Physical Oceanography*, **19**, 572–595.

Gregory, D. N., 2004: Climate: A database of temperature and salinity observations for the northwest Atlantic. Technical Report DFO Can Sci. Advis. Sec. Res. Doc. 2004/075, MEDS.

Grey, S. M. and K. Haines, 1999: Climatological hydrography of the North Atlantic. *Int. WOCE Newsletter*, **36**, 23–25.

Groisman, P. Y., R. W. Knight, D. E. Easterling, T. R. Karl, G. C. Hegerl, and V. N. Razuvaev, 2005: Trends in intense precipitation in the climate record. *Journal of Climate*, **18**, 1326–1344.

Häkkinen, S., 2002: Freshening of the Labrador Sea surface waters in the 1990s: Another great salinity anomaly? *Geophysical Research Letters*, **29**, 24, 2232, doi:10.1029/202GL015243.

Häkkinen, S. and P. B. Rhines, 2004: Decline of Subpolar North Atlantic Circulation During the 1990s. *Science*, **304**, 555–559.

Hátún, H., A. B. Sandø, H. Drange, and M. Bentsen, 2005: Seasonal to Decadal Temperature Variations in the Faroe-Shetland Inflow Waters. AGU Geophysical Monograph Series; 158.

Hatun, H., A. B. Sando, H. Drange, B. Hansen, and H. Valdimarsson, 2005: Influence of the Atlantic subpolar gyre on the thermohaline circulation. *Science*, **309**, 1841–1844.

Houghton, R. W. and M. H. Visbeck, 2002: Quasi-decadal Salinity Fluctuations in the Labrador Sea. *Journal of Physical Oceanography*, **32**, 687–701.

Hurrell, J. W., 1995: Decadal trends in the North Atlantic oscillation regional temperatures and precipitation. *Science*, **269**, 676–679.

Hurrell, J. W., Y. Kushnir, G. Ottersen, and M. Visbeck, 2003: *The North Atlantic Oscillation: Climate Significance and Environmental Impact*. Geophysical Monograph Series, 134, 279 pp.

IPCC, 1996: *Climate Change 1995: The Science of Climate Change, Contribution of Working Group I to the Second Assessment Report of the Intergovernmental Panel on Climate Change*, J. T. Houghton, L. G. M. Filho, B. A. Callander, N. Harris, A. Kattenberg, and K. Maskell, eds., Cambridge Univ. Press, Cambridge, 572 pp.

Jacobsen, P. K., M. H. Ribergaard, D. Quadfasel, T. Schmith, and C. W. Hughes, 2003: The near surface circulation in the northern North Atlantic as inferred from lagrangian drifters: variability from the mesoscale to interannual. *Journal of Geophysical Research*, **108**.

Josey, S. A. and R. Marsh, 2005: Surface freshwater flux variability and recent freshening of the North Atlantic in the eastern subpolar gyre. *Journal of Geophysical Research*, **110**, C05008.

Joyce, T. M., C. Deser, and M. A. Spall, 2000: The relation between decadal variability of subtropical mode water and the north atlantic oscillation. *Journal of Climate*, **13**, 2550–2569.

Kara, A. B., P. A. Rochford, and H. E. Hulburt, 2003: Mixed layer depth variability over the global ocean. *Journal of Geophysical Research*, **108(C3)**, 1–15.

Kara, A. B., P. A. Rochford, and H. E. Hurlburt, 2000: An optimal definition for ocean mixed layer depth. *Journal of Geophysical Research*, **105**, 16803–16821.

Katsman, C. A., M. A. Spall, and R. S. Pickart, 2004: Boundary Current Eddies and Their Role in the Restartification of the Labrador Sea. *Journal of Physical Oceanography*, **34**, 1967–1983.

Khatiwala, S., P. Schlosser, and M. Visbeck, 2002: Rates and mechanisms of water mass transformations in the Labrador Sea as inferred from tracer observations. *Journal of Physical Oceanography*, **32**, 666–686.

Kistler et al., 2001: The NCEP-NCAR 50-year reanalysis: Monthly means CD-ROM and documentation. *Bulletin of the American Meteorological Society*, **82**, 247–267.

Kulan, N. and P. G. Myers, 2007: Comparing two climatologies of the Labrador Sea: Geopotential vs. isopycnal. *Atmosphere-Ocean*, in revision.

Lab. Sea Group, 1998: The Labrador Sea Deep Convection Experiment. *Bull. Am. Met. Soc.*, **79**, 2033–2058.

Lankhorst, M. and W. Zenk, 2006: Lagrangian observations of the middepth and deep velocity fields of the northeastern Atlantic Ocean. *Journal of Physical Oceanography*, **36**, 43–63.

Lavender, K. L., R. E. Davis, and W. B. Owens, 2000: Mid-depth recirculation observed in the interior Labrador and Irminger seas by direct velocity measurements. *Nature*, **407**, 66–69.

—, 2002: Observations of Open-Ocean Deep Convection in the Labrador from Subsurface Floats. *Journal of Physical Oceanography*, **32**, 511–526.

Lavender, K. L., W. B. Owens, and R. E. Davis, 2005: The mid-depth circulation of the subpolar North Atlantic Ocean as measured by subsurface floats. *Deep-Sea Research I*, **52**, 767–785.

Lazier, J., R. Hendry, A. Clarke, I. Yashayaev, and P. Rhines, 2002: Convection and restratification in the Labrador Sea, 1990-2000. *DS1*, **49**, 1819–1835.

Lazier, J. R. N., 1973: The renewal of the Labrador Sea water. *Deep Sea Research*, **20**, 341–353.

—, 1980: Oceanographic conditions at O. W. S. Bravo 1964-1974. *Atmosphere-Ocean*, **18**, 227–238.

Lazier, J. R. N. and D. G. Wright, 1993: Annual Velocity Variations in the Labrador Current. *Journal of Physical Oceanography*, **23**, 659–678.

Levitus, S., 1982: Climatological atlas of the world ocean. Technical Report 13, U.S. Department of Commerce, National Oceanographic and Atmospheric Administration.

—, 1994: World Ocean Atlas 1994 CD-ROM sets. Technical Report Informal Report 13, U.S. Department of Commerce, National Oceanographic and Atmospheric Administration.

Levitus, S., J. I. Antonov, T. P. Boyer, and C. Stephens, 2000: Warming of the World Ocean. *Science*, **287**, 2225–2229.

Li, H. and B. Chen, 2005: The evolution of precipitable water associated with the Asian and Australian monsoons as revealed from MODIS/SSMI, ECMWF and NCEP reanalysis data sets. *Geophysical Research Letters*, **32**.

Lilly, J. M., P. B. Rhines, F. Schott, K. Lavender, J. Lazier, U. Send, and E. D'Asaro, 2003: Observations of the Labrador Sea eddy field. *Prog. in Oceanogr.*, **59**, 75–176.

Lilly, J. M., P. B. Rhines, M. Visbeck, R. Davis, J. R. N. Lazier, F. Schott, and D. Farmer, 1999: Observing deep convection in the Labrador Sea during winter 1994/95. *Journal of Physical Oceanography*, **29**, 2065–2098.

Loder, J. W., B. Petrie, and G. Gawarkiewicz, 1998: The costal ocean off northeastern North America: A large-scale view. *The Sea, Volume 11*, A. R. Robinson and K. H. Brink, eds., John Wiley and Sons, Inc., 105–133.

Lozier, M. S., W. B. Owens, and R. G. Curry, 1995: The climatology of the North Atlantic. *Prog. Oceanog.*, **36**, 1–44.

M G Bosilovich, S. D. S. and G. K. Walker, 2005: Global changes of the water cycle intensity. *Journal of Climate*, **18**, 1591–1608.

MacDonald, A. M., T. Suga, and R. G. Curry, 2001: An Isopycnally Averaged North Pacific Climatology. *J. of Atm. and Ocean. Tech.*, **18**, 394–420.

Marsh, R., B. de Cuevas, A. C. Coward, H. L. Bryden, and M. Álvarez, 2005: Thermohaline circulation at three key sections in the North Atlantic over 1985-2002. *Geophysical Research Letters*, **32**, L10604, doi:10.1029/2004GL022281.

Marshall, J. and F. Schott, 1999: Open-ocean convection: Observations, theory, and models. *Rev. Geophys.*, **37**, 1–64.

McCartney, M. S., 1992: Recirculating components to the deep boundary current of the northern North Atlantic. *Prog. in Oceanogr.*, **29**, 283–383.

Molinari, R. L., R. A. Fine, and W. D. Wilson, 1998: The arrival of recently formed Labrador Sea Water in the Deep Western Boundary Current at 26.5 degrees N. *Geophysical Research Letters*, **25**, 2,249–2,252.

Myers, P. G., 2002: SPOM: A Regional Model of the Sub-polar North Atlantic. *Atmosphere-Ocean*, **40**, 445–463.

—, 2005: Impact of freshwater from the Canadian Arctic Archipelago on Labrador Sea Water formation. *Geophysical Research Letters*, **32**.

Myers, P. G. and C. Donnelly, 2007: Water mass transformation and formation in the labrador sea. *Journal of Climate*, in revision.

Myers, P. G., A. F. Fanning, and A. J. Weaver, 1996: JEBAR, bottom pressure torque and Gulf Stream seperation. *Journal of Physical Oceanography*, **26**, 671–683.

Myers, P. G., S. Grey, and K. Haines, 2005: A Diagnostic Study of Interpentadal Variability in the North Atlantic Ocean Using a Finite Element Model. *Ocean Modelling*, **10**, 69–81.

Myers, P. G., S. A. Josey, B. Wheler, and N. Kulan, 2007a: Interdecadal variability in Labrador Sea precipitation minus evaporation and salinity. *Progress in Oceanography*, **73**, 341–357.

Myers, P. G., N. Kulan, and M. H. Ribergaard, 2007b: Irminger Water variability in the West Greenland Current. *Geophysical Research Letters*, in press.

Mysak, L. A., D. K. Manak, and R. F. Marsden, 1990: Sea-ice anomalies observed in the Greenland and Labrador Seas during 1901-1984 and their relation to an interdecadal Arctic climate cycle. *Clim. Dynamics*, **5**, 111–133.

NOAA, 1988: Data Announcement 88-MGG-02. *Digital relief of the Surface of the Earth*, National Geophysical Data Center, Boulder, Colorado, [Available at http://www.ngdc.noaa.gov].

Peterson, B. J., R. M. Holmes, J. W. McClelland, C. J. Vorosmarty, R. B. Lammers, A. I. Shiklomanov, I. A. Shiknomanov, and S. Rahmstorf, 2002: Increasing river discharge to the Arctic Ocean. *Science*, **298**, 2171–2173.

Petrie, B. and C. Andersen, 1983: Circulation on the Newfoundland continental shelf. *Atmosphere-Ocean*, **21**, 207–226.

Pickart, R. S., M. A. Spall, and J. R. N. Lazier, 1997: Mid-depth ventilation in the western boundary current system of the sub-polar gyre. *Deep-Sea Research I*, **44**, 1025–1054.

Pickart, R. S., M. A. Spall, M. H. Ribergaard, G. W. K. Moore, and R. F. Milliff, 2003: Deep convection in the Irminger Sea forced by the Greenland tip jet. *Nature*, **424**, 152–156.

Pickart, R. S., D. J. Torres, and R. A. Clarke, 2002: Hydrography of the Labrador Sea during Active Convection. *Journal of Physical Oceanography*, **32**, 428–457.

Pickart, R. S., D. J. Torres, and P. S. Fratantoni, 2005: The East Greenland spill jet. *Journal of Physical Oceanography*, **35**, 1037–1053.

Reverdin, G., F. Durand, J. Mortensen, F. Schott, H. Valdimarsson, and W. Zenk, 2002: Recent changes in the surface salinity of the North Atlantic subpolar gyre. *Journal of Geophysical Research*, **107**.

Reynaud, T. H., 1994: *Dynamics of the Northwestern Atlantic Ocean: A Diagnostic Study*. Ph.D. thesis, McGill Iniversity, Montreal, QC, Canada.

Reynaud, T. H., A. J. Weaver, and R. J. Greatbatch, 1995: Summer mean circulation of the northwestern Atlantic Ocean. *Journal of Geophysical Research*, **100**, C1, 779–816.

Rhein, M., J. Fischer, W. M. Smethie, D. Smythe-Wright, R. F. Weiss, C. Mertens, D. H. Min, U. Fleischmann, and A. Putzka, 2002: Labrador Sea Water: Pathways, CFC Inventory, and Formation Rates. *Journal of Physical Oceanography*, **32**, 648–665.

Ribergaard, M. H., 2006: Oceanographic investigations off West Greenland 2005. Technical Report 06/001, NAFO Scientific Council Documents.

Schmidt, S. and U. Send, 2004: Origin and composition of seasonal Labrador Sea freshwater. *Journal of Physical Oceanography*, submitted.

Schmitt, R. W., P. S. Bogden, and C. E. Dorman, 1989: Evaporation minus precipitation and density fluxes for the North Atlantic. *Journal of Physical Oceanography*, **19**, 1208–1221.

Simmons, A. J. and J. K. Gibson, 2000: The era-40 project plan. Technical Report ERA-40 Project Report Series No. 1, ECMWF.

Smethie, W. M. and J. H. Swift, 1989: The tritium: krypton-85 age of Denmark Strait Overflow Water and Gibbs Fracture Zone Water just south of Denmark Strait. *Journal of Geophysical Research*, **94**, 8,265–8,275.

Smith, J. N., E. P. Jones, S. B. Moran, W. M. Smethie, and W. E. Kieser, 2005: Iodine 129/CFC 11 transit times for Denmark Strait Overflow Water in the Labrador and Irmenger Seas. *Journal of Geophysical Research*, **110**, doi: 10.1029/2004JC002516.

Spall, M. A., 2004: Boundary Currents and Watermass Transformation in Marginal Seas. *Journal of Physical Oceanography*, **34**, 1197–1213.

Steffen, E. L. and E. A. D'Asaro, 2002: Deep Convection in the Labrador Sea as Observed by Langrangian Floats. *Journal of Physical Oceanography*, **32**, 475–492.

Steffen, K., S. V. Nghiem, R. Huff, and G. Neumann, 2004: The melt anomaly of 2002 on the Greenland Ice Sheet from active and passive microwave satellite observations. *Geophysical Research Letters*, **31**.

Stein, M., 2004: Climatic overview of NAFO Subarea 1, 1991-2000. *J. Northw. Atl. Fish. Sci.*, **34**, 29–40.

Stephens, C., J. I. Antonov, T. P. Boyer, M. E. Conkright, R. A. Locarnini, T. D. O'Brien, and H. E. Garcia, 2002: World Ocean Atlas 2001 Volume 1: Temperature. NOAA Atlas NESDIS 49.

Stramma, L., D. Kieke, M. Rhein, F. Schott, I. Yahayaev, and K. P. Koltermann, 2004: Deep water changes at the western boundary of the subpolar North Atlantic during 1996 to 2001. *Deep-Sea Research I*, **51**, 1033–1056.

Stramma, L. and M. Rhein, 2001: Variability in the Deep Western Boundary Current in the equatorial Atlantic at 44°W. *Geophysical Research Letters*, **28**, 1623–1626.

Straneo, F., 2006: Heat and Freshwater Transport through the Central Labrador Sea. *Journal of Physical Oceanography*, **36**, 606–628.

Straneo, F., R. S. Pickart, and K. Lavender, 2003: Spreading of Labrador sea water: an advective-diffusive study based on Langrangian data. *Deep-Sea Research I*, **50**, 701–719.

Straneo, F. and F. Saucier, 2007: The Outflow from Hudson Strait into the Labrador Sea. *Deep-Sea Research I*, submitted.

Talley, L. D., 2003: Shallow, Intermediate, and Deep Overturning Components of the Global Heat Budget. *Journal of Physical Oceanography*, **33**, 530–560.

Talley, L. D. and M. S. McCartney, 1982: Distribution and Circulation of Labrador Sea Water. *Journal of Physical Oceanography*, **12**, 1189–1205.

Thierry, V., E. de Boisson, and H. Mercier, 2007: Rapid changes in the properties of the Reykjanes Ridge Mode Water over 1990-2006. *Deep Sea Research*, submitted.

Thompson, K. R., J. R. N. Lazier, and B. Taylor, 1986: Wind-Forced Changes in Labrador Current Transport. *Journal of Geophysical Research*, **91**, 14,261–14,268.

Trenberth, K. E. and J. M. Caron, 2001: Estimates of Meridional Atmosphere and Ocean Heat Transports. *J. of Climate*, **14**, 3433–3443.

Vinje, T., 2001: Fram Strait ice fluxes and atmospheric circulation: 1950-2000. *Journal of Climate*, **14**, 3508–3517.

Walsh, J. E. and D. H. Portis, 1999: Variations of precipitation and evaporation over the North Atlantic Ocean, 1958-1997. *Journal of Geophysical Research*, **104**, 16613–16631.

Weaver, A. J. and E. S. Sarachik, 1991: Evidence for Decadal Variability in an Ocean General Circulation Model: An Advective Mechanism. *Atmosphere-Ocean*, **29**, 197–231.

Webb, D. J., 1993: An ocean model code for array processor computers. Technical Report 324, Institute of Oceanographic Sciences, Wormley, U.K.

Yashayaev, I., 2006: Recent changes in oceanographic conditions in the Labrador Sea. *Journal of Physical Oceanography*.

Yashayaev, I. M. and I. I. Zveryaev, 2001: Climate of the Seasonal Cycle in the North Pacific and the North Atlantic Oceans. *Int. J. Climatol.*, **21**, 401–417.